FP   10:30 AM - 12:30 PM

B406B-B407

Modulators

William Burns, *CODEON Corp., USA, Presider*

FP1   (Invited)   10:30 AM

Hi Perf LiNbO3 Modulators

M. Sugiyama, *Fujitsu Labs., Atsugi, Japan,*
Email: msugi@jp.fujitsu.com.

The recent progress in the development of external LiNbO3 modulators is summarized here. An OTDM modulator, a polarization independent modulator and a low drive modulator are introduced.

1. Introduction

Optical communication systems operating at 10 Gb/s or 40 Gb/s require modulators with such characteristics as a broad bandwidth, low drive voltage, and low insertion loss. LiNbO3 Mach-Zehnder modulators[1-3] with a traveling-wave electrode have a high potential for WDM systems because of their low insertion loss, low-frequency chirp, and wavelength-independent characteristics. Therefore LiNbO3 modulators have been used widely for high speed and long haul transmission system, since all problems on unstability were solved in the early 1990s.[4,5]
In this paper, we introduce our developed LiNbO3 modulators that are effective for high-bit-rate communications.

2. OTDM modulator

We proposed and fabricated the 40 Gb/s OTDM modulator as shown in Fig. 1[1]. The OTDM modulator integrates a 20 G 1x2 switch, two 20 Gb/s modulators, and a multiplexer on a chip. The first stage of the 1x2 switch is driven by a 20 GHz electrical clock. The second stage consists of two Mach-Zehnder modulators with a bandwidth of over 20 GHz. The final stage is a multiplexer using an intersecting 3 dB coupler.

The total optical insertion loss is 8 dB. The drive voltage of the first stage switch is 5.5 V at 20 GHz and that of the second stage modulators is 5.7 V for 20 Gb/s signals. The E/O bandwidth is more than 20 GHz. Fig. 2(a) shows the optical clock generated with the first stage. Fig. 2(b) is the RZ optical signal at the rear part of the modulator in the second stage. Fig. 2(c) shows the 40 Gbs/ optical signal at the end of the waveguide. Thus, we achieved a modulation at 40 Gb/s with 20 GHz electrical clock signals and two independent 20 Gb/s electrical signals. This is a demonstration of 40 Gb/s modulation and this technology can also be applied to modulations higher than 40 Gb/s.
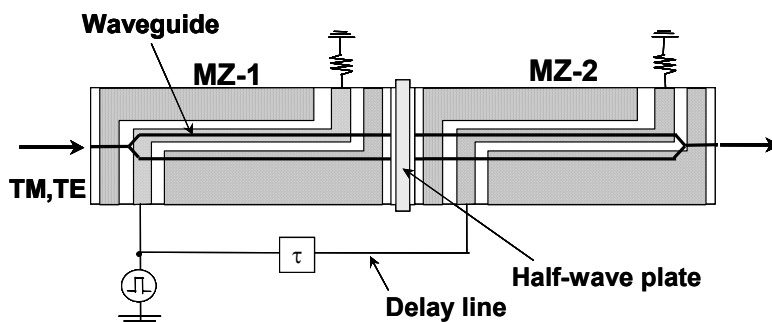

Fig. 1. Schematic of OTDM modulator

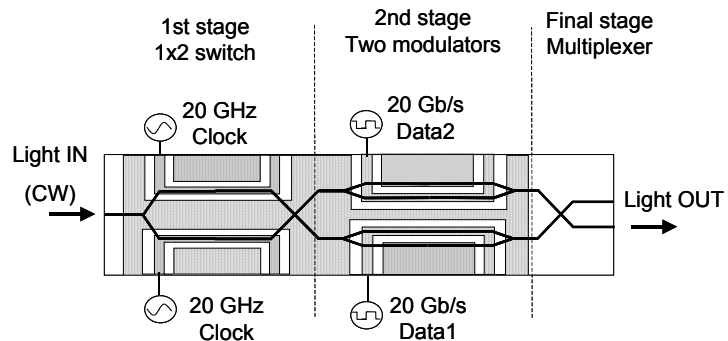(a) 20 Gb/s clock(first stage)   (20 ps/div.)

(b) 20 Gb/s RZ pattern(second stage)   (20 ps/div.)

(c) 40 Gb/s pattern (final stage)   (10 ps/div.)
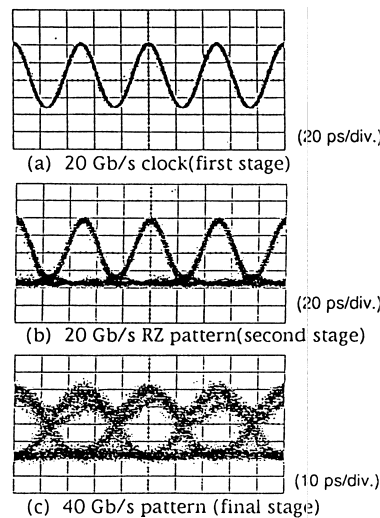
Fig. 2. Waveform of OTDM modulator.

3. Polarization independent modulator

Since LiNbO3 modulators have polarization dependency, their applications are limited to systems with polarized light sources. Polarization independent modulators enable systems in which unpolarized light sources are used.
We developed a polarization independent modulator with a tandem electrode and a half-wave plate, as shown in Fig. 3[2]. The half-wave plate, which acts as a TE/TM mode converter, is located at the center of the Mach-Zehnder waveguide. This structure contributes to the function of the polarization-independence, and ensures a match between the light and microwave velocities.
A 0.85-μm-thick Si-dioxide buffer layer and a 0.1-μm thick Si film were deposited on the substrate. Two traveling-wave electrodes 24-μm thick and 25-mm long were then patterned. This construction resulted in a match between the light and microwave velocities. The chip was 1.2-mm wide and 60-mm long. A groove 20-mm wide and 200-

mm deep was cut between the two electrodes using a dicing saw. A 12-μm-thick half-wave plate, which acts as a TE/TM mode converter, was inserted into the groove and fixed in place with a UV-curable adhesive.
The fiber-to-fiber insertion loss was 5.1 dB, including the 2 dB loss of the half-wave plate. The PDL remained at 0.2 dB. The driving voltage was 3.3 V DC (Fig. 4) and 4.5 V for 10 Gb/s signals. Fig. 4 shows that the same drive voltage and the drive point were obtained for each type of polarized input. The extinction ratio was 20 dB or more for both polarized input lights. An electrical 3-dB bandwidth was achieved at over 10 GHz.
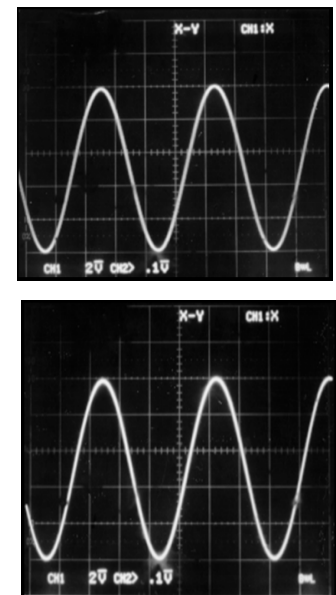

Fig. 4. Applied voltage vs. optical power for incident light of (a) TM mode and (b) TE mode. (L:2 V/div.)

4. Low drive voltage modulator

Current 40 Gb/s modulators require a drive voltage of about 5 V for single-drives and 3 V for dual-drives. Low drive voltage is required to reduce the cost, size and power consumption of 40 Gb/s transmitters.
We optimized the structure of the dual-drive modulator to reduce the drive voltage [3]. We measured Vπ and microwave attenuation and obtained their dependency on the interaction length and the gap between signal and ground electrodes. From these data, we found that a wide-gap and long electrode was effective for a low drive voltage. We defined the interaction length of 60 mm and gap of 50 μmthat were twice as large as those of conventional modulators.
We fabricated and packaged a dual-drive modulator with a novel design. The optical fiber to fiber insertion loss was 6 dB and the extinction ratio 27 dB, these values being suitable for practical use. Fig. 5 shows the S-parameters and the optical response. The 6 dB bandwidth of S21 was 30

Fig. 3. Schematic of polarization independent modulator.

GHz. The S11 was low enough because impedance matching was obtained. An effective refractive index of 2.15 was estimated from the S21 phase. The 3 dB bandwidth of optical response was 28 GHz. Eye diagrams of the driving signal and optical output in a PRBS 2^{31}-1 are shown in Fig. 6. Clear eye openings were obtained with a drive voltage of 0.9 V.
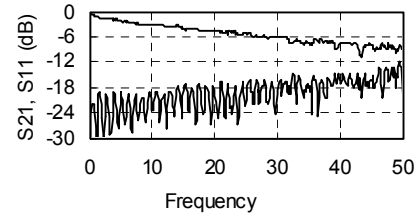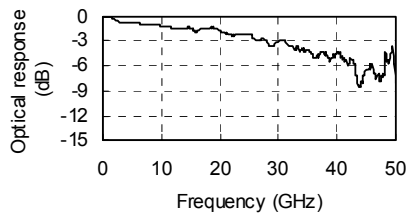

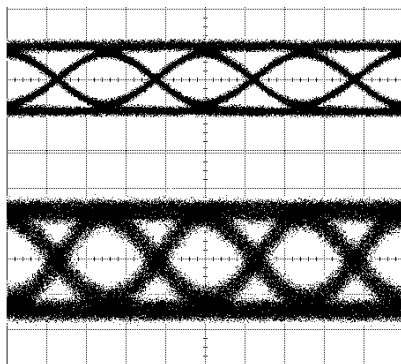
Fig. 5. Frequency response of low-drive-voltage modulator.

Fig. 6. Eye diagram at 40 Gb/s.

5. Conclusions

I believe that LiNbO$_3$ modulator will continue to be a key device in future high speed and long haul communication systems. Therefore the small size and low cost are considered to be more important especially in the WDM systems.

References

[1] R.C.A Alferness, IEEE Trans. Microwave Theory Tech., vol. MTT-30, pp. 1121-1137 (1982).
[2] K. Noguchi, O. Mitomi et al., IEEE J. Lightwave Technol., vol. LT-13, pp. 1164-1168 (1995).
[3] M. Minakata, Proc. SPIE, vol. 4532 (2001).
[4] I. Sawaki, H. Nakajima et al., CLEO'86 MF2 (1986).
[5] M. Seino, T. Nakazawa et al., OFC'92 PD-3 (1992).
[6] M. Doi, et al., Photonics in Switching '96 PThB1, pp. 172-173 (1996).
[7] S. Taniguchi, et al., CLEO /Pacific Rim 2001 ME1-2 I-90 (2001).
[8] M. Sugiyama, et al., OFC02 PD-FB6 (2002).

FP2   **11:00 AM**

A Repetition Rate Upgrade from 10 to 40 GHz for Laser Sources

K. Yiannopoulos, K. Vyrsokinos, N. Pleros, C. Bintjas, T. Houbavlis, H. Avramopoulos, *National Technical University, Athens, Greece;* G. Guekos, *Swiss Federal Institute of Technology, ETH, Hoenggerberg, Zurich,* Switzerland, *Email: kyianno@cc.ece.ntua.gr.*

We demonstrate a simple method for upgrading the repetition rate of 10 GHz optical sources to 40 GHz. It employs a Fabry-Perot filter and the saturation properties of a Semiconductor Optical Amplifier.

1. Introduction

Optical fiber transmission is accomplished with extremely sophisticated and expensive systems and research has traditionally focused in developing techniques to allow multiplexing of as many channels as possible over the same physical fiber layer, so as to divide the plant cost between them and to reduce the transmission cost per individual channel. Hero experiments have continued to set new, remarkable records using both WDM and/or OTDM techniques [1-4]. Key to these achievements has been the availability of ultra-fast laser sources. The recent change in the telecommunications business cycle has however created a new reality for transmission and networking systems: they must be of low initial cost and modest performance, but readily upgradeable in terms of capability to meet performance needs as these grow.

In the present communication we demonstrate a novel, simple and stable laser source, at 40 GHz nominal repetition rate. It consists of a 10 GHz gain switched, short pulse DFB, which is followed by a Fabry-Perot filter (FPF), with 40 GHz free spectral range (FSR) or 4 times the repetition rate of the initial pulse train [5-6]. At the output of the FPF, the pulses of the 40 GHz pulse train have exponentially decreasing amplitudes and these are next nearly equalized in a semiconductor optical amplifier (SOA) using its nonlinear gain saturation. The technique is simple and lends itself to be employed for the easy upgrade from 10 GHz to 40 or higher repetition rates of laser sources, using one passive and one active (but dc driven) component and without the need for any high frequency microwave driver circuits and amplifiers. The technique could in principle be useful to increase the repetition rate of several lower rate sources and share the upgrade cost of the FPF and SOA between them. This is especially since a single FPF may multiply simultaneously the repetition frequency of several laser sources and since single SOAs have been shown in multi-wavelength amplification [7] and multi-wavelength sources [8].

2. Concept and Experimental Setup

Fig. 1 shows the experimental layout of the proposed optical source. The initial pulse train was generated with a DFB laser source gain switched at 9.97163 GHz at 1549.2 nm, producing 8.8 ps pulses after linear compression in a DCF fiber of total dispersion of –54.27 ps/nm. These pulses were then nonlinearly compressed in a two-stage fiber compressor comprising of an EDFA and alternating sections of DSF and SMF fiber, so that after filtering in a 2 nm filter the signal pulses had a temporal width of 3.2 ps. The compressed pulse train was next further amplified and fed into the Fabry-Perot filter. The FPF was a coated fused quartz substrate with FSR equal to 39.88652 GHz and a modest finesse of 50. Assuming that the input to this FPF is the initial pulse train, its output is a periodic sequence of 4 pulses that are
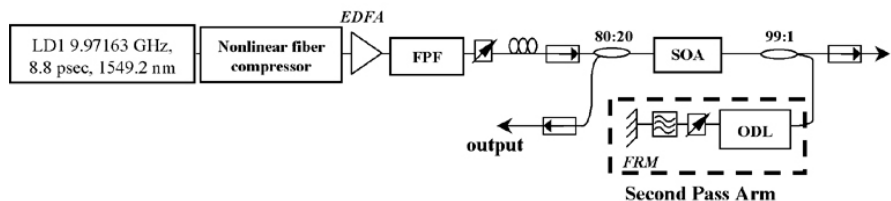

Fig. 1. Experimental setup. FPF: Fabry-Perot Filter, FRM: Faraday Rotator Mirror, ODL: Optical Delay Line

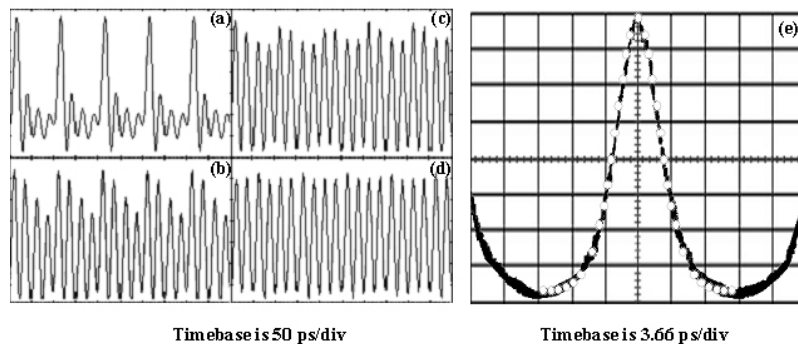Fig. 2. (a) Compressor output, (b) Fabry-Perot filter output, (c) Output after first SOA pass (d) Output after second SOA pass and (e) Second harmonic autocorrelation trace with the white dots indicating the fitted profile.

Fig. 3. RF Spectra at the (a) Output of the Compressor, (b) Output of the Fabry-Perot filter and (c) Output of the 40 GHz Pulse Source. Amplitude Scale is 10 dB/div and Frequency Scale is 4 GHz/div

exponentially decreasing to -1.65 dB from first to last, at a rate equal to the FSR of the FPF.

Clearly this amplitude modulation is far too high for a potential laser transmitter source, but this pattern may be reduced subsequently in a SOA using its nonlinear saturation properties. In our experiment the SOA was a commercially available device (Optospeed S.A.) of ridge waveguide structure, with small signal gain of 24 dB at 1549.2 nm, when driven at 700 mA dc current and 3 dB polarization gain dependence. Experimental measurements and numerical simulations revealed that single pass through the SOA could significantly reduce the amplitude modulation but could not remove it altogether. For this reason the outgoing pulse train from the SOA was re-introduced for a second pass, in a counter-propagating direction. By arranging for the second pass through the SOA to counter-propagate the first, the amplitude modulation in the pulse train may be further reduced if the higher amplitude pulses from the two directions are adjusted to temporally meet in the SOA. The arm arranged to provide this second pass through the SOA therefore included a variable optical delay line (ODL), a power attenuator, a 2.8 nm bandpass filter to remove out of band noise from the SOA and a Faraday rotator mirror. With this arrangement three adjustments are provided to reduce the amplitude pattern: the degree of saturation of the SOA that can be controlled by adjusting the power of the two beams with the attenuators VOA1 before the SOA and VOA2 at the second pass arm and the timing adjustment with ODL.

3. Results and Discussion

VOA1 and VOA2 were adjusted to provide 850 μW and 80 μW of power for the first and second pass respectively. At this input power the first pass through the SOA results in its heavy saturation and sets its point of operation in the non-linear regime. In passing through the SOA for the second time and with the ODL adjusted so that the pulses meet with their respective pairs in amplitude in the SOA, the pulses experience the saturated gain and modify it slightly so as to have their amplitude modulation nearly, totally, eliminated. Fig. 2 shows the pulse trains at the output of (a) the fiber compressor, (b) after the FPF, (c) after the first pass through the SOA and finally (d) after its second pass. Monitored on a 40 GHz photodiode and sampling oscilloscope, the amplitude modulation, defined as the ratio of higher to lower pulse, after the FPF was measured to be 1.65 dB, after the first pass through the SOA reduces to 0.8 dB and finally is further reduced to 0.15 dB after the second pass through the SOA. Fig. 2(e) depicts the autocorrelation trace of the output pulse stream fitted with a hyperbolic secant profile. Assuming the hyperbolic secant profile, the pulses have a FWHM of 3.8 ps, marginally increased from 3.5 ps at the input of the SOA due to modal gain difference and birefringence in the SOA. The output power was 680 μW.

Fig. 3 shows the microwave spectra of the optical pulse trains measured on a 50 GHz spectrum analyzer: Fig. 3(a) is the spectrum of the 10 GHz pulse train after the fiber compressor, Fig. 3(b) after the FPF and Fig. 3(c) after the second pass through the SOA. This figure shows that the combination of the FPF with the double pass through the SOA, results in effective suppression (in excess of 26 dB) of the 10 GHz component while the 20 and 30 GHz frequency components are suppressed by approximately 35 dB. Analysis of the microwave spectra at the output of the SOA reveals that the amplitude modulation of the signal is below 0.25 dB, in close agreement to the measurements made with the sampling oscilloscope. Clearly the use of a FPF with larger finesse can further reduce this amplitude modulation.

Even though the source presented here used a bulk FPF, it proved to be operationally stable in laboratory conditions and provided unchanging pulse trains for several hours at a time. To further assist the stability of the source obvious improvements include the use of a fiber Fabry-Perot filter of optimized finesse and a SOA with low polarization gain dependence.

4. Conclusion

In conclusion we have presented a novel method for producing 40 GHz pulses. Our technique employs a gain switched short pulse 10 GHz source whose output is introduced in a Fabry-Perot filter with 40 GHz FSR to generate the 40 GHz signal and is doubly passed through a SOA to remove the resulting amplitude modulation. The source has been shown to display amplitude modulation below 0.25 dB and stable operation. The source was built from commercially available components, does not require any 40 GHz microwave circuits and provides a relatively easy upgrade path to higher repetition rates for 10 GHz laser sources.

References

[1] H. Bissessur, G. Charlet, W. Idler, C. Simonneau, S. Borne, L. Pierre, R. Dischler, C. De Barros and P. Tran, "3.2 Tbit/s (80x40 Gbit/s) phase-shaped binary transmission over 3x100 km with 0.8 bit/s/Hz efficiency," Electron. Lett., Vol. 38, No. 8 , April 2002, pp. 377 –379.
[2] A.H. Gnauck, G. Raybon, S. Chandrasekhar, J. Leuthold, C. Doerr, L. Stulz, A. Agarwal, S. Banerjee, D. Grosz, S. Hunsche, A. Kung, A. Marhelyuk, D. Maywar, M. Movassaghi, X. Liu, C. Xu, X. Wei and D.M. Gill, "2.5 Tb/s (64x42.7 Gb/s) Transmission Over 40x100 km NZDSF Using RZ-DPSK Format and All-Raman-Amplified Spans," in Proceedings of Optical Fiber Conference 2002, Post-deadline Paper FC2.
[3] H. Sugahara, K. Fukuchi, A. Tanaka, Y. Inada and T. Ono, "6,050 km transmission of 32x42.7 Gb/s DWDM signals using Raman-amplified quadruple-hybrid span configuration," in Proceedings of Optical Fiber Conference 2002, Post-deadline Paper FC6.
[4] M. Nakazawa, T. Yamamoto and K. R. Tamura, "1.28 Tbit/s-70 km OTDM transmission using third- and fourth-order simultaneous dispersion compensation with a phase modulator," Electron. Lett. , Vol. 36, pp. 2027-2029, 2000.
[5] T. Sizer, "Increase in Laser Repetition Rate by Spectral Selection," IEEE J. Quantum Electron., Vol. 25, No. 1, Januaey 1989, pp. 97-103.
[6] D.K. Serkland, G. D. Bartolini, W.L. Kath, P. Kumar and A.V. Sahakian, "Rate Multiplication of a 59-GHz Soliton Source at 1550 nm," IEEE J. Lightwave Technol., Vol. 16, No. 4, April 1998, pp. 670-677.
[7] A.H. Gnauck, L.H. Spiekman, J.M. Wiesenfeld, L.D. Garrett, "Dynamic Add/Drop of 8-of-16 10-Gb/s Channels in 4x40km Semiconductor-Optical-Amplifier-Based WDM System," in Proceedings of Optical Fiber Conference 2000, Post-deadline Paper PD39.
[8] K. Vlachos, K. Zoiros, T. Houbavlis and H. Avramopoulos, "10 Simultaneously Mode-locked and Synchronized Channels at 30 GHz from Fiber Ring Laser," in Proceedings of Optical Fiber Conference 2000, Vol. 2, pp. 344-346.

FP3   **11:15 AM**

Variable Optical Frequency Shifter Using Multiple Quasi-Phase-Matched LiNbO₃ Wavelength Converters

O. Tadanaga, M. Asobe, H. Miyazawa, Y. Nishida, H. Suzuki, *NTT Photonics Laboratories, NTT Corporation, Atsugi, Kanagawa, Japan, Email: tadanaga@aecl.ntt.co.jp.*

We describe an optical frequency shifter that uses two 4-channel multiple quasi-phase-matched LiNbO₃ wavelength converters. We obtained ten different outputs by varying the pump wavelength combination for the two wavelength converters.

1. Introduction

An all-optical wavelength converter is a key device for constructing future large-capacity and flexible wavelength-division multiplexed (WDM) networks. 1.55-μm-band quasi-phase-matched (QPM) wavelength converters based on difference frequency generation (DFG) in periodically poled LiNbO₃ (LN) are promising because of their novel features, such as the simultaneous conversion of multiple WDM channels, high-efficiency, low noise, and transparency as regards bit-rate and data format [1]. We have already reported a double-conversion optical frequency shifter (DC-OFS) that employs two QPM-LN wavelength converters [2]. This DC-OFS provides WDM signals with a uniform optical frequency shift by the amount of the frequency difference of two pump lights. However, the amount of shift for the DC-OFS is limited considerably because the QPM bandwidth of the conventional QPM-LN wavelength converters used in the work is only about 0.2 nm. If we wish to construct a flexible optical node system such as an optical cross-connect (OXC), we must develop an OFS that allows us to vary the shift. In this paper, we describe a novel variable-destination DC-OFS that uses two 4-channel multiple-QPM-LN wavelength converters. We achieved ten different outputs by changing the pump wavelength combination for the two wavelength converters.

2. Concept of DC-OFS

The DC-OFS is based on double wavelength conversion using DFG in QPM-LN wavelength converters. Figure 1 is a schematic drawing of the principle of the DC-OFS when it is operated in a $\chi^{(2)}$-cascaded scheme. When a pump light (ω_{p1}) and a signal light (ω_{signal}) are injected into a QPM-LN wavelength converter, the pump light generates a second-harmonic (SH) light ($2\omega_{p1}$). A converted signal light, $\omega_{conv.}$ (= $2\omega_{p1} - \omega_{signal}$), is then generated by means of a parametric interaction between the SH light and the signal light. In multi-channel-conversion, each channel is converted in accordance with the relation described above [see Fig. 1(a)]. When a second pump light, ω_{p2} (= $\omega_{p1} + \Delta$), and a signal light, which is the signal converted in the first conversion, are injected into a second QPM-LN wavelength converter, the frequency difference between the first input signal and the second converted signal is twice as large as that between the two pump lights [Fig. 1(b)]. This system provides a uniform frequency shift (2Δ) for all the input lights without changing their order in the wavelength dimension. The magnitude and direction of the shift in the DC-OFS can be varied by fabricating two converters with an appropriate frequency difference between the two pump lights in a double wavelength conversion. In order to realize flexible characteristics with this type of DC-OFS we utilized multiple-QPM-LN wavelength converters that have a continuously-phase-modulated domain structure. These multiple QPM-LN wavelength converters allow multi-wavelength pumping with a minimal loss of efficiency. In addition, various number and frequency spacings can be designed and devised in the multiple QPM structure. The number of different shift destinations can be increased up to MxN by utilizing multiple-QPM-LN wavelength converters with M- and N-channel multiple QPM conditions for the first and second conversions, respectively. The magnitude of the frequency shift can be varied in accordance with the optical frequency difference between the two pump lights.
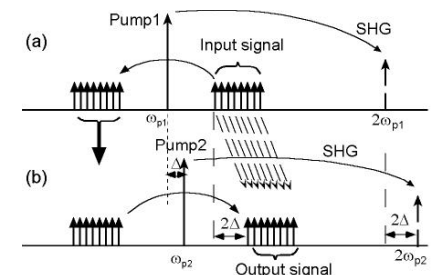

Fig. 1. Principle of DC-OFS using $\chi^{(2)}$-cascaded scheme.

3. Experiments
3.1. Device fabrication
We used 3-inch z-cut non-doped congruent LN substrates to fabricate the QPM-LN wavelength

converters. The substrates were periodically poled by means of an electrical poling method. The periods were 14.75 μm. Phase of the periodic poling was continuously modulated in order to satisfy the QPM condition at 4 different wavelengths. We fabricated the waveguides using the annealed proton exchange (APE) method. After proton exchange in pure benzoic acid using a SiO$_2$ mask, the substrate was annealed in an oxygen atmosphere. We fabricated two types of 4-channel QPM-LN wavelength converter; one with a 210 GHz spacing, and the other with a 420 GHz spacing.

3.2. Experimental setup

Figure 2 is a schematic diagram of the experimental OFS setup. All the light sources were CW tunable semiconductor lasers. We used a $\chi^{(2)}$ cascading scheme [1]. A signal light around 1530 nm and a pump light (pump 1) amplified by an erbium-doped fiber amplifier (EDFA) were injected into the first QPM-LN wavelength converter through a WDM coupler. The converted signal lights in the L-band were used as input signals in the second conversion through an L-band-pass filter. These input signal lights in the L-band and pump light (pump 2) were amplified by other EDFAs, and injected into the second QPM-LN wavelength converter. Signal lights converted in the second conversion were measured by an optical spectrum analyzer.

The operating temperatures were 100.5°C and 102.2°C for the first and the second QPM-LN wavelength converters, respectively. Each QPM-LN allowed 4 different pump wavelengths. The wavelengths of pump 1 were 1548.6, 1550.3, 1552.0 and 1553.7 nm, and the wavelengths of pump 2 were 1547.0, 1550.3, 1553.7 and 1557.0 nm. Figure 2(b) shows the relation between the two pump lights, where Δ is 210 GHz. The individual pump wavelengths were denoted as 1a, 1b, 1c, and 1d for pump 1, and 2a, 2b, 2c, and 2d for pump 2. In this case, the 4x4 combination of two pump lights provides 10 patterns of frequency differences because some combinations exhibit the same values. Therefore we can obtain 10 different shifts from this DC-OFS by selecting different combinations of the two pump wavelengths. The maximum number of patterns, (16), for the DC-OFS utilizing two 4-channel QPM-LN wavelength converters can be achieved by optimizing the wavelength and the spacing of the multiple QPM structures.
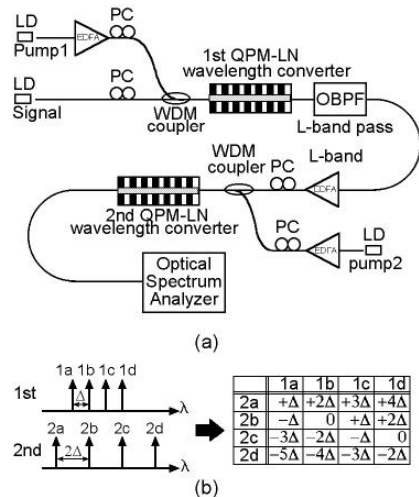

(a)

(b)

Fig. 2. Experimental setup and pump wavelength relation.

4. Results and discussion

First, we measured the spectra after the two 4-channel QPM-LN wavelength converters to confirm the principle of the DC-OFS. Figure 3(a) shows the output spectra after the first converter for 4 different pump wavelengths. It can be seen that the input signal was converted in accordance with the wavelength of pump 1. Figure 3(b)

shows the output spectra after the second converter when the input was the longest wavelength signal converted in the first conversion. A pump wavelength shift by 420 GHz relocated the converted signal by 840 GHz. We also confirmed that the remaining three signals converted in the first conversion could be converted appropriately by the second conversion.

Figure 4 shows the output spectra of the DC-OFS. We succeeded in demonstrating all the conversions of the 4x4 combination shown in Fig. 2(b). Note that the amount of shift is twice as large as the frequency difference of the two pump lights. All the signals exhibited a 420 GHz spacing from -10Δ to +8Δ with a reasonably small deviation resulting from the fact that the pump wavelengths were not tuned precisely. The magnitude of the shift agreed well with that expected from the principle. The direction of the shift was blue, red, and "0", and the output wavelength range was as broad as 30 nm.

Although we used one channel for the input signal in this study, it is clear that the DC-OFS can be operated with multi-channel inputs or a variable input [2]. Since the number of QPM structures in a single device for practical use is limited by the efficiency of the QPM-LN wavelength converter, the use of two multiple QPM-LN wavelength converters is an attractive way of providing flexibility with this type of DC-OFS.
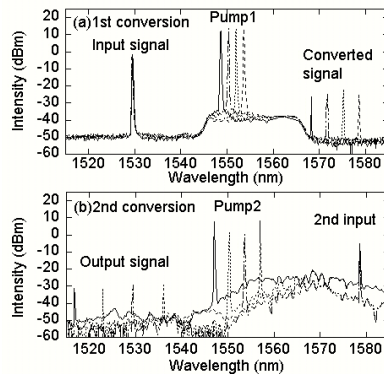

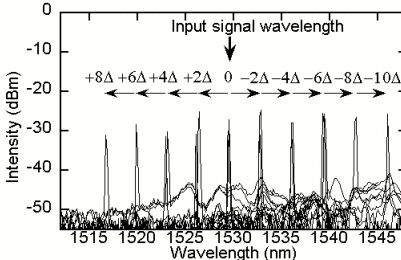Fig. 3. Output spectra after (a) first conversion and (b) second conversion.

Fig. 4. Output spectra of the DC-OFS.

5. Summary

We described a double-conversion optical frequency shifter that uses two 4-channel multi-quasi-phase-matched LiNbO$_3$ wavelength converters. One channel signal was converted to shorter and longer wavelength directions, and the same wavelength by changing the pump wavelengths. We obtained ten different outputs spread across a wavelength range of as broad as 30 nm. A double-conversion optical frequency shifter with such features as a broadband and variable output is attractive for use in future flexible WDM optical communication networks.

References

[1] M. H. Chou, I. Brener, M. M. Fejer, E. E. Chaban, and S. B. Christman, "1.5-μm-band wavelength conversion based on cascaded second-order nonlinearity in LiNbO$_3$ waveguides," *IEEE Photon. Technol. Lett.* 11, pp. 653-655 (1999).
[2] O. Tadanaga, M. Asobe, H. Miyazawa, Y. Nishida, and H. Suzuki, "A 1-THz optical frequency shifter using quasi-phase-matched LiNbO$_3$ wavelength converters," *Tech. Digest of OFC2002*, ThDD1, pp. 592-593 (2002).

FP4   **11:30 AM**

Tunable All-Optical Control of Wavelength Conversion of 5 ps Pulses by Cascaded Sum- and Difference Frequency Generation (cSFG/DFG) in a Ti:PPLN Waveguide

Y. Min, J. Lee, Y. Lee, W. Grundkoetter, V. Quiring, W. Sohler, *University of Paderborn, Paderborn, Germany, Email: sol_ym@physik.uni-paderborn.de.*

A 10 GHz, 5 ps pulse stream (λ_s=1554.8 nm) was wavelength converted in a Ti:PPLN channel waveguide by exploiting cSFG/DFG. The wavelength shift could be optically controlled in a 15 nm wide range by the wavelength of a control beam.

Introduction

Wavelength converters are considered to be key elements of future dense WDM optical networks. They enable contention resolution, wavelength reuse and effective use of the vast fiber bandwidth. Moreover, tunability of a wavelength converter can further enhance the flexibility of network systems by facilitating reconfigurable dynamic wavelength routing [1].

Cascaded three-wave mixing ($\chi^{(2)} : \chi^{(2)}$) processes in periodically poled LiNbO$_3$ (PPLN) waveguides are most promising to realise all-optical wavelength conversion with high efficiency. Two different methods have been demonstrated including cascaded difference frequency generation (cDFG) [2] and cascaded sum and difference frequency generation (cSFG/DFG) [3]. cDFG offers a wide range of transparency, negligible excess noise due to spontaneous parametric emission, a high conversion efficiency and polarization independent operation [4]. However, fast all-optical tuning of the wavelength shifted signal is not possible [5].

In order to achieve optically tunable wavelength conversion, we recently proposed and experimentally demonstrated wavelength conversion and tuning based on cSFG/DFG [3]. Two cw pump waves of different wavelengths were used to convert a cw signal to the sum frequency and to generate a wavelength shifted idler by subsequent DFG with the second pump. As a consequence, the idler wavelength can be tuned by changing the wavelength of the second pump.

In this contribution, we demonstrated for the first time tunable all-optical wavelength conversion of 5 ps pulses based on cSFG/DFG in a single Ti:PPLN channel waveguide. The device was numerically analysed and wavelength conversion and tuning was experimentally demonstrated.

Numerical Analysis

Fig.1 shows the schematic diagram of the operation principle of the device exploiting cSFG/DFG process. In this process, five different waves interact with each other simultaneously in the Ti:PPLN channel waveguide. The signal (λ_s) and the pump (λ_p) generate the sum frequency (λ_{sf}) perfectly phase matched. At the same time, a control wave (λ_c) interacts with the sum frequency wave (λ_{sf}) to generate an idler (λ_i) by DFG. However, this process is slightly phase mismatched, but obeyes of course energy conservation $1/\lambda_{sf}=1/\lambda_i+1/\lambda_c$. This relation is plotted as dashed line in Figure 1(b) for fixed λ_c. Though not ideally phase matched the DFG conversion efficiency is only slightly reduced in comparison to a phase matched interaction.

(a)

$$\omega_s + \omega_p \rightarrow \omega_{sf} : \text{SFG}$$

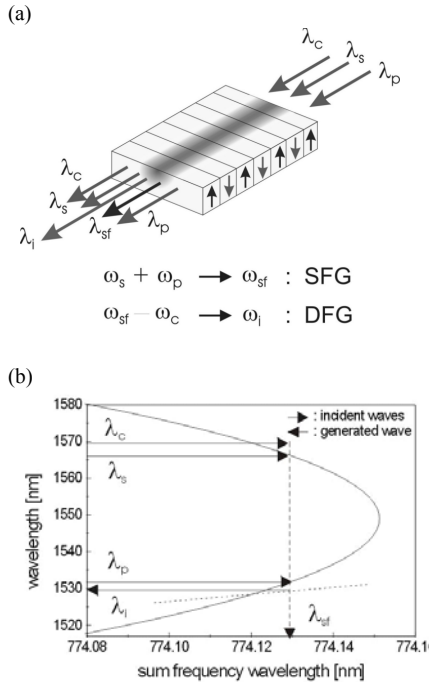$$\omega_{sf} - \omega_c \rightarrow \omega_i : \text{DFG}$$

(b)

Fig. 1. (a) Schematic diagram of cSFG/DFG in a Ti:PPLN channel waveguide and (b) phase matching characteristics for three-wave mixing processes involved. The dashed line represents energy conservation ($1/\lambda_{sf}=1/\lambda_i+1/\lambda_c$) for fixed λ_c

For the numerical calculations, signal pulses (λ_s) were assumed as Gaussian-type 5 ps pulses with 10 GHz repetition rate; pump and control were considered as cw waves. The coupled wave equations for the nonlinear optical processes were numerically solved using a fast fourier transform (FFT) split-step propagation method. The (average) input power of the signal was 7.7 mW, the control power was assumed to be 161 mW as in the experiments. The length and width of the Ti:PPLN channel waveguide were assumed to be 6 cm and 7 μm , respectively. 19 pm/V was taken as d_{33} value of $LiNbO_3$ and optical losses for infrared and sum frequency waves were assumed to be 0.15 dB/cm and 0.3 dB/cm, respectively.
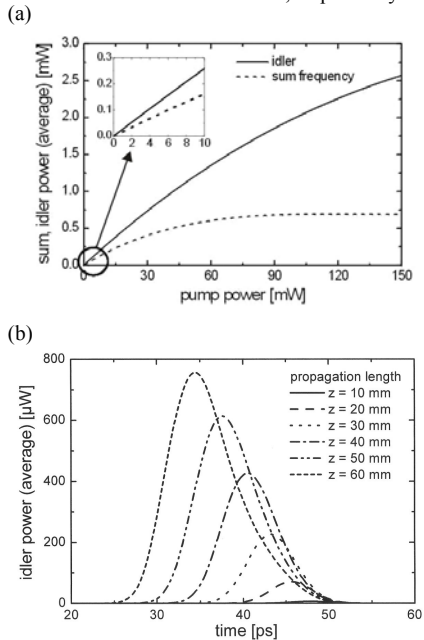
(a)

(b)

Fig. 2. (a) Calculated average sum frequency and idler power, respectively, as function of the pump power and (b) temporal evolution of the idler pulse at different positions in the waveguide, assuming a pump power level of 2.8 mW.
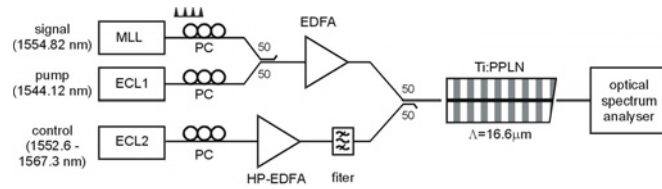

Fig. 3. Schematic diagram of experimental set-up.

Fig. 2 (a) presents the calculated sum frequency and idler power, respectively, as function of the pump power. The inset gives a magnified characteristic at low pump power levels to allow a comparison with experimental results. The maximum idler power of 2.6 mW is achieved with 150 mW of pump power. Fig. 2 (b) shows the temporal evolution of the idler pulse along the waveguide. The broadening of sum frequency and signal/idler pulses is due to the group velocity mismatch (3 ps/cm). At the output, the pulse width is 9 ps. The conversion efficiency defined as the ratio of generated idler power to the input signal power is -4.8 dB at 150 mW of pump power.

Experimental results and discussion
To demonstrate all-optical wavelength conversion by cSFG/DFG, a 8-cm-long Ti:PPLN channel waveguide of 16.6 μm microdomain period was fabricated. One side of the sample was angle polished in order to avoid internal multiple reflections. Phase matching wavelength and conversion efficiency for second harmonic generation (SHG) are 1549.45 nm and 650%/W, respectively, at 153.3°C. The effective nonlinear interaction length is ~6 cm calculated from the SHG bandwidth of $\Delta\lambda$=0.18 nm; the waveguide propagation losses are 0.15 dB/cm around λ=1550 nm.
Figure 3 shows the schematic diagram of the experimental set-up. Transform limited gaussian pulses (λ_s=1554.82 nm) of 5ps width and 10 GHz repetition rate of a mode-locked fiber laser were combined by a 3 dB-coupler with the cw pump wave (λ_p=1544.12 nm) of an extended cavity semiconductor laser (ECL1) and amplified simultaneously by an EDFA. The control wave delivered by the ECL2 was amplified by a high power EDFA (HP-EDFA). Amplified spontaneous emission (ASE) was to a large extent suppressed by a tunable band pass filter. All three waves were polarisation-controlled by fiber optic polarisation controllers (PC). They were superimposed by another 3 dB-coupler and launched together into the channel waveguide by fiber butt-coupling. The transmitted signal, pump, and generated idler were observed as function of the wavelength using an optical spectrum analyser.
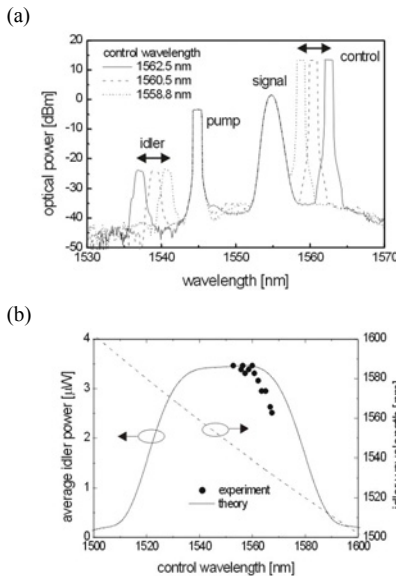
(a)

(b)

Fig. 4. (a) Optical spectra taken at the output of the Ti:PPLN wavelength converter at different control wavelengths and (b) average idler power versus another wavelength.

Fig. 4(a) shows the optical spectra for three different wavelengths of the control wave measured with 2 nm resolution; averaged optical power levels are given. The coupled (peak) power of signal and control were adjusted to be equal (161 mW). The coupled pump power was 2.8 mW. Pump and signal generate optical pulses at λ_{sf}=774.7 nm by SFG. These pulses serve as pump for the DFG-process with the control wave; idler pulses are generated. Their (calculated) evolution along the waveguide is shown in Fig. 2(b). The idler wavelength changes with the control wavelength according to energy conservation (see Fig 4a). Due to group velocity dispersion the idler pulses are broadened to about 9 ps half width according to our calculations. The average idler power was measured to be -24.6 dBm. Figure 4(b) shows the average idler power as function of the control wavelength together with a calculated normalised response. The wavelength of the control wave could be tuned from 1552.65 nm to 1567.30 nm (limited by the EDFA gain bandwidth), resulting in an idler wavelength from 1546.24 nm to 1531.6 nm. The theoretical result predicts an even wider tuning range of more than 50 nm.

Conclusions
For the first time, tunable all-optical wavelength conversion of 5-ps pulses based on cascaded SFG/DFG was demonstrated in a Ti:PPLN channel waveguide of homogeneous microdomain periodicity. The overall efficiency was about -25 dB defined by the ratio of average idler to signal power. However, theory predicts that it can be easily increased to -4.8 dB just by adjusting the pump power level to 150 mW (see Fig. 2(a)); this will be investigated in the near future. The 3 dB bandwidth of the idler tuning range is about 56 nm.

References
1.Jaafar M. H. Elmirghani, et al., "All-optical Wavelength conversion : Technologies and Applications in DWDM Network," IEEE Commun. Magazine, p.86, March 2000.
2. K. Gallo, et.al., "Efficient wavelength shifting over the erbium amplifier bandwidth via cascaded second order processes in lithium niobate waveguides," Appl. Phys. Lett., 71, 1020 (1997).
3. J. H. Lee, et al., "All-optical wavelength shifting and tuning in a Ti:PPLN channel waveguide by cascaded sum and difference frequency generation," Opt. Lett., *to be submitted* (2002).
4. H. Suche, et al., "All Optical Wavelength Conversion and Switching in Ti:PPLN-Waveguide," in Proc. International Topical Meeting on Photonics in Switching, p. 34, Cheju, Korea (2002).
5. Bo Chen, et al., "All-Optical Variable-In Variable-Out Wavelength Conversions by Using MgO:LiNbO$_3$ Quasiphase Matched Wavelength Converter," Jpn. J. Appl. Phys., 40, 1370 (2001).

FP5 **11:45 AM**

Wavelength Converter Operating on Strict Frequency Grid Using a Single Side Band Optical Modulator in a Circulating Loop

A. Takada, *NTT Network Innovation Laboratries, NTT Corporation, Yokosuka, Kanagawa, Japan;*
E. Yamazaki, J. Park, *NTT Network Innovation Laboratories, NTT Corporation, Yokosuka, Kanagawa, Japan, Email:*
takada@exa.onlab.ntt.co.jp.

A wavelength converter and a variable wavelength light source that operate on strict frequency grid are proposed and demonstrated using a single side band optical modulator in a re-circulating fiber loop configuration.

1. Introduction

Wavelength conversion is attracting considerable attention for use in photonic routers that must be capable of setting 'virtual wavelength paths' [1]. To date, many kinds of wavelength conversion techniques have been proposed: Optical-Electrical-Optical (OEO) conversion, cross gain/phase modulation using nonlinear materials such as semiconductor optical amplifiers and optical fibers, and parametric conversion using $\chi^{(2)}$ or $\chi^{(3)}$ effect in parametric materials. Optical frequency shift type-wavelength conversion using a single side band (SSB) electrooptic modulator (EOM) [2-3] has several attractive features. It needs no other light source, its operation is independent of the optical modulation format of the input signal light, and it has capability of strict frequency shift identical to the modulation frequency injected into the EOM. However, the frequency shift is limited by the modulation-bandwidth of the EOM and driving circuit. This paper introduces a novel configuration for a wideband wavelength converter that uses an SSB optical modulator in a fiber loop. The optical frequency of the input signal light shifts successively as the light circulates the loop. Therefore, a large degree of frequency shifting on a strict frequency grid is obtained. The proposed configuration is also useful for a wide-band variable-wavelength light source or optical frequency comb generator. Experimental demonstrations show error-free 375 GHz frequency shift for wavelength conversion and 3.7 THz-wide variable-wavelength light source.

2. Configuration and principle

The configuration of the wavelength converter is shown in Fig.1. Input light, with wavelength of λ_i, passes though circulator-1 and is reflected by the Fiber Bragg Grating-1 (FBG-1) whose reflecting center wavelength equals that of the input light. The reflected light passes through FBG-2, whose reflecting wavelength λ_o is longer or shorter than λ_i, and experiences an optical frequency shift in the SSB-modulator (SSB-Mod). The frequency-shifted light is then passes FBG-1, because the reflection bandwidth of the FBG-1 is set to narrower than the frequency shift by the SSB-Modulator.

This means that the optical frequency of the input light is shifted successively as the light circulates the loop till the wavelength of the circulating light in the loop reaches the reflection wavelength of FBG-2. The circulating light, whose wavelength equals that of FBG-2, is reflected by FBG-2 and launched to the output port though circulator-2. Therefore, the required wavelength converted light that lies exactly on the frequency grid is obtained by adjusting the wavelength of FBG-2 to the one of the frequency grid and the modulation frequency of the SSB modulator to the grid spacing. The optical amplifier (EDFA in Fig.1) is inserted to compensate loop loss from passive devices and conversion loss of the SSB-Modulator. This configuration also acts as wavelength variable light source and optical frequency comb generator [4-5] all that is needed is a CW light with standardized optical frequency as the input.

3. Experiment and results

A monolithic waveguide SSB-modulator [2] with the basic structure shown in ref [3] was used in the loop. The driving frequency of the SSB-modulator was 25 GHz. The optical spectra of un-modulated and modulated output light in single transmission are shown in Fig.2 (a). The input light is CW. The SSB-modulator is adjusted to shift the input light to the longer wavelength side. The suppression ratio of the fundamental input mode was larger than 45 dB and the required -1th (neighboring longer wavelength to the input light) to 1th, 2th, and -2th modulation side-band power ratios were larger than 25 dB.

We converted the wavelength of an input signal light modulated with 5 Gbit/s non-return to zero (NRZ), 2^{11}-1 pseudo-random bit sequence (PRBS) format. The wavelength of the input light and center reflection wavelength of FBG-1 was set to the same 1549.8 nm. The reflection bandwidth (FWHM) and reflectivity of FBG-1 and -2 were 11 GHz and 95 %, respectively. The center reflection wavelength of FBG-2 was 1552.8 nm. Figures 2 (b) and (c) show the spectra obtained at the monitor port and output port of circulator-2, respectively. These spectra show that the input light circulated 15 times in the loop, was wavelength-shifted a total of 3 nm (375 GHz in frequency) and launched to the output. The bit error rate performance is shown in Fig. 3. The lines (a) and (b) show BERs for back-to-back and after wavelength conversion. An optical pre-amplifier EDFA followed by an optical band pass filter was used in the receiver. Error free wavelength conversion was confirmed. The power penalty is considered to be attributed to the spectral filtering effect in both FBG-1 and -2, degradation in signal to noise ratio of the circulating light due to ASE from loss compensating EDFA, and interference between required the output mode and the spurious sideband generated from the SSB-modulator. The wavelength conversion of 10 Gbit/s signal with lower power penalty may be available by using properly designed FBGs for 10 Gbit/s signal.
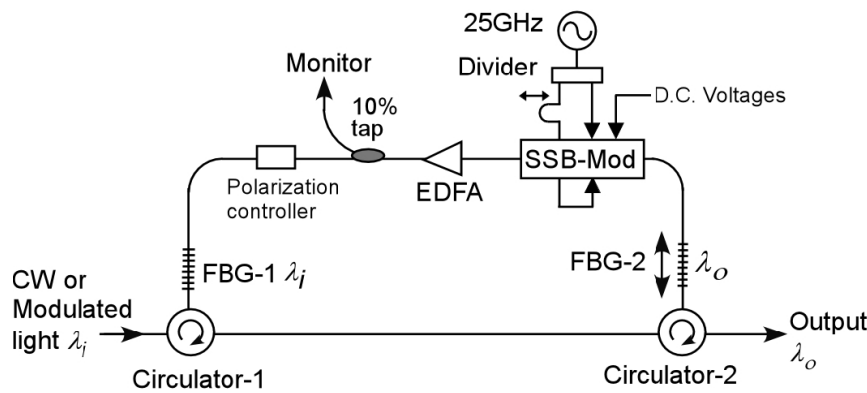

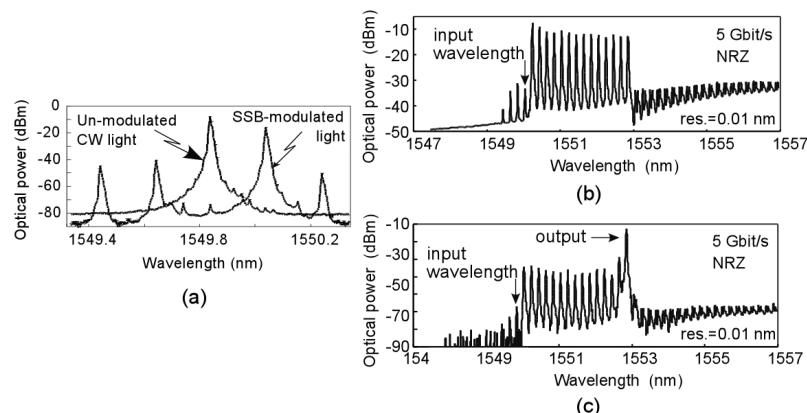Fig. 1. Configuration of wavelength converter and wavelength variable light source

Fig. 2. (a) Frequency shift by single-pass SSB-Modulator, (b) Optical spectrum in loop measured by monitor port, and (c) output spectrum from circulator-2
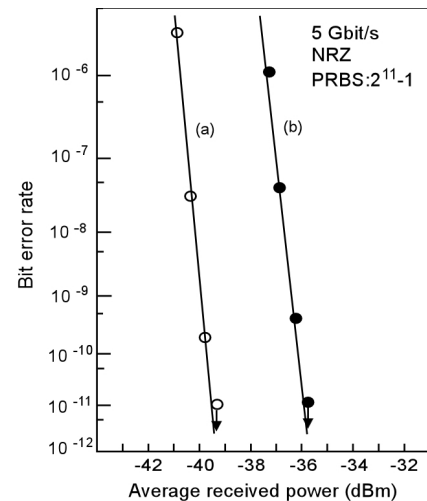

Fig. 3. Bit error rate performance

Wideband optical frequency comb [4-5] was generated by removing output FBG-2 and introducing CW light into the loop. The monitored optical spectra are shown in Fig. 4. Figures (a) and (b) show the spectra for the SSB-modulator adjusted to shift the input light to shorter and longer wavelength sides, respectively. The adjustment is achieved by varying the DC biases of three Mach-Zehnder interferometers forming the SSB-modulator [2]. Fig.4 (c) shows magnified portion of the spectrum around 1546 nm in Fig.4 (a). The degradation in optical SNR is found from Fig.4 (a), (b) to be about 0.18 dB/circuit. The optical frequency comb was successfully generated in the wavelength range from the input wavelength λ_i to λ_i -16 nm (about 80 circuits) and λ_i to λ_i +14 nm (about 70 circuits) with SNR larger than 20 dB.
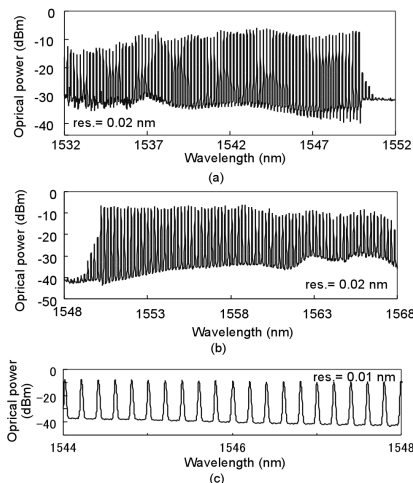
Fig. 4. Spectra in the loop without FBG-2

This indicates that a light with arbitrary wavelengths over a 30 nm (3.75 THz in frequency) range that exactly follow a frequency grid can be achieved with a variable FBG.

4. Conclusion
A novel configuration for a wavelength converter and a variable wavelength light source operating on strict frequency grid was proposed and demonstrated. The 375 GHz frequency shift as a wavelength converter and 3.7 THz-wide variable-wavelength light source are successfully demonstrated.

References
[1] N. Nagatsu et al., IEEE J. of Select. Areas Commun., vol. 14, pp. 893-902, Jun. 1996.
[2] S. Shimotsu et al., in Proc. OFC 2001, Anaheim, U.S.A., Mar. 2001, paper WK3-2.
[3] M. Izutsu, et al., J. of Quantum Electron., vol. 17, pp. 2225-2227, Nov. 1981.
[4] M. Kourogi et al., IEEE Photon. Technol. Lett. Vol. 8, p. 1698, 1996.
[5] H. Sanjoh et al., in Proc. ECOC'02, Copenhagen, Denmark, Sep. 2002, paper 3.3.5.

FP6   **12:00 PM**

Integrated DQPSK Transmitter for Dispersion-Tolerant and Dispersion-Managed DWDM Transmission

R. Griffin, R. Johnstone, R. Walker, S. Wadsworth, A. Carter, M. Wale, *Bookham Technology, Towcester, United Kingdom, Email: robert.griffin@bookham.com.*

We demonstrate GaAs integration of an encoder for optical DQPSK transmission. Experiments demonstrate application to dispersion-tolerant 10 Gb/s transmission over an uncompensated fiber span up to 250 km, and high spectral efficiency 20 Gb/s transport.

1. Introduction
There is currently renewed interest in the development of differential phase-shift key (DPSK) for optical transmission, with increasing evidence that DPSK exhibits superior transmission performance compared to on-off-key (OOK) in DWDM transmission systems [1]. While binary DPSK has been recognized for many years, we have recently demonstrated quadrature signaling - DQPSK [2],[3] - where parallel bit streams are encoded to one of four possible phase states. Compared to conventional OOK, optical DQPSK offers improved tolerance to chromatic dispersion and polarization mode dispersion (PMD), together
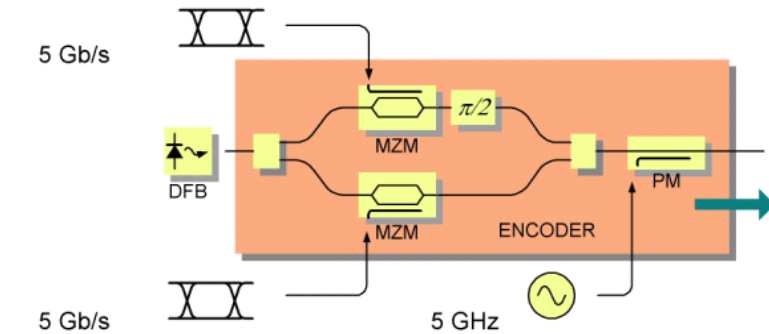
with increased spectral efficiency, while requiring the same OSNR for a given bit rate.

To enable wide application of optical DQPSK, integration of optical functionality is required to provide high performance, compact size and cost-effective manufacturing. Here we describe the realization of a high-functionality GaAs/AlGaAs single-chip DQPSK encoder, which we employ to demonstrate key features of optical DQPSK. We utilize the inherent advantages of DQPSK to address multiple applications: transmission of 10 Gb/s over 250km of SMF without dispersion compensation, and transmission of 20 Gb/s with high spectral efficiency.

2. Single-Chip GaAs/AlGaAs Optical DQPSK Encoder
As outlined in [2], an optical DQPSK link consists of digital precoder, electro-optic encoder, and an optical delay-and-add decoder used with balanced detection. Here we focus on the development of the encoder. While there are alternative encoder realizations which can provide mapping of electrical bits to optical phase states, our simulations suggest that best performance is achieved using Mach-Zehnder modulators (MZMs) arranged within a Mach-Zehnder super-structure, as shown in Fig. 1. Each of the MZMs is biased for minimum dc transmission and driven with a data signal with amplitude $2V_\pi$ at a bit rate $B/2$. An optical phase difference of $\pi/2$ is maintained between upper and lower branches, ensuring quadrature addition of the optical fields on recombination. A phase modulator (PM) is also shown in Fig. 1 after the recombiner, which can be driven with a sinusoidal clock signal to provide chirp on the DQPSK signal. As shown in the results below, additional chirp allows extended reach for uncompensated transmission.

For practical implementation, integration of these multiple functions is essential in order to reduce footprint, reduce assembly, and provide suitable stability. We have successfully integrated a DPQSK encoder like Fig. 1 onto a single chip using a GaAs/AlGaAs integration platform. This improves our previous design by incorporating the additional phase modulator, together with modifications which allow transmission experiments with long pattern lengths. The optical waveguides consist of ribs etched into the surface of a GaAs/AlGaAs slab-waveguide. Optical inputs to the twin, parallel MZMs are from a 1×2 splitter via compact S-bends. Similar S-bends furnished with phase-shift electrodes route the modulator outputs to the 2×2 optical combiner, a device that introduces a nominal $\pi/2$ phase difference between the two optical paths. Identical split and recombine elements are also used within each travelling-wave MZM. The MZMs use a microwave slow-wave technique to achieve the RF/optical velocity-match needed to achieve wide bandwidth with low drive voltage. The phase modulator at the output is a traveling wave structure similar to the Mach-Zehnder electrodes. A low-loss integrated two-photon absorption (TPA) monitor on the GaAs chip after the recombiner provides a photocurrent proportional to $\langle I(t)^2 \rangle$, where $I(t)$ is the instantaneous output intensity. The TPA photocurrent, ~ 1µA, is equivalent to

detection of the output signal with a fast photodiode followed by an RF diode detector. The RF power carried by the optical signal under DQPSK modulation is minimum at optimum bias, and provides a convenient error signal for closed loop control of the phase difference between upper and lower optical paths. The 52mm × 3.5mm GaAs/AlGaAs chip was co-packaged together with a DFB laser to provide a high-performance small-footprint module, shown in Fig. 2. Typical optical output power of 1 mW under DQPSK modulation was realized for several modules.
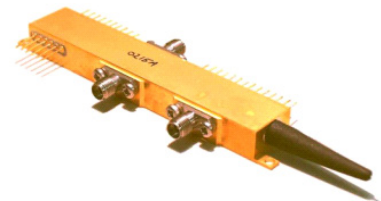

Figure 2: DQPSK transmitter module containing GaAs encoder together with DFB laser source.

3. Experimental Setup
Data from a pattern generator was used to provide inputs I_k and Q_k to the DQPSK encoder. Both data and complementary data outputs of the pattern generator were used, with a relative time delay of 2.2 ns to approximate uncorrelated data. For a net transmission rate of 10 (20) Gb/s, the pattern generator was clocked at 5 (10) GHz. The MZMs exhibited bandwidths ~ 15 GHz, with V_π < 3.5V. Standard 10 Gb/s drivers were used to amplify the signals to 7V peak-peak, corresponding to $2V_\pi$ for the MZMs. RF phase shifters were used to synchronize I_k and Q_k data terms. Each MZM was biased for minimum optical output in the absence of an RF signal.

A simplified decoder consisting of a single Mach-Zehnder interferometer (MZI) with balanced detection was used, and either output u_k or v_k could be measured by appropriate adjustment of the decoder phase. The MZI was a fiber interferometer with a commercial fibered receiver with 15 GHz bandwidth. For 10 (20) Gb/s operation, the nominal MZI delay was 200 (100) ps. For decoder stabilization, a control loop was implemented using a second pilot tone together with an RF diode detector after the balanced receiver. No precoder circuit was employed for measurement, and hence there was a deterministic mapping of data from input to output. To allow BER measurements, the error detector was programmed with the expected data sequence incorporating the DQPSK mapping. For transmission of real traffic, a precoding function is required as given in [2].

4. Dispersion-Tolerant Transmission
For ring architectures in metropolitan networks, dispersion-tolerant transmission is an attractive feature, since dispersion compensation adds considerable cost and complexity. DQPSK provides inherent dispersion tolerance since data is transmitted at a symbol rate half that of the channel bit rate. For transmission at 10 Gb/s over standard

Figure 1: Schematic illustration of optical DQPSK encoder, showing configuration for 10Gb/s transmission.

singlemode fiber with dispersion ~ 17 ps/nm.km, DQPSK can provide reach up to 150 km, providing significant improvement over conventional on-off-key. Further improvement is realized, however, by additional chirp generated by a phase modulator at the encoder output. With a small sinusoidal modulation of ~ 0.2 rad amplitude, correctly phased with the data, substantially greater reach can be achieved. Whereas this synchronous phase modulation can improve dispersion tolerance, even small values of chirp within the individual MZMs of the encoder are detrimental to transmission.

Transmission was performed over SMF28 fiber with dispersion 15.8 ps/nm.km at 1535 nm. Measurements were performed for 10 Gb/s transmission using 2^{21}-length modified PRBS patterns. Excellent back-to-back sensitivity of DQPSK was achieved, demonstrating the high waveform quality achieved from the transmitter. By driving the phase modulator at the clock frequency and optimizing amplitude and relative phase, low dispersion penalty was recorded for spans up to 250 km, as shown in the results in Fig. 3a and 3b.
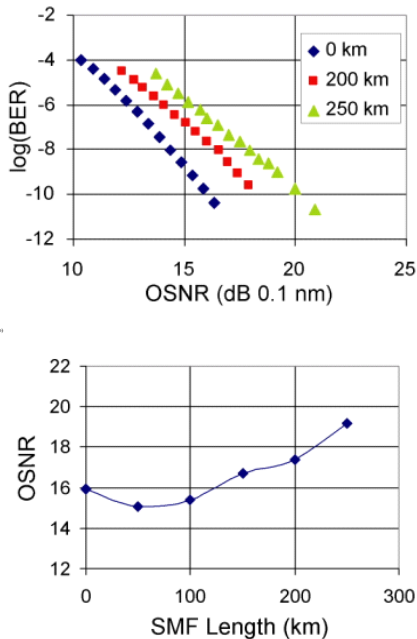

Figure 3: (a) measured BER as a function of OSNR; (b) required OSNR to achieve a BER of 10^{-9}.

Dispersion-Managed Transmission
To make most efficient use of fiber infrastructure for long-haul transmission, it is desirable to maximize the spectral efficiency of optical transport. For point-to-point systems where dispersion management is employed, 20 Gb/s DQPSK offers an attractive option. At this data rate, DQPSK effectively provides parallel transmission of two OC-192 data streams on a single optical channel, providing increased capacity while maintaining a standard interface. Since transmitting 2 bits per symbol inherently halves the optical spectral width compared to binary signalling, DQPSK offers increased channel packing, potentially allowing 20 Gb/s transmission with 25 GHz channel spacing without the need for polarization interleaving/multiplexing to reduce cross-channel interaction.

To illustrate the potential spectral efficiency of DQPSK, we have demonstrated tolerance to tight optical filtering, which is a requisite for close channel spacing. A 20 Gb/s DQPSK signal was generated with the same encoder setup as above, but with the pattern generator clocked at 10 GHz. Here additional phase modulation was not applied. For decoding, an optical add-and-delay filter with 100ps delay was employed. To perform optical filtering, a 50 GHz de-interleaver operating in loop-back was used together with an optical

circulator, providing an optical filter with FWHM 11 GHz. The 20 Gb/s DQPSK optical spectrum before and after optical filtering is shown in Fig. 4(a). The spectral width after filtering was 6.9 GHz, measured with 2 GHz resolution bandwidth. The narrow width of the DQPSK spectrum provides excellent tolerance to optical filtering, as demonstrated by the eye diagrams at the receiver shown in Fig 4(b) and Fig 4(c). Required OSNR to achieve a BER of 10^{-9} before and after filtering was measured to be 19.3 dB and 21.6 dB respectively. We expect that optimization of the optical filter will allow DWDM transmission with a spectral efficiency of 0.8 b/s/Hz.
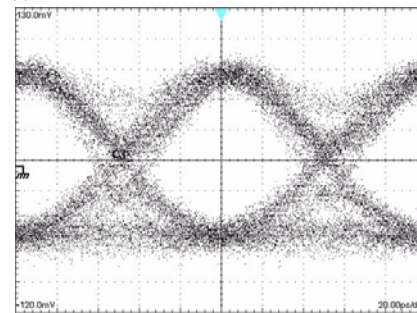
(a)
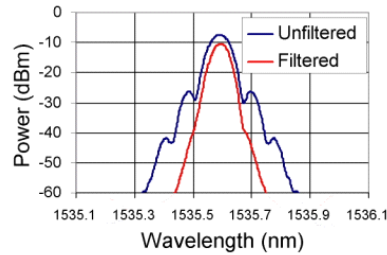
(b)
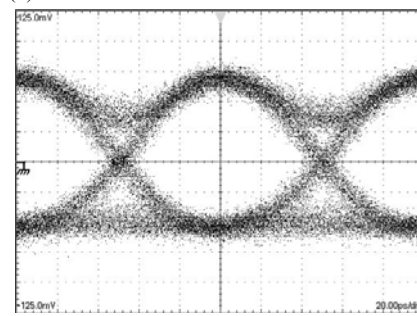
(c)

Figure 4: (a) Measured 20 Gb/s DQPSK optical spectrum; (b) 20 Gb/s received eye without optical filtering; (c) 20 Gb/s received eye after optical filter with 11 GHz FWHM.

5. Summary
A multi-function single-chip DQPSK encoder fabricated in GaAs/AlGaAs has been co-packaged together with a DFB laser to realize an integrated DWDM DQPSK transmitter module. Experiments using the module have demonstrated key advantages of DQPSK for dispersion-tolerant and dispersion-managed operation. Transmission of 10 Gb/s over 250 km of uncompensated fiber has been demonstrated. For 20 Gb/s operation, optical filtering with 11 GHz FWHM has shown low power penalty, illustrating the potential for high spectral efficiency in long-haul DWDM systems.

6. References
[1] A. H. Gnauck et al, "2.5 Tb/s (64×42.7 Gb/s) transmission Over 40×100 km NZDSF using RZ-DPSK format and all-Raman-amplified spans," *OFC'02*, paper FC 2 (2002).
[2] R. A. Griffin and A. C. Carter, "Optical differential quadrature phase-shift key (oDQPSK) for high capacity optical transmission," *OFC'02*, paper WX 6 (2002).

[3] R. A. Griffin et al, "10 Gb/s Optical Differential Quadrature Phase Shift Key (DQPSK) Transmission using GaAs/AlGaAs Integration" *OFC'02*, paper FD 6 (2002).

FP7   **12:15 PM**

Suppression of Optical Harmonics in Wavelength Conversion Using Optical Single-Sideband Modulator

T. Kawanishi, M. Izutsu, *Communications Research Laboratory, Koganei, Japan, Email: kawanish@crl.go.jp.*

For wavelength conversion using an optical SSB modulator, we proposed a novel technique for suppression of undesired harmonics, which gives the conventional theoretical limit of SNR, by feeding the fundamental and 3rd order harmonic rf-signals.

1. Introduction
In wavelength-domain-multiplexing (WDM) optical networks, wavelength conversion is a key technology for cross-connection at switching nodes [1]. Nonlinear effect between lightwaves whose wavelength are different, such as four-wave-mixing in optical fibers, cross phase modulation in semiconductor optical amplifier, and so on, are often used to obtain wavelength conversion, by which bit-stream data on a WDM channel can be copied to the other channel [2]. Pumping light sources are used in these techniques, so that the switching time from one WDM channel to the other channel is dominated by that of the pumping light source. The wavelength can be tuned by changing temperature or current density in the light source. But, it is difficult to change the wavelength in a few nano second without losing stability of the source. Recently, we reported wavelength conversion by using an optical single-sideband (SSB) modulator consisting of four optical phase modulators [3-6]. The wavelength of the output lightwave depends on rf-signal frequency and dc-bias voltage fed to the modulator, which can be electronically controlled. We demonstrated high-speed wavelength switching using an SSB modulator and a fiber Bragg grating [7]. By sweeping the rf-signal frequency, we get a photonic sweeper whose output wavelength can be swept agilely. This is useful for precise measurement of optical components for WDM systems. However, the output lightwave contains undesired components due to imperfection of the modulator and the electric signal feeding circuits, which decreases signal-to-noise-ratio (SNR) of the output. In addition, optical harmonic generation in phase modulations also causes a drop of the SNR. The effect due to the imperfection can be reduced by improvement of the modulator and circuits. On the other hand, the optical harmonic generation gives the theoretical limit of the SNR in the wavelength conversion using an SSB modulator as reported in previous works [3,4]. In this paper, in order to increase the SNR larger than the conventional theoretical limit, we propose a novel technique to reduce the optical harmonic generation by feeding two rf-signals whose frequencies are fm (fundamental) and 3fm (3rd order).

2. Principle of operation
Fig.2 Principle of operation
The SSB modulator consists of parallel four optical phase modulators as shown in Fig.1. The phases of electric field induced on the phase modulators are 0, 90, 180 and 270 degrees. The SSB modulator has a pair of Mach-Zehnder structures, so that we can apply rf-signals of 0, 90, 180 and 270 degrees by feeding a pair of rf-signals with 90 degrees phase difference at two rf-ports (RF A/RF B) [6]. The rf-signals can be obtained by using rf 90 degrees hybrid coupler. The optical phase differences are also 90 degrees. Amplitudes of electric fields and lightwaves should be balanced. When the intensity of the electric field is so small that we can neglect high-order harmonic generation at the optical phase modulation, the output optical spectrum consists of only one component

the first order lower or upper sideband. Thus, the optical frequency difference between the input and output is equal to the frequency of the rf-signal applied to the electrodes on the phase modulator. The unbalance in amplitude of lightwave or electric signal in the phase modulators causes generation of undesired component. Phase fluctuation in electric signal and lightwave also decrease the SNR. For simplicity, we consider an ideal condition where the amplitudes are perfectly balanced and the phase fluctuations are zero. Even in this case, undesired components are generated by nonlinearity of optical phase modulation, which gives the theoretical SNR limit. In addition to the first order sideband component, high-order harmonic components whose optical frequency is $f0+nfm$ ($f0$: input lightwave frequency, fm: rf-signal frequency, n: order of harmonic), are generated at the phase modulators. Even order components ($f0+2nfm$) are eliminated by interference between the outputs of the phase modulators. On the other hand, half of the even order components come out from the output port of the SSB modulator. The first order lower ($f0-fm$) or upper ($f0+fm$) sideband is the major component, and is the desired component in the output lightwave from the SSB modulator. We can choose one from $f0-fm$ or $f0+fm$ components by adjusting the dc-bias voltage. Here, we consider that the major component is $f0+fm$ component. In this case, $f0-fm$ component is eliminated, but $f0-3fm$ component comes out from the SSB modulator. Components of $f0-3fm$, $f0+5fm$, $f0-7fm$, $f0+9fm$ and higher order are in the output of the SSB modulator. In experimental setups, the harmonic components higher than 5th order are so small that the SNR can be approximately expressed by $J1(A)/J3(A)$, where A is the amplitude of the rf-signal. Jn is the n-th order the first kind Bessel's function. $J1(A)$ shows the amplitude of the desired component. Thus, in conventional configurations [3-6], the highest SNR we can get is $J1(A)/J3(A)$.
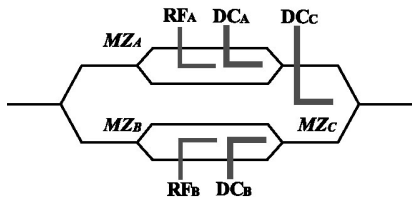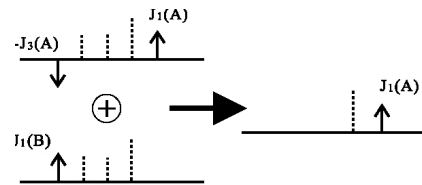

Fig.1. Optical SSB modulator

Fig. 2. Principle of operation

Fig.2 shows the principle of high order harmonic suppression. In addition to the rf-signal (fm rf-signal, henceforth) which generates the major $J1(A)$ and the third order $J3(A)$ optical spectra components, a rf-signal whose frequency is $3fm$ (3fm rf-signal, henceforth) fed to the modulator, in order to compensate $f0-3fm$ component. The amplitude of $f0-3fm$ component due to 3fm rf-signal is $J1(B)$, where B is the electric field intensity of 3fm rf-signal at the phase modulators. Thus, when $J3(A)$ is equal to $J1(B)$ and the phase difference between the components generated by fm and 3fm rf-signals is 180 degrees, the optical $f0-3fm$ component becomes zero. This is the basic principle of proposed method. The dc-bias voltage is adjusted to eliminate the first order lower sideband ($f0-fm$ component generated by fm rf-signal). Thus, $f0-3fm$ component due to 3fm rf-signal is also eliminated and $f0+3fm$ component is generated when 3fm rf-signal is just combined at the input port of the 90 degrees hybrid couplers.

To generate $f0-3fm$ component and eliminate $f0+3fm$ component, the 3fm rf-signal phase of the port RF B should be 270 degrees with respect to that of the port RF A, when the fm rf-signal phase of the port RF B is 90 degrees with respect to that of the port RF A. Such signals can be obtained by using a pair of 90 degrees hybrid couplers and combiners. Here, we propose a simple setup using two input ports of a 90 degrees hybrid coupler, as shown in Fig. 3. A pair of fm and 3fm signals with 90 and 270 degrees phase delays can be taken out from a pair of the output ports of the hybrid coupler. In this setup, the hybrid coupler has three functions: 1) combine the fm rf-signal with the 3fm rf-signal, 2) make 90 degrees phase delay for fm rf-signal and 270 degrees phase delay for 3fm rf-signal, 3) distribute the rf-signals to the two ports. We note that higher order components, for example, $f0+5fm$, and so on become larger due to nonlinearity of the phase modulation, when the $f0-3fm$ component becomes zero. Thus, we should minimize the total power of all undesired harmonics instead of elimination of the $f0-3fm$ component. The ratio of amplitudes of fm and 3fm rf-electric signals (B/A) that gives maximum SNR is shown as a function of A, in Fig. 4. The wavelength conversion efficiency $J1(A)$, which is also shown in Fig.4, has a maximum of -4.70dB when A (normalized to be induced phase at a phase modulator) is 1.81rad. Fig. 5 shows numerically calculated SNR of our proposed technique and that of the conventional setup. SNR is defined as a ratio of the $f0+fm$ component and the sum of the $f0-3fm$ and $f0+5fm$ components. SNR with 3fm rf-signal is 36.3dB when the conversion efficiency is -6.2dB ($A=1.2$), while SNR without 3fm rf-signal is 24.1dB.
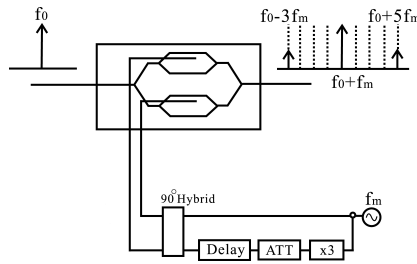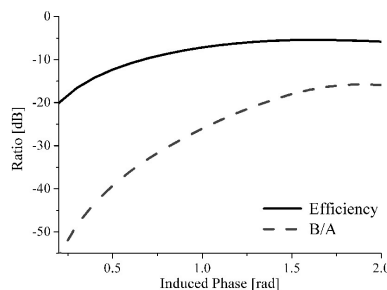

Fig. 3. Experimental setup

Fig. 4. Converision efficiency and ratio of fundamental and 3rd order rf-signals
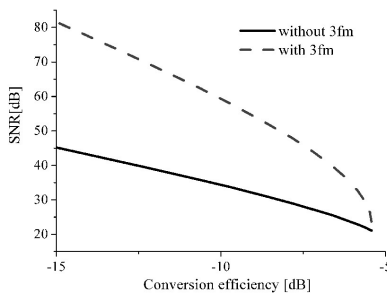

Fig. 5. SNR versus conversion efficiency

3. Experimental results and conclusion

Fig. 6 shows the output spectra of the SSB modulation for three cases: 1) Wavelength conversion using our proposed technique, 2) Wavelength conversion using the conventional technique, 3) Input lightwave (turning of rf-signals and dc-bias adjusted to maximize optical power). The rf-signal frequency fm was 6GHz, and the power at each rf ports (RF A and RF B) was 26.6dBm. The 3fm rf-signal power was 5.9dBm. The conversion efficiency was -5.8dB. The suppression ratio of 3rd order harmonic ($f0+3fm$) was 10.4dB. In conclusion, we proposed a novel technique for suppression of undesired harmonic component in wavelength conversion using an optical SSB modulator. We can reduce 3rd order undesired optical harmonic, and obtain high SNR larger than the conventional theoretical limit, by feeding fundamental and 3rd order harmonic rf-signals simultaneously with 90 and 270 degrees phase delays. By using one rf hybrid coupler, we constructed a simple setup for this technique, and demonstrated suppression of 3rd order optical harmonic component.
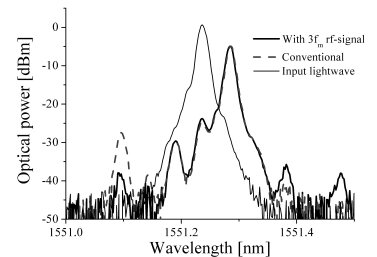
Fig. 6. Output spectra

References
[1] H. Harai, M. Murata, and H. Miyahara, "Heuristic Algorithm of Allocation of Wavelength Convertible Nodes and Routing Coordination in All-Optical Networks," J. Lightwave Technol., Vol. 17, 535-545 (1999).
[2] S. J. B. Yoo, "Wavelength conversion technologies for WDM network applications," J. Lightwave Technol., Vol. 14, 955-966 (1996).
[3] S. Shimotsu, S. Oikawa, T. Saitou, N. Mitsugi, K. Kubodera, T. Kawanishi and M. Izutsu, "Single Side-Band Modulation Performance of a LiNbO3 Integrated Modulator Consisting of Four-Phase Modulator Waveguides," IEEE Photon. Tech. Lett., Vol. 13, 364-366 (2001).
[4] S. Shimotsu, S. Oikawa, T. Saitou, N. Mitsugi, K. Kubodera, T. Kawanishi and M. Izutsu, "LiNbO3 Optical Single-Sideband Modulator," OFC 2000, PD-16.
[5] S. Shimotsu, M. Izutsu, T. Kawanishi, S. Oikawa and M. Sasaki, Wideband "Frequency conversion with LiNbO3 optical single-sideband modulator," OFC 2001, WK3-1.
[6] K. Higuma, S. Oikawa, Y. Hashimoto, H. Nagata and M. Izutsu, "X-cut lithium niobate optical single-sideband modulator," Electro. Lett., Vol. 37, 515-516 (2001).
[7] T. Kawanishi, M. Izutsu, S. Oikawa and K. Higuma, High-speed wavelength switching by using an optical single-sideband modulator, CLEO 2002.

Challenges in Intelligent Transport Network Restoration

J. Yates, G. Li, *AT& T Labs - Research, Florham Park, NJ, Email: jyates@research.att.com.*

Protocols and mechanisms developed for rapid restoration in intelligent transport networks require careful design to ensure cost efficient, secure and rapid failure recovery. This paper highlights many of these challenges and some potential solutions.

1. Introduction

Rapid failure recovery is fundamental to building reliable transport networks. Mesh restoration promises cost effective failure recovery compared with legacy ring networks [1], and is now seeing large-scale deployment [1].
Intelligence for network functions such as automated provisioning, topology and resource discovery and failure recovery is being moved into network elements through the emergence of distributed transport control planes. Proprietary implementations are deployed, while overlapping and competing standards bodies are developing counterparts, by extending virtual circuit management protocols from the packet realm. The Internet Engineering Task Force (IETF) is extending Internet Protocol (IP)-based protocols used in the Multi-Protocol Label Switching (MPLS) control plane to define Generalized Multi-Protocol Label Switching (GMPLS). GMPLS is envisioned as a common control plane managing multiple technologies, including IP / MPLS and a range of transport technologies. The International Telecommunication Union (ITU) is reviewing and extending the IETF protocols to form an ITU transport control plane standard. In addition, the ATM forum and ITU are extending the PNNI protocols designed for controlling ATM networks to provide another transport control plane standard.
Although restoration is a critical component of emerging control plane standards, there are still many challenges yet to be addressed. This paper discusses some of these. We focus on restoration within a common control plane, and on interworking challenges across technologies, and across different control planes.

2. Restoration challenges within a common control plane

Restoration mechanisms efficiently share spare restoration capacity by re-establishing connectivity after failure at each node along the restoration route. The bandwidth along restoration paths can be reserved before failure or may be dynamically identified and allocated after failure [2].
Restoration schemes involve a common set of steps, including restoration path selection, fault detection and notification, and signaling for failure recovery. We discuss each of these and challenges that must be addressed.

Restoration path selection
The major benefit of intelligent transport network restoration comes from the sharing of restoration capacity among multiple connections that fail independently. Effective restoration path calculation will enhance sharing of capacity, thus reducing spare capacity requirements. In restoration schemes that dynamically search for capacity after failure, effective restoration path calculation may also minimize the amount of crankback required when signaling messages encounter links with insufficient spare capacity, thereby speeding restoration. If the restoration paths are pre-
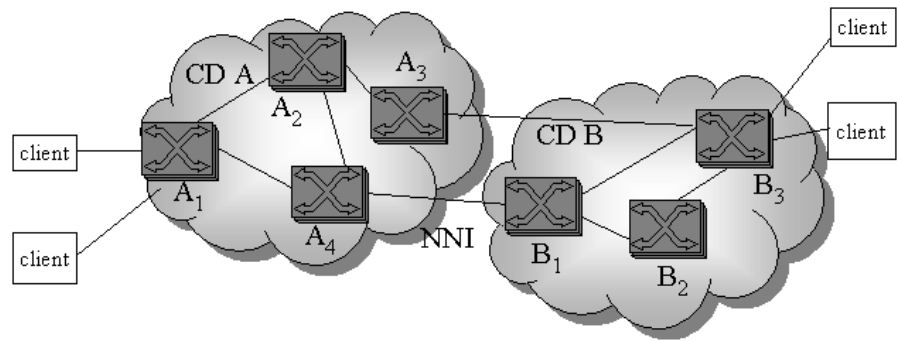

Figure 1. Two control domains.

planned, a single, physically diverse restoration path may be calculated for each connection. Algorithms used for pre-planning restoration routes are relatively easy to design for centralized calculation where a complete view of network resources is available, but designing algorithms that efficiently pre-calculate restoration routes without requiring the advertisement of excessive amounts of information is an important area of research. In addition, pre-calculating restoration paths requires an accurate representation of the Shared Risk Link Groups (SRLGs) used to define links with common risks of failure. Although SRLGs can be identified from manually entered databases, these databases, like any information source managed via manual processes, are often erroneous. Automating the identification of SRLGs is an important outstanding issue in developing a truly automated, reliable network [3].

Fault detection and notification
Once a failure occurs, it must be detected, and nodes responsible for restoration must be notified. SONET and SDH utilize opto-electronic conversion and alarm notifications transmitted within overhead bytes in the SONET/SDH payload to provide fault detection, isolation and notification. However, fault detection is more challenging in all-optical networks – power monitoring can be used to detect loss of light, but failures causing signal quality degradations are more challenging to identify and are a topic of continuing research. In addition, physical layer failure notification is not feasible in all-optical networks, requiring control plane intervention.

Signaling for rapid connection recovery
Upon receipt of a failure notification, the nodes responsible for initiating restoration commence a signaling procedure that is used to recover connectivity. Adapting existing signaling mechanisms and procedures will generally speed standards and implementation development compared with creating completely new signaling protocols, making it attractive to extend existing provisioning signaling mechanisms to restoration. However, restoration signaling has its' own unique requirements and challenges distinct from provisioning. For example, provisioning requests tend to arrive one at a time, whereas a major failure may result in a "message storm" as large numbers of connections simultaneously attempt to restore. This can lead to significant queuing of signaling messages and corresponding processing delays. One solution is to aggregate multiple signaling messages into a single message, although this introduces complexities into the restoration signaling design and implementation. Studies of the benefits achieved using signaling aggregation and its associated complexity are necessary.
Delving further into the signaling scheme, the point at which cross-connection is performed within the signaling procedure also impacts how rapidly failure recovery is achieved. In general, signaling mechanisms include one request message that traverses from source to destination, and then an end-to-end reply message from destination to source. Restoration would be fastest if cross-connection were performed as each node receives the request message. This would be fine

except for the case when contention occurs – when the two cross-connects (XCs) on either side of a link attempt to simultaneously allocate the same channel to two different connections. If this occurs and the cross-connection is made on the request message, then we may temporarily end up with two customers connected who should not have been – sensitive data could potentially be sent to the wrong customer. This scenario is known as misconnection, and is unacceptable for even a short period of time. One solution is to require that at least the first cross-connect along a path not be performed until all contention has been resolved. Using this approach slows restoration, but ensures that misconnection is avoided.
The cross-connect architecture itself can also significantly impact restoration times. For cross-connects with cross-connection times exceeding signaling message processing times, if cross-connection is serial (i.e., a cross-connect can only be started once the previous cross-connect has completed), then the restoration time will be dominated by the time it takes to execute the desired cross-connects in a given XC. For example, if we have a cross-connect time of 5msec, and 200 connections being recovered through an XC, then the time to recover all connections exceeds 1 second if each one is executed in turn. Alternatively, if cross-connections can be executed in parallel, then the restoration time can be dramatically decreased to a little more than the signaling time (in fact, 5msec + signaling time). Thus, for "slow" cross-connects, it is crucial that multiple cross-connects are executed in parallel.
There are numerous other technical challenges beyond what we have been able to discuss here [4]. For example, a reliable control plane software design is crucial to building a reliable transport network, and multi-service priority restoration is required to support multiple service types within a single restoration procedure.

3. Interworking issues

Ideally, a single standard with a limited set of restoration schemes would allow service providers to select equipment from different vendors and have them interoperate. However, the industry has created a plethora of standards, proprietary control plane implementations and restoration mechanisms. This leads to immediate inter-working challenges – the Optical Internetworking Forum (OIF) and ITU are addressing these through the development of a Network-to-Network Interface (NNI) designed to provide distributed inter-working across different control domains all managed by a single service provider. A *control domain* (*CD*) is a sub-network in which all nodes run a common control plane. Figure 1 illustrates two control domains, interconnected by a two pairs of XCs.
The NNI is addressing interworking by aiming for a single standard that will allow provisioning across multiple control domains. Restoration can be achieved within each control domain without requiring complicated interworking. However, this leaves nodes interconnecting control domains (known as border nodes) as single points of failure along each connection. Thus, it is desirable that control domains have dual interconnection (e.g., two links between CD A and CD B in Fig-

ure 1) and that there be restoration mechanisms to recover connections passing through a failed border node. Such restoration mechanisms are yet to be addressed, but must be designed to operate across a range of control domain control planes and transport technologies.

Transport layer connection restoration provides reliable links to higher layer services. However, failures involving higher layer devices, such as port failures and node failures, cannot be recovered using transport network restoration. Large IP networks today utilize IP layer protocols to re-route traffic around failed routers, interfaces and links. Transport layer failure recovery is often used, but is not necessary if IP layer mechanisms exist. Due to the unreliable nature of IP routers today, ISPs often use a dual router architecture, in which each central office (CO) contains two routers designed so that if one fails, traffic is automatically re-routed via the other. Studies have shown that utilizing transport layer failure recovery is significantly more expensive with a dual router architecture than using unprotected transport connections and allowing IP to re-route traffic upon failure [5]. This is due to the fact that little additional capacity is required to handle SRLG failures beyond that required to handle router failures. If routers were more reliable – eliminating the need for two routers at each CO - then optical layer restoration can be more cost effective than IP layer recovery. An integrated approach may provide the most cost effective solution [5]. For IP, at least, building a reliable router is an important requirement for transport layer restoration to become imperative. Thus routers need first to develop mechanisms for hitless software upgrades, non-stop routing, 1:N interface protection and so on.

4. Conclusions
Fast mesh restoration is critical in designing an intelligent transport network. However, there are numerous research, implementation and political challenges that remain to be addressed in developing cost-effective, secure and rapid mesh restoration.

5. References
[1] B. Cortez, "The Emerging Intelligent Optical Network: Now a Reality," *OFC* 2002.
[2] E. Mannie, editor, "Generalized Multi-Protocol Label Switching (GMPLS) Architecture," Internet Draft, 2002.
[3] P. Sebos *et al.,* "Effectiveness of Shared Risk Link Group Auto-Discovery in Optical Networks," *OFC* 2002.
[4] R. Doverspike and J. Yates, "Challenges for MPLS in Optical Network Restoration," *IEEE Commun. Mag.*, Feb. 2001.
[5] S. Phillips *et al.*, "Network Studies in IP/Optical Restoration," *OFC* 2002.

FQ2   **11:00 AM**

Local Optimization of Shared Backup Channels in Optical Mesh Networks

E. Bouillet, J. Labourdette, G. Ellinas, S. Chaudhuri, *Tellium, Oceanport, NJ, Email: ebouillet@tellium.com.*

This paper illustrates the complexity of assigning backup-channels in shared-mesh-protected optical networks. We propose a distributed recurring method to solve this problem, and show that substantial savings are achievable.

1. Introduction
Wavelength Division Multiplexed (WDM) networks that route optical connections using intelligent optical cross-connects (OXCs) is firmly established as the core constituent of next generation networks. With connection rates reaching tens of Gigabits/s, preventing and repairing failures is increasingly becoming an integral part of the network design process. In this work we consider two categories of end-to-end path restoration as supported in Tellium Aurora Optical Switch™ (see also [3,4]). Other categories include line protection and re-provisioning[7], these are not considered here. In end-to-end dedicated (1+1) mesh protection (Figure 1.), the ingress and egress OXCs of the failed connection attempt to restore the signal on a predefined backup path that is disjoint, or diverse, from the primary path. Path diversity guarantees that primary and backup paths will not simultaneously succumb to the same failure. This approach requires large amount of capacity, that is more than the working capacity since backup paths are longer than working paths. However the backup path remains "live" in permanence, thus saving crucial path-setup latency when recovery takes place. In shared mesh restoration (Figure 2.), backup paths can share capacity if the corresponding primary paths are mutually diverse. Compared to dedicated (1+1) mesh protection, this scheme allows considerable saving in terms of capacity required[3]. In addition, the backup resources can be utilized for lower priority pre-emptible traffic in normal network operating mode. However recovery is slower than dedicated (1+1) mesh protections, essentially because it involves signaling and path-setup procedures to establish the backup path.

They are two different policies to assign the protection channels: (1) pre-assign the protection channels to each backup-path before failure occurrence, or (2) rely on the protection mechanism to select the channels from a pool of reserved channels after failure occurrence[6]. Although more cost-efficient, approach (2) requires time-consuming inter-node communication to agree on the channel assignment, and to it we prefer approach (1), which can achieve sub-200ms restoration times in large networks[2]. However the gain in restoration time is paid for with additional complexity to fill up the backup-to-channel lookup tables at each node during provisioning (when speed is less of an issue.) We show in this paper that this operation is tantamount to a graph-coloring problem. In particular we show how a first fit based assignment can be easily improved using a graph-coloring algorithm. We finally discuss an application of this algorithm to migrate service protections from 1+1 mesh protection to shared mesh protection.

2. Shared Mesh Protection Provisioning using Vertex Coloring
We use the term Shared Risk Optical Group (SROG) to indicate a group of optical equipment that share a common risk of failure. Two mesh restored protection paths are "compatible" and may share a protection channel if their respective primary paths are SROG disjoint. Although only single SROG failures are considered here, the description of the algorithm can easily be transposed to protect against node failure as well: replace SROG by node where it applies. Otherwise they are said to be "conflicting". Given a group of protection paths traversing a common link, the problem is to assign the minimum number of protection channels to the paths in the link in accordance to the rules of sharing. Typical online provisioning algorithm assigns protection channels on a first-come first-serve basis and reserve new channels when sharing is not possible with present protection channels. In this approach the number of protection channels depends ultimately on the order of arrival of the protection
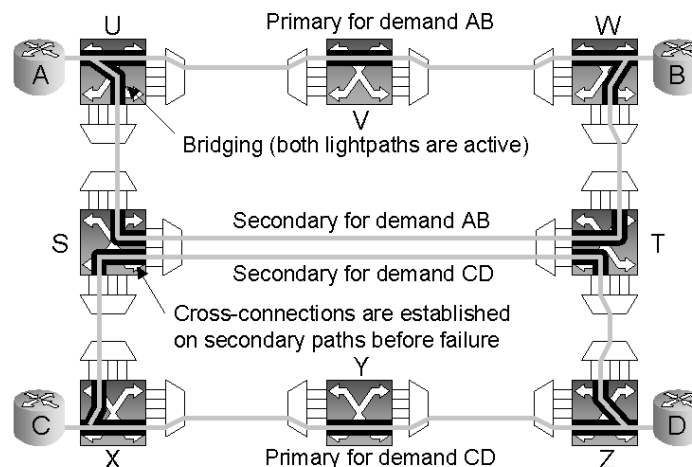

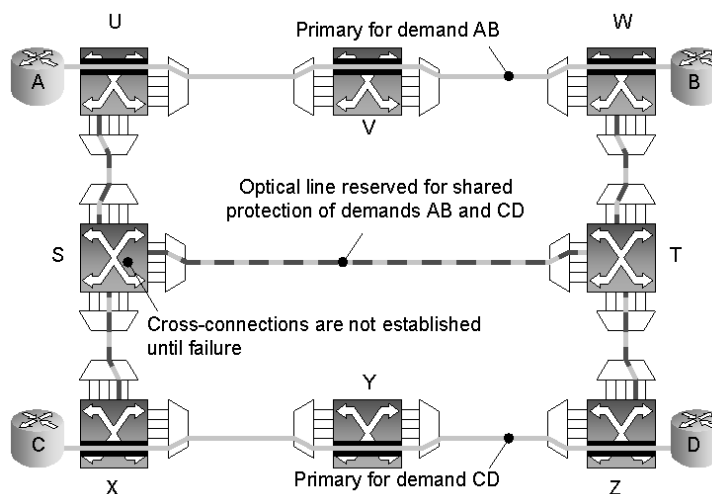Figure 1. Dedicated (1+1) Mesh Protection
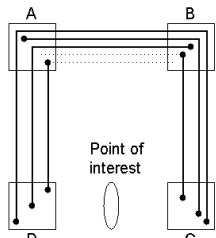

Figure 2. Shared Mesh Protection

Fig (3a) Network consists of 4 nodes, 4 links and 5 lightpaths.

Order	Demand
1	AD
2	CD
3	BC
4	AC
5	BD

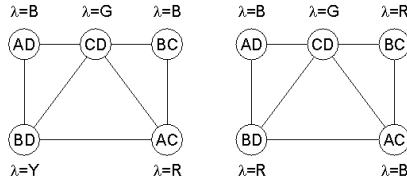Table (3b) Order in which lightpaths are routed

Fig (3c) Online coloring for link D-C requires 4 colors (B,G,R,Y)

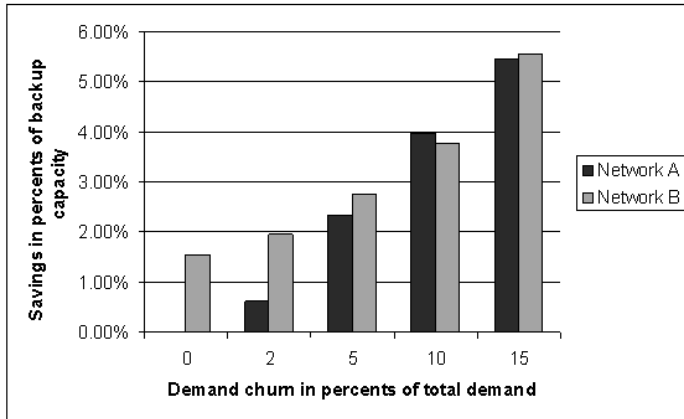Fig (3d) Optimized coloring for link D-C requires 3 colors (B,G,R)

Figure 4.

paths. Since the order cannot be determined in advance, an optimization algorithm must be invoked at regular intervals to reassign the channels. In this write-up we show that finding the optimum channel assignment is equivalent to solving a vertex-coloring problem.

The allocation of protection channels is tantamount to a vertex-coloring problem: given the set of all restoration paths that intersect on a given link, represent every path as a vertex, and connect with an edge every pair of vertices whose corresponding paths are conflicting. Assign a distinctive color to each protection channel, and allot a protection channel to each path, that is color the vertices. Clearly, two vertices cannot be allotted the same color if they are connected by an edge, since the corresponding restoration paths are conflicting and cannot share a channel. The objective is to minimize the number of protection channels (respectively number of colors) required to accommodate all backup paths (respectively color all vertices), while avoiding conflicts.

This problem is known to be NP-hard, however there are many heuristics that can be used to compute sub-optimal solutions. A vertex-coloring algorithm that offers a good tradeoff between quality and runtime complexity is DSATUR[1].

Example
Consider the example of Figure 3 above (3a through 3d.) The figure illustrates five lightpaths {AD,CD,BC,AC,BD} and their protections, routed in a 4-node ring network. All the protections traverse link e_{CD}. The demands are provisioned following the sequence indicated in Table 3b. If we use a typical online shared mesh protection provisioning, and apply the graph representation presented earlier to e_{CD}, we obtain the "coloring" shown in Figure 3c. Even though a single failure in this example affects at most three primaries, this coloring consumes 4 colors, indicating that 4 protection channels are required. An optimized coloring yields the solution shown in Figure 3d, which consumes only 3 colors. Comparing 1c and 1d, we observe that a new channel (R) should have been allotted to the protection path of demand (BC) instead of sharing channel (B) with the protection of demand (AD). This solution however is not considered because not optimal when the third demand is being provisioned (that is {AD,CD,AC} are routed and {BD}

has not yet arrived) since at that time it would consumes 3 channels instead of 2.

3. Implementation and Applications
The optimized channel reassignment is a low priority procedure. It can be a program thread running in background, or at regular intervals. The information necessary to accomplish this task is available locally in every OXC and independent of non-adjacent OXCs. Thus each OXC can run a copy of the algorithm in a distributed manner, locally and independently of other OXCs. A change in the allocation of a protection channel needs only to be propagated to its end-points. Since protection channels are "booked" and actually not cross-connected until a restoration occurs, the task amounts to no more than modifying and exchanging sharing databases between pairs of nodes. For every OXC-pair connected by at least one optical line, the OXC with highest IP address is delegated to perform the task.

A byproduct of the optimized channel reassignment is that it can be used to migrate the protection paths of mesh dedicated protections to shared mesh protections if desired. By changing their protection type to shared mesh protections, we allow the thread to apply the channel reassignment optimization to these services. The algorithm does not optimize the routes of the backup paths however, and the resulting solution is thus not as efficient as a re-optimization algorithm that re-routes the backup paths to maximize sharing[5].

4. Experiments
For our experiments we compare the benefits of local protection channel optimization on two realistic core mesh networks. Network A consists of shared-mesh capable optical switches in 46 cities interconnected by 75 fiber-trunks and loaded with 570 lightpaths. Network B consists of 61 switches, 88 fiber-trunks, and 419 lightpaths. For each network, we provision all the demands in sequence, using various values of demand churns (expressed in percent of the total demand), and perform a local channel optimization after all the demands are routed. We measure the amount of protection channel required before and after optimization and report the saving in % of total backup capacity in Figure 4. Our measurements indicate that as the demand churn increases, the

number of protection channels that can be freed becomes substantial.

5. Conclusion
This document proposes a distributed method that rearranges the allocation of shared channels reserved for restoration, with objective to minimize the number of allotted channels. This algorithm can be implemented as an independent background process to supplement existing provisioning algorithms. It is effective to correct suboptimality inherent to a first fit based provisioning, or seize on improvement opportunities that are brought forth by demand churn.

6. References
[1] Daniel Brélaz, "New Methods to Color the Vertices of a Graph," Communications of the ACM, Vol 22, Num 4. April 1979.
[2] A. Akyamac, S. Biswas, J.F. Labourdette, S. Chaudhuri, K. Bala, "Ring Speed Restoration and Optical Core Mesh Networks," NOC'02, Darmstadt Germany, Jun. 2002.
[3] J.F Labourdette, E. Bouillet, R. Ramamurthy, G. Ellinas, S. Chaudhuri, K. Bala, "Routing Strategies for Capacity Efficient and Fast Restorable Mesh Optical Networks," Photonic Network Communications, pp. 219-235, July-Dec 2002.
[4] G. Ellinas, et al., "Routing and Restoration Architectures in Mesh Optical Networks," Optical Networks Magazine, Jan-Feb 2003.
[5] E. Bouillet, P. Mishra, J.F. Labourdette, K. Perlove, S. French, "Lightpath Re-optimization in Mesh Optical Networks," NOC'02, Darsmstadt Germany, Jun. 2002.
[6] S. Datta, et al, "Efficient Channel Reservation for Backup Paths in Optical Mesh Networks," IEEE GLOBECOM 2001, San Antonio, TX, Nov. 2001.
[7] J. Doucette, W.D. Grover, "Comparison of Mesh Protection and Restoration Schemes, and the Dependency on Graph Connectivity," 3rd International Workshop on the Design of Reliable Communication Networks, Budapest, Hungary, Oct. 2001.

FQ3   **11:15 AM**

Capacity Requirements for Network Recovery from Node Failure with Dynamic Path Restoration

G. Shen, W. Grover, *TRLabs and Department of Electrical and Computer Engineering, University of Alberta, Edmonton, AB, Canada, Email: gshen@trlabs.ca.*

Node failure is not as frequent as span failure but recent events have emphasized its importance in network planning. We study the effects on capacity design if full or partial recovery from node failures is provided using failure-specific path restoration.

1. Introduction
Most studies of restorable networking consider span failures as the primary class of failure scenario. It is, however, often noted that because of its end-to-end orientation, a path restoration mechanism has an inherent ability also to respond to node failures. The spare capacity that ensures 100% span restorability is not necessarily adequate to ensure any particular target level of recovery from a node failure, however. Pre-planned shared backup path protection (SBPP) [1] does inherently protect transiting flows against node loss if primary and backup paths are all node disjoint. But SBPP also generally requires more spare capacity than dynamic path restoration and, due to its fixed pre-planned nature, has an inherently lower availability against to dual failure scenarios. It is of interest, therefore, to consider how much extra spare capacity an adaptive path restorable network needs to support node recovery, beyond that needed for span restorability. Other studies [2, 3, 4] have considered node recovery issues but to our knowledge the specific questions we ask, and the particular mechanism [6] and capacity design model [5] we consider are novel
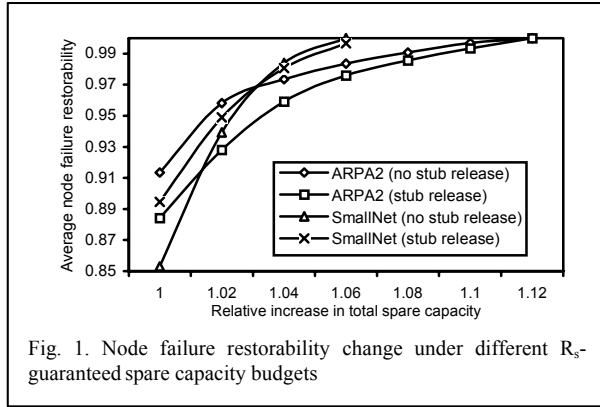
Fig. 1. Node failure restorability change under different R_s-guaranteed spare capacity budgets
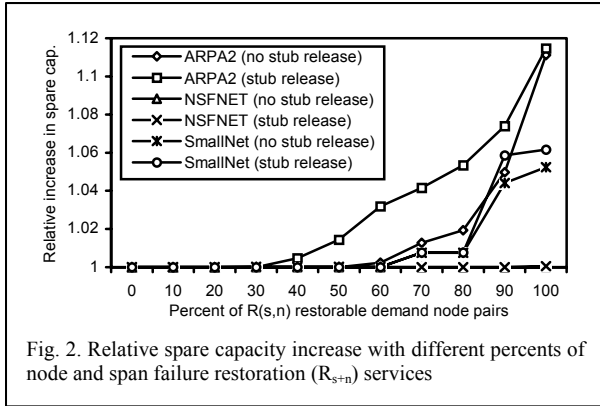

Fig. 2. Relative spare capacity increase with different percents of node and span failure restoration (R_{s+n}) services

and useful. Note that in studies on "node restoration," it is actually recovery of the transiting paths through a failed node that is intended. Service paths originating or terminating at the failed nodes cannot be restored by these methods. From one standpoint a node failure is like several concurrent span failures, suggesting large amounts of extra spare capacity would be needed. On the other hand, source/sink demands at the failed node are omitted from the recovery goal. So it is unclear in advance how much extra spare capacity is needed. With this in mind, the study poses three questions:

• *Under suitable optimization, what are the maximum levels of node recovery that can be achieved with no more total spare capacity than required to ensure 100% span restoration?*
• *How much additional spare capacity is required to guarantee both 100% node and span restoration compared to span restorability only?*
• *How does capacity depend on the mix of services in a multiple Quality of Protection (multi-QoP) context (considering mixes of service with no protection, span failure protection, and both node and span protection)?*

2. Methods and Results
To address these questions, we extend the prior model for dynamic adaptive path-restorable capacity design [5] and assume that there is at least enough wavelength conversion at each OXC node to make wavelength blocking insignificant. Three new design models were developed.

A) Design for 100% span and node failure restoration

This design model finds the minimal amount (and distribution) of spare capacity that guarantees 100% span restorability and 100% recovery of transiting demands at failed nodes. It is based on the conventional capacity design model for path restoration [5] with the addition of restorability and spare capacity constraints for each node failure scenario. This is the most straightforward (and potentially expensive) design approach.

B) Design to support Multi-QoP
This is an extension of the first model to consider three QoP levels. These are: (1) R_0 restorability: this is a wholly best-efforts class with no assured restorability, (2) R_s : this class is assured of restorability against any span failure, but receives only best efforts recovery for node failure. (3) R_{s+n} : A lightpath in this class enjoys assured restorability against any span or node failure (other than its own end-nodes). The design model places spare capacity so that all the affected traffic demands that require R_s or R_{s+n} restorability can be fully restored upon a span failure, and all the affected traffic demands that require R_{s+n} restorability can be fully restored upon a node failure. R_0 working capacity is effectively ignored in the spare capacity design problem, but would receive best-efforts restorability in real time within the spare capacity remaining after re-routing for R_s or R_{s+n} service classes.

C) Maximal node recovery under a spare capacity budget
This design model allows us to set a budget on total spare capacity (above that where 100% span restoration is feasible) and optimize the distribu-

tion of spare capacity for the highest achievable node failure recovery level as well. In Models A and B the objective function is minimum cost or capacity, but here it is to minimize the total *unrestored transiting demand over all node failures*. By varying the budget amount this model can be used to systematically study the trade-off between cost and node recovery level.
Each of these design models is also implemented with and without "stub release" (the conversion of surviving channels on failed paths into available spare capacity as per [5,6]). In the context of node recovery, stub release means that the surviving lightwave channels of paths transiting the failed node (which *will* be restored) and of paths sourced at the failed node (which will *not* be restored) are both available as spare capacity for the restoration effort. This is a failure-specific restoration response to exploit available capacity, in contrast to the fixed response of SBPP-planned paths to a failure anywhere along its route. The failure-specific re-routing may be either found adaptively in real time [6], or also pre-planned and stored in the OXC nodes.
We evaluate the performance of the design models on five well-known topologies: ARPA2 (21-nodes 25-spans), NSFNET (14,21), SmallNet (10,22) from [5], Cost 239 (11,26), and the (55, 63) topology from www.level3.com. Lightpath demands were generated following a uniform random distribution on the range [1…20] for each node-pair. For the larger Level3 test case only the largest 30% of demand pair volumes are employed for computational reasons. Note that this demand model makes demands between distant nodes as intense as between neighbors, creating relatively large numbers of transiting paths at nodes. This is the more challenging case for node recovery compared to demand models with a gravity-like localization effect. A single shortest route is used for each working demand but the design models consider all possible distinct routes between each node pair for each failure scenario for spare capacity placement. The design problems were all solved within half an hour with AMPL/CPLEX 7.1, except Level3, which took several hours.
Table 1 summarizes the results. The first (double) row is obtained using Model C to maximize node recovery given a budget equal to that of a span-restorable design only. This represents the intrinsic potential for node restorability with no more capacity than needed for conventional span failure restoration. Note how high this "free" node recovery capability can be - almost 100% in many cases and always at least 78%. The recovery levels are lower *with* stub release (at first somewhat counter-intuitively) because the basic networks to handle span failures only also have significantly less spare capacity when using stub release. The second and third rows show the relative amounts of extra spare capacity and total cost increase for the network to wholly support R_{s+n} services, as compared with the network supporting R_s services only. The values are surprisingly marginal. Consistent with the very high intrinsic R_n, NSFNET and Level3 require almost no added capacity to support 100% node recovery. And in no case was more than 10% extra spare capacity needed to ensure 100% node recovery. These findings suggest that the "abandonment" of source/sink paths at the failed node in measuring node recovery levels is a more dominant effect than the fact that node failure is like multiple span failures, especially on sparse topologies.
Fig. 1 shows the results of using Model C to study node recovery levels with various total spare capacity budgets. Starting from the point of the spare capacity designed just for 100% span restoration, a very small budget increase gives a great improvement of node failure restorability. For example, there is 9% restorability improvement when there is 2% spare capacity increase for the ARPA2 network without stub release. However, the improvement rate tends to slow down after that. For SmallNet without stub release, a budget increase from 4% to 12% can only bring about 3% restorability improvement. The explanation seems to be related to the approach to 100% R_n itself. Under a small budget, there is a large num-

Table 1. Node failure restorability, redundancy increase, and total cost increase for various network design cases

Networks		ARPA2	NSFNET	SmallNet	Cost239	Level3
Intrinsic node failure restorability	No stub release	91.35%	99.84%	85.30%	78.89%	95.59%
	Stub release	88.43%	99.60%	89.40%	82.85%	99.998%
Redu. increase (R_{s+n} vs. R_s)	No stub release	10.0%	0.02%	2.6%	3.4%	4.1%
	Stub release	9.7%	0.03%	2.8%	1.4%	0.1%
Total cost inc. (R_{s+n} vs. R_s)	No stub release	5.2%	0.01%	1.7%	2.4%	2.0%
	Stub release	5.3%	0.02%	1.9%	1.0%	0.001%

ber of un-restorable lightpaths, hence many chances to make improvements. At higher budgets there are fewer unrestored lightpaths remaining to be made restorable in any "easy" way. Finally Fig. 2 shows the results on the relative spare capacities required to support multi-QoP services. For simplicity of presenting results we assume a mix of only R_s and R_{s+n} services (no R_0). We find that the spare capacity designed for R_s restorability alone can serve up to 30% (for ARPA2 with stub release), 50% (for ARPA2 without stub release), 60% (for SmallNet), and almost 100% (for NSFNET) R_{s+n} services in the networks as well. This implies that without any additional spare capacity over the conventional designs, a network can still serve a large number of higher –level QoP services.

3. Concluding Remarks

This work shows that, overall, it is surprisingly easy to support node recovery in path-restorable networks. Very high levels of premium service class guarantees (services assured of both span and node recovery) can apparently be supported with no more spare capacity than needed to give all services span restorability alone. Conversely if 100% node recovery is desired by design it took at most 10% extra capacity to provide this. This knowledge and related design methods are useful in themselves and to further inform the comparison of failure-specific path restoration to the SBPP pre-planning scheme.

4. References

[1] W.D. Grover, J. Doucette, "Design of a meta-mesh of chain sub-networks: ... ," *JSAC* 20, 47-61 (2002).
[2] A. Chiu, J. Strand, "Joint IP/optical layer restoration after a router failure," *OFC 2001*, pp. MN5/1 -MN5/2.
[3] D. Stamatelakis, W.D. Grover, "IP layer restoration and network planning based on virtual protection cycles," *JSAC* 18, 1938–1949 (2000).
[4] Y. Liu, D. Tipper, "Successive survivable routing for node failures," *Globecom 2001*, pp. 2093-2097.
[5] R.R. Iraschko, M. MacGregor, W.D. Grover, "Optimal capacity placement for path restoration in STM or ATM mesh survivable networks," *IEEE Tran. Net.* 6, (1998), 325-336.
[6] R.R. Iraschko, W.D. Grover, "A highly efficient path-restoration protocol ...,"*JSAC*, vol.18, no.5, May 2000, pp. 779- 793.

FQ4   **11:30 AM**

FASTeR: Shared Restoration Without Signaling

V. Poosala, C. Phadke, *Bell Labs, Lucent Technologies, Murray Hill, NJ;* A. Shandilya, *Univ. of Rochester, Rochester, NY, Email: poosala@research.bell-labs.com.*

We present a novel technique for rapid restoration in optical/electrical mesh networks that does not incur signaling or cross-connect setup latencies. We show that it easily meets the 50ms requirement in most scenarios.

Introduction

The last few years have witnessed the introduction of optical and electrical mesh networks as an alternative to SONET ring networks. One of the key benefits of mesh networks is the improved bandwidth utilization coming from shared restoration. Unlike the traditional 1+1 protection schemes which reserve 50% of the bandwidth for protection, shared restoration allows multiple demands to share backup links and hence reserves less capacity. However, the speed of restoration is an issue with this scheme. Many classes of traffic, especially voice traffic, require paths to be restored very fast, often within 50ms [2]. It is easy to meet this requirement with 1+1 protection - data is always sent on the primary and backup paths and the end node picks the best signal. This is not the case with shared restoration where the backup paths are only set up after the failure. Typ-
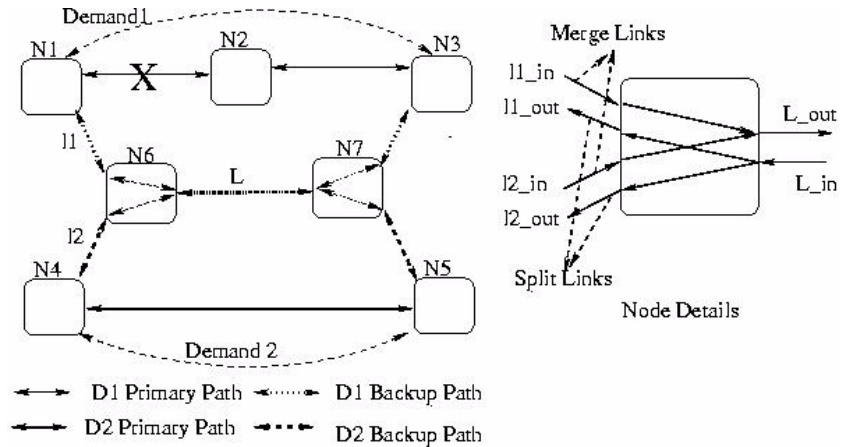

Figure 1: Split Merge Node Configuration.

ically, this process involves signaling to setup cross-connects(XCs) which can be time-consuming in large networks using slower XC technologies.

Motivated by these issues, we have developed a rapid restoration mechanism that works for both optical and electrical mesh networks, with a primary goal of eliminating the signaling and XC latencies.

Related Work: Much of the earlier work on shared restoration has focused on routing and design algorithms and our technique is complementary to those results. A mechanism called ROLEX for fast restoration was proposed in [1] and its implementation in GMPLS/RSVP was given in [3]. However, ROLEX also incurs cross-connect and signaling latencies, which are the primary bottlenecks addressed in our solution.

Solution

We consider a mesh network consisting of cross-connect nodes (XCs) connected by DWDM systems. Each wavelength between two adjacent nodes is considered to be a link. The edge nodes are assumed to have OEO capability. Traffic consists of unit-wavelength demands between the edge-nodes, protected through shared restoration. Each demand is associated with a *primary path* and a precomputed *backup path* for the entire path or per link. For clarity, we assume bi-directional traffic using the same path in both directions and bi-directional failures for our discussion and present the modifications for uni-directional cases where necessary.

The basic idea behind our solution, called FASTeR (FAst Signal-free Traffic Restoration), is as follows. Even before any failure occurs, all the backup paths are set up using certain special features of the XCs, in contrast with the traditional approach where the backup paths are only pre-computed but not actually setup until failure occurs. On failure, the end-nodes of the failed demand immediately start sending data on the backup path, without any prior signaling. The details are described next.

We present our solution to cover a wide-range of generic hardware with the following characteristics, rather than assuming specific XC technology like 3D MEMS.

1. Coupling/Multicasting: The node can merge multiple in-links (*merge links)* onto the same out-link; and multicast data from an in-link to multiple out-links (*split links).*

2. Selection: The node will send light from only one of the merge links onto the out-link. One of the ways this may operate is as follows. All the merge links are in a "non-blocked" state when there is no light on any of them. When there is light on one of them it goes onto the out-link and in parallel the node blocks the others within certain *blocking time.* The links remain blocked until the light stops. There is a chance for garbling the data if light comes on the other links before they

are blocked, which is handled by our scheme. Blocking is known to be a simpler operation than setting up a XC and is expected to take much less time. E.g., it is possible to achieve blocking times in nanoseconds using LiNbO3 and in micro-seconds to few milliseconds using ferro-electric crystals, MEMS [5]; however, our scheme can tolerate much higher blocking times as shown later.

Note that many of the current XCs already provide a similar ``bridge-merge'' functionality to support 1+1 protection, typically combining up to two or four ports. The main focus of this paper, however, is on the overall scheme; more specific details of the hardware are outside its scope.
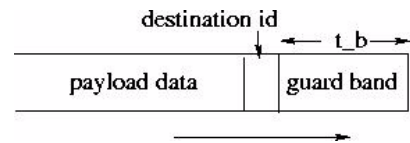

Figure 2: Message Format.

Path Setup: When a demand arrives, its backup path can be computed using any routing algorithm and the XCs are configured as follows. Consider a node where two or more backup links l_1 - l_n merge onto a single backup link L. The links l_1 - l_n in the incoming fiber are configured as merge links, merging onto the outgoing L. The links l_1 - l_n in the outgoing fiber are configured as split links, with light from the incoming L multi-cast onto them. This is illustrated in Figure 1. By default, the backup links carry no light and hence all the merge-links are non-blocked. A protocol like RSVP can be extended to implement the necessary messages.

Restoration: On a network failure, the end-nodes of the failed demand (N1, N3 in the figure) send data out on their backup paths, preceded by a *guard band* equal to the blocking time and a header containing the destination node identifier (see Figure 2). When this light reaches an intermediate node over a merge link, it will be sent over the corresponding shared link while blocking the other merge links. If there are near-simultaneous failures in the network, multiple transmissions may arrive on the merge links before blocking is completed. This can result in garbling of data for that time duration. By choosing a guard band equal to the blocking time, the corruption is restricted to the guard band. The signal is multi-cast onto the split links when encountered, ultimately reaching the other end-node. On receiving light on the backup link, the end node skips the guard band, reads the header, and picks up the data only if the id in the header matches its own.

Essentially, blocking replaces the more complex cross-connect setups and multi-casting eliminates the need to process address headers in the internal nodes.

Note that, due to the multi-casting, data may go on parts of the network that were not in the backup

path being restored. This can lead to unnecessary blocking if there are simultaneous failures. As an optimization, signals can be sent on a different channel to stop the multi-casting. This can be done after the data has been sent without impacting restoration times. If the hardware does not support automatic blocking on merge links, this signal can also be used to block the other merge links, of course at a higher blocking time.

Failure to Restore: Restoration may fail for various reasons, e.g., blocked merge link, failure in the backup path. It may even cause a deadlock where two simultaneously failed demands block each other on two different nodes. All these cases are handled through a time-out mechanism at the end-nodes. After sending the data out on the backup path, the end-nodes wait for a time equal to the maximum time for successful restoration. If data is not received on the backup path, the end node stops data transmission and retries after a random interval (similar to exponential backoff in Ethernet), up to a maximum number of attempts. This step differs for uni-directional traffic and failures, where the destination will need to send a signal to the source to notify the receipt of data on the backup path. We have also shown that there is no possibility of deadlocks with uni-directional traffic [4].

End of Backup Transmission: Once data transmission ends on the backup path, e.g., when the primary path becomes operational, the nodes unblock the merge links.

Performance
The FASTeR scheme does not incur any signaling or cross connect setup latencies. The time taken to restore a backup path of n links after failure detection is $(n * t_l + t_b + t_h)$, where t_l is the average link latency, t_b is the blocking time at an XC and t_h is the header processing time at the destination. In contrast, the time taken by a traditional approach in which the nodes forward the signal after setting up the cross-connect is $((n-1) * (t_l + t_h + t_c)) + ((n-1) * (t_a + t_l) + t_a) + n * t_l)$ where t_c is the cross-connect setup time and t_a is the ACK processing time. If the node forwards the signal prior to setting up the cross-connect, the time taken is $((n-1) * (2t_l + t_h + t_a) + t_c + t_a)$. For comparison, we have tabulated the above times for ranges of cross-connect times and blocking times for two different signal times. Here, $n = 10$, $t_l = 1$ms, $t_a = 0.05$ms.

t_h	t_b	t_c	Restoration Time		
			FASTeR	Fwd-Before-XC	Fwd-After-XC
.3	.1-35	5-100	10-45	36-131	78-933
3	.1-35	5-100	13-48	60-155	102-957

Table 1: Restoration Times For Various Schemes (all times in ms)

Note that even with an unrealistically large blocking time of 35ms, FASTeR still meets the 50ms requirement. In contrast, the signaling-based schemes fail to do so in most scenarios. All the schemes are likely to take longer when restoring several demands simultaneously - but the FASTeR scheme will suffer to a lesser extent due to fewer operations.

Conclusion
Shared restoration is critical to the success of mesh networking. In this paper, we proposed a novel mechanism for ultra-fast shared restoration. The scheme requires certain additional support from XCs, but eliminates XC setups and signaling latencies. At the core of our solution is a technique for fast circuit switching which can be applied to other problems like burst switching. We are currently working on routing algorithms for FASTeR and further experimentation.

[1] Robert D. Doverspike and Gokhan Sahin and John L. Strand and Robert W. Tkach. Fast restoration in a mesh network of optical cross-connects. *OFC*, 1999.
[2] Walter J. Goralski. SONET. McGraw-Hill Professional, 2nd edition, 2000.
[3] Guangzhi Li and Jennifer Yates and Robert Doverspike and Dongmei Wang. Experiments in fast restoration using GMPLS in optical/electronic mesh networks. *OFC*, 2001.
[4] Chitra Phadke and Vishy Poosala. DataFirst - A Zero-wait Circuit Switching Mechanism. *Bell Labs Technical Report*, 2002, Bell Labs.
[5] J.A. Walker and K.W. Goossen and S.C. Arney. Mechanical anti-reflectio switch (MARS) device for fiber-in-the-loop applications. *IEEE/LEOS 1996 Summer Topical Meetings*.

FQ5   11:45 AM

Hybrid Centralized/Distributed Approach to Optical Network Restoration

F. Yu, D. Wang, R. Sinha, G. Li, B. Doverspike, C. Kalmanek, *AT&T Labs – Research, Florham Park, NJ, Email: fyu@eecs.berkeley.edu*.

We propose a hybrid centralized/distributed approach to restoration in networks with "intelligent" cross-connects. This approach achieves low restoration capacity and fast restoration speed, while requiring few control plane changes.

1. Introduction
Many carriers are migrating away from SONET ring restoration for their core transport networks and replacing it with mesh restoration through "intelligent" O-E-O cross-connects (XC). The mesh restoration is typically provided via two fiber-disjoint paths: a service path and a restoration path [1]. Two standard approaches for restoration in cross-connect networks have been proposed. In a *centralized* approach, a centralized server (e.g., a Network Management System - NMS) maintains a view of the entire network and is responsible for selecting paths and sending commands to the XCs to establish the connections. In the *distributed* approach, the source node of a connection selects paths based on local information and sets up connections by sending signaling messages from the source node to other XCs along the path. An advantage of centralized control is better use of resources (link and channel
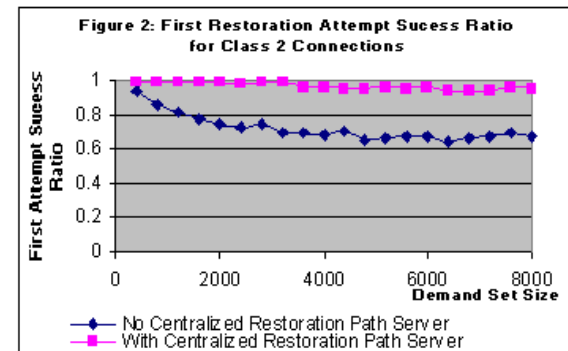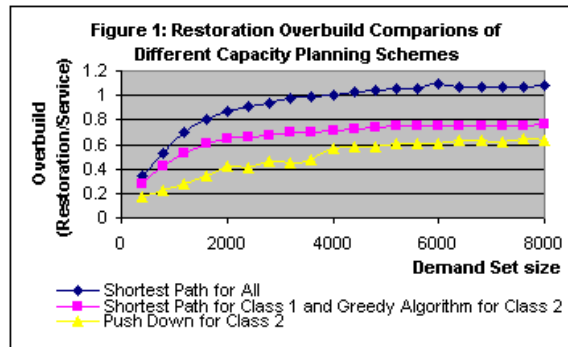
capacity) by optimization of path selection. The main advantages of distributed control are speed, both for service and restoration path set-up, and avoidance of the high cost and development effort to customize centralized systems to control specific network elements. Currently, there is a trend towards distributed control. However, to keep signaling simple, a common approach is to not distribute information about restoration paths. As a result each source node employs simple path-selection heuristics (such as "shortest path"). In this paper we propose and analyze a hybrid solution that utilizes a centralized restoration "path server" to optimize the restoration path selection, yet utilizes distributed control to compute service paths and set up service/restoration paths. The objective is to achieve very fast provisioning, fast restoration upon network failure, and more efficient use of capacity.

Our approach consists of the following features. First, since it might be computationally intensive to request an "optimized" restoration path from a centralized server when a connection is provisioned, we propose some possible alternatives. Second, since many carriers offer multiple levels of restoration priority for services and install capacity in discrete units (such OC-48 to OC-192), we propose a path-selection heuristic that includes two levels of restoration priority and minimizes the restoration capacity in the appropriate granularity.

We establish the benefit of the hybrid approach over the distributed approach through simulation experiments in a typical intercity backbone network. The comparisons are a) the restoration overbuild (the ratio of extra restoration capacity to service capacity) of our path-selection heuristic compared to the pure distributed case with shortest-path selection and b) restoration process efficiency. We design the network capacity under the assumption of a centralized scheme and then measure how many connections are restored in the "first" attempt. The two approaches are compared using the same network capacity and demand matrix.

2. Role of Restoration Path Server
In order to compute the restoration path, the path server must synchronize its topology database with the physical network topology, perhaps by integrating the path server into a vendor-supplied EMS that maintains this information. The distributed control plane is assumed to be able to obtain a restoration path from the path server. The connection provisioning procedure in this hybrid

Figure 1: Restoration Overbuild Comparisons of Different Capacity Planning Schemes

Figure 2: First Restoration Attempt Sucess Ratio for Class 2 Connections

approach is the following: when a XC receives a connection request, it first selects and establishes the service path, then sends a restoration path request to the path server along with the service path information. The server selects an efficient restoration path based on the service priority and other network usage. If the path server is unable to select a restoration path due to insufficient capacity, it has the option to re-optimize the restoration paths of some or all previously established connections and then download new information to the source nodes. During a failure event, no communication exchange is required between XC and the restoration path server, and the restorations start simultaneously at different source nodes. This avoids the latency of centralized restoration.

Another alternative to speed up the restoration path selection is to allow initial selection of a simple restoration path, such as min-hop, by the source node. Then, on a regular cycle (e.g., once a day), the centralized server recomputes the restoration paths of some or all connections and then downloads these new restoration paths at a convenient time. Because there could be only few connections with sub-optimal paths between restoration path re-optimization events, such an approach can achieve virtually the same performance as optimal path selection, but without the real-time penalty of computing paths on a per-connection basis. In both alternatives, a node makes a restoration path request after a control plane reboot.

The advantages of the hybrid approach are summarized here: (1) The network achieves both the speed of distributed restoration and the use of optimized restoration paths; (2) This capability can be added to cross-connect platforms with no or minimal change to existing signaling mechanisms; (3) The path server allows carriers to customize restoration to their own specifications, while avoiding modifications to distributed vendor XC solutions. Carriers can reflect restoration requirements that are not easily captured in vendor distributed path selection methods, such as a particular Shared Risk Group (SRG) topology (e.g., shared fiber span or WDM structures), or service criteria (e.g., priority of connections).

3. Centralized Path Selection Algorithm
In this section, we describe our capacity planning heuristic called ***pushdown*** that optimizes restoration paths to minimize the total restoration capacity. Suppose that capacity is purchased in units of OC-48, the XC employs STS-1 switching granularity, and the network supports two types of connection services: class 1 and class 2. Class 1 services have more stringent restoration time requirements than class 2 services. The inputs to the pushdown algorithm include the network topology, service connections in STS-1 units and service type, as well as service paths for all connections. The output is an SRG-disjoint restoration path for each service connection. Since the time to establish a restoration path depends on the number of path hops [3], the pushdown algorithm selects minimum hop SRG-disjoint restoration paths for class 1 connections. For class 2 connections, the pushdown algorithm selects an SRG-disjoint path, while attempting to minimize the total number of OC-48s.

The pushdown algorithm is based on a greedy online algorithm described in [2]. It operates in two phases. In the first phase, we consider one service connection at a time and apply a locally optimal algorithm. In the second phase, we try to do a global optimization. We maintain an array $failneed_k[e]$ for each link k, where $failneed_k[e]$ denotes the needed restoration capacity on link k when SRG e fails. In order to provide 100% restoration for any single SRG failure, link k must place at least $M_k = \max_e failneed_k[e]$ STS-1s. For example, if $M_k = 49$ STS-1 units, then two OC-48s of capacity must be provisioned on link k. However, it is possible that only one SRG failure requires two OC-48s and all the remaining SRG failures require only one OC-48 of capacity. Thus, we try to select alternative restoration paths for some of the service paths with a goal of bringing M_k down to one OC-48. Reducing one OC-48 on

link k and fixing the required OC-48s on all other links k accomplishes this. As a result, a few service paths can no longer be restored on link k. Then we try to select alternative restoration paths for these service connections without increasing the required capacity on all links. If we succeed, we pushed down one OC-48. If we fail, we restore the original restoration paths and repeat this process with the next link. We iterate until no OC-48 can be pushed down.

4. Performance Evaluation
For our simulation study, we used a 95-node, 164-link network representative of an intercity backbone network. The demand sets are based on the private line demand distribution of a large intercity backbone. We assume requests for bandwidth occur in units of STS-1, STS-3, or STS-12 and that 25% of connections are class 1 while 75% connections are class 2. We compare our pushdown algorithm with a solution that consists of disjoint shortest restoration paths solution and other published heuristics. For every demand set, we calculate the total number of OC-48s required for each restoration scheme. Figure 1 shows the restoration overbuilds for different demand sets. The top curve is the overbuild requirement for the SRG-disjoint minimum hop restoration path. The middle curve is the overbuild requirement using the algorithm provided in paper [2]. As shown, the pushdown algorithm reduces the restoration overbuild up to 50% compared with the shortest path algorithm, and 15% compared with the greedy algorithm in [2].

To evaluate restoration process efficiency, we compared our proposed approach with a fully distributed approach (using min-hop paths) with the same network and demand matrix models. We used the pushdown algorithm to plan the capacities and evaluated the restoration success ratio by simulation of the distributed restoration process. Both approaches restore nearly 100% of class 1 connections in the first attempt since we always give higher priority to class 1 connections in our simulator. Figure 2 shows the results for class 2 connections. Our approach restores nearly 100% of class 2 connections in the first attempt. In contrast, the distributed approach can only restore 60% of class 2 connections at first attempt under high demand load.

5. Conclusion
We proposed a hybrid distributed/centralized approach for optical network restoration that combines the merits of centralized and distributed solutions. It avoids the scalability issues of centralized solutions by using a distributed control plane for service path computation and service/restoration path provisioning. The hybrid approach improves the first restoration attempt success rate by 40% compared with the distributed approach. We also presented a restoration path computation algorithm. Simulation results show that our algorithm saves up to 50% of restoration capacity compared with the shortest path

algorithm and 15% compared with a previously published greedy algorithm.

6. Reference
[1] R. Doverspike, et al., "Fast restoration in a mesh network of optical cross-connects," OFC 99.
[2] G. Li, et al., "Efficient distributed path selection for shared restoration connections," IEEE INFOCOM 2002.
[3] E. Bouillet, et al., "Enhanced Algorithm Cost Model to Control Tradeoff in Provisioning Shared Mesh Restored Lightpaths," OFC 2002.

FQ6   **12:00 PM**

A Novel Bidirectional Wavelength Division Multiplexed Passive Optical Network with 1:1 Protection

T. J. Chan, Y. C. Ku, C. K. Chan, L. K. Chen, F. Tong, *Chinese University of Hong Kong, Shatin, Hong Kong Special Administrative Region of China, Email: tjchan1@ie.cuhk.edu.hk.*

We propose a novel network architecture for WDM-PON which offers 1:1 protection capability. In case of any fiber cut between remote node and ONUs, the affected ONU can re-route the wavelength channels via the adjacent ONU.

1. Introduction
There has been a tremendous growth in optical access networks due to the availability of low cost optical components in recent years. Passive optical networks (PONs) [1] does not require electric power supply at the remote node (RN), which greatly eases the network maintenance, thus it is considered to be one of the most promising approach to allow further penetration of fiber towards the subscriber side. However, in conventional PONs, both upstream and downstream bandwidths have to be time-shared among all optical network units (ONUs). Therefore, new schemes on WDM-PONs [2] [3] have been proposed to further enhance the total system capacity. Little work has been done to offer protection capability in both conventional PONs and WDM-PONs except fiber-cut detection methods. Whenever a fiber link from the RN to the ONU is broken, the affected ONU will become unreachable from the optical line terminal (OLT), leading to enormous loss in data and business. In this paper, we propose a novel network architecture for WDM-PON which offers 1:1 protection capability in both downstream and upstream fiber connections. The traffic for both directions can be re-routed via the adjacent ONU if any fiber cut between the RN and an ONU occurs.

2. Network Design
Fig. 1 shows our proposed network architecture. The RN comprises an array-waveguide grating (AWG) and N 1x2 3-dB couplers to route the
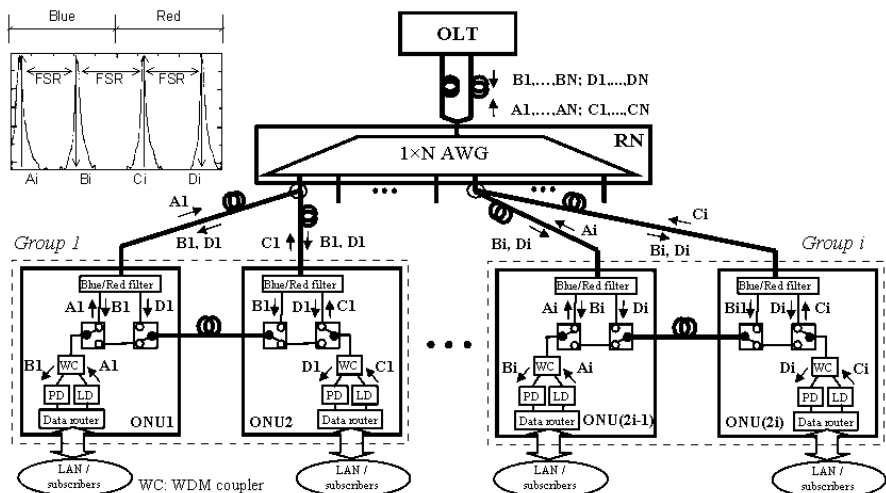

Fig. 1: Proposed network architecture for WDM-PON with protection and restoration

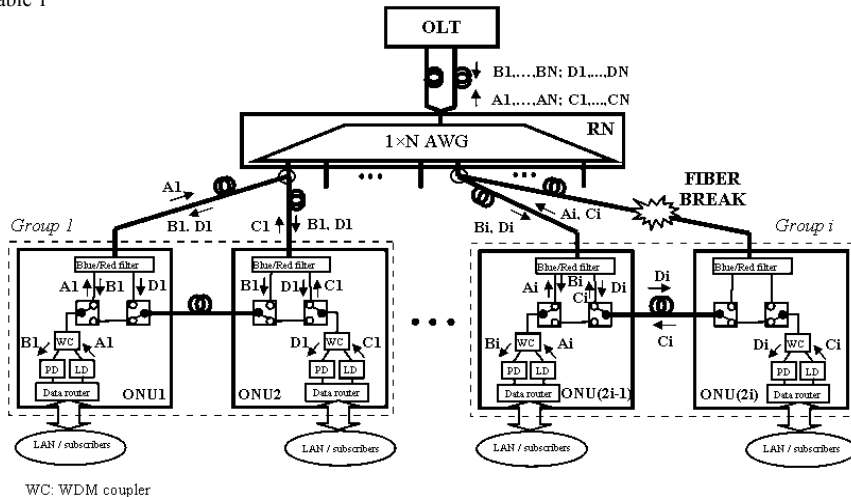| Channel no	Wavelength value	Channel no	Wavelength value	Channel no	Wavelength value	Channel no	Wavelength value
A1	1532.29	B1	1539.37	C1	1546.52	D1	1553.73
A2	1533.07	B2	1540.16	C2	1547.33	D2	1554.54
A3	1533.86	B3	1540.95	C3	1548.11	D3	1555.34
A4	1534.64	B4	1541.75	C4	1548.91	D4	1556.15
A5	1535.43	B5	1542.54	C5	1549.72	D5	1556.96

Table 1

Fig. 2: Network restoration when the fiber link between RN and ONU(2i) is broken
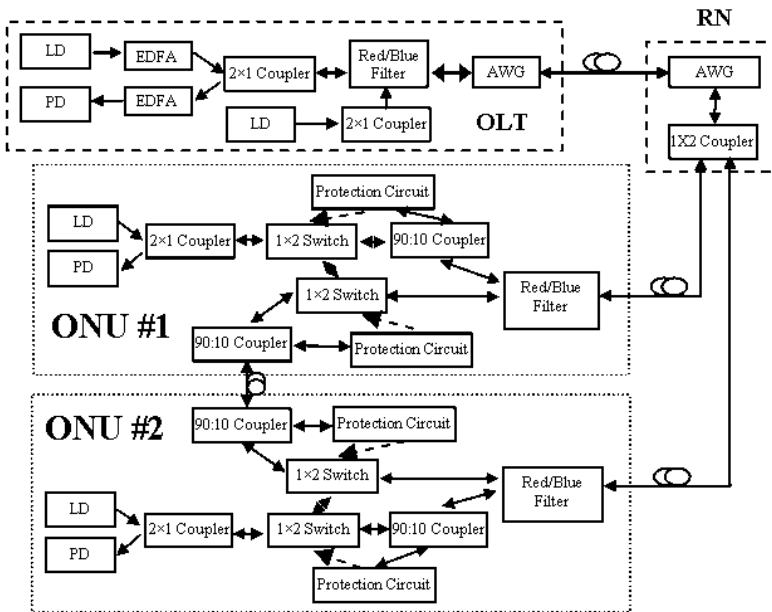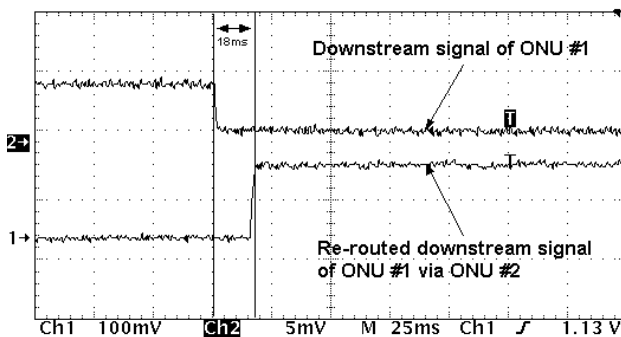

Fig. 3: Experimental Setup

Fig. 4: Switching time measurement

wavelength channels to the ONUs. Every two adjacent ONUs are assigned to a group. Each ONU in a group is separately connected to the same output port of the AWG via the fiber coupler. In each group of ONUs, a single piece of fiber is used to connect the two ONUs to provide an alternative path. Whenever there is a possible fiber cut between an ONU and the RN, it can still route its upstream and downstream traffic to/from the OLT via its adjacent ONU in the same group. Thus an ONU can protect its adjacent ONU from being isolated due to fiber cut, although each of them can still serve their respective connected subscribers in both normal and protection modes. A mutual 1:1 protection is therefore achieved.

Under normal operation (see Fig. 1), the downstream wavelengths, Bi and Di, are carried on the fiber link connecting to $ONU(2i-1)$ and the same composite signal is also delivered to $ONU(2i)$. At the front-end of $ONU(2i-1)$, its destined downstream wavelength, Bi, will be filtered out by the Red/Blue filter and so is Di in $ONU(2i)$. The use of the WDM coupler is to separate the upstream and the downstream wavelengths within the ONU. For upstream wavelengths, Ai from $ONU(2i-1)$ and Ci from $ONU(2i)$ will pass through their own Red/Blue filters and their respective fiber links. They are then combined before being fed into the same output port of the AWG. Under normal operation, there will be no traffic running on the fiber link connecting two ONUs in the same group.

For each ONU, two distinct wavelengths are assigned for upstream and downstream signals. Moreover, as two adjacent ONUs in the same group are actually connecting to the same output port of AWG at the RN, we make use of the spectral periodicity property of AWG to support the set of working and re-routed wavelengths. The upstream wavelengths (Ai, Ci) and downstream wavelengths (Bi, Di) in the ONU group i, i.e. $ONU(2i-1)$ & $ONU(2i)$, are spaced by one free-spectral-range (FSR) of the AWG, thus one AWG port can support the transmission and routing of all four wavelength channels (see the inset of Fig. 1) simultaneously. Table 1 shows the example of the wavelength assignment for a WDM-PON with 10 ONUs.

In case of fiber cut at the fiber link connecting to $ONU(2i)$, for example, the optical switches inside both ONUs in the same group would be reconfigured as illustrated in Fig. 2. Both upstream and downstream wavelengths of the isolated $ONU(2i)$ will be routed to the $ONU(2i-1)$ via the single fiber connecting between them. Conversely, $ONU(2i)$ protects $ONU(2i-1)$ in a similar way. With this protection mechanism, a fast restoration of the broken connection can be achieved, with minimal affect on the existing traffic.

Assuming the transmitted powers from the LDs in the ONUs are 0 dBm, the receiver sensitivities of the photodiodes at the OLT are -24dBm (at 2.5Gb/s), the insertion losses of optical switches, AWG, Red/Blue filters and WSC are 1dB, 5dB, 1dB and 1dB, respectively; the optical power margin will be 10dB in the re-routing path of upstream traffic, and so is that in downstream traffic. Therefore, a transmission distance of more than 40km can be achieved.

3. Experimental Results

Fig. 3 shows the experimental setup to demonstrate the principles of the bi-directional transmission and protection operations of the proposed WDM-PON network. The 1550nm DFB laser diodes (LD) used were 2.5Gb/s, directly modulated, while each of the arrayed-waveguide gratings (AWGs) had 16 channels with 100-GHz channel spacing and had an FSR of 12.8nm. Each Red/Blue filter had a bandwidth of about 18nm in each passband. On the OLT side, EDFAs were inserted in front of the AWG in order to compensate the components' insertion losses and to achieve the required transmitted power. Using this setup, we measured the switching time in case of fiber cut between ONU #1 and the RN. The optical power of the downstream signals from RN and from ONU #2 were monitored and the result was shown in Fig. 4. The upper waveform showed the downstream signal from RN to ONU #1 while the lower was the re-routed downstream signal via
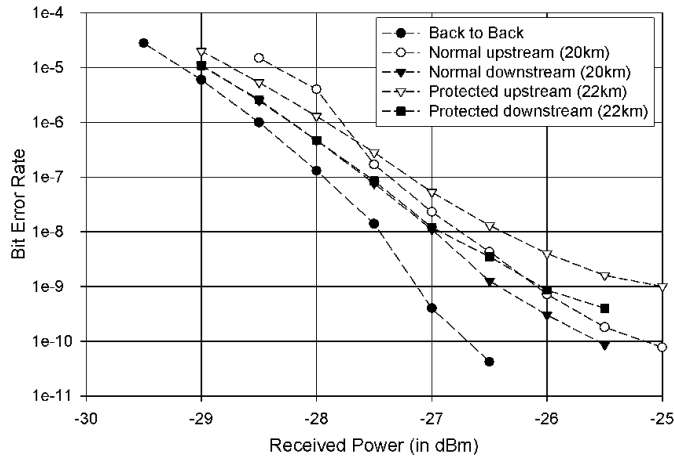
Fig. 5: BER measurements of 2.5Gb/s upstream and downstream traffic in normal and protected modes

ONU #2. The switching time was measured to be about 18ms and this corresponded to the network traffic restoration time.

We have also measured the bit-error-rate (BER) performance using 2.5Gb/s 2^{23} -1 PRBS data for both the upstream and the downstream traffic; and the measurement results were depicted in Fig. 5. In normal operation, both the upstream and the downstream wavelengths travelled through a transmission distance of 20km between the OLT and the ONU. Then, the fiber link between the RN and ONU1 was intentionally disconnected to simulate the fiber cut scenario. With our automatic protection mechanism, the fiber cut was detected and both the upstream and downstream wavelengths serving ONU1 were automatically switched to the fiber link (2km) between the two ONUs. Both wavelengths were then routed back to the OLT via the fiber link between ONU2 and the RN. Thus, the re-routed wavelengths travelled though a distance of 22km between the OLT and the ONU1. In all cases, the measured receiver sensitivities at 2.5-Gb/s varied from -25dBm to -26.5dBm. The additional 2-dB power penalty with respect to the back-to-back measurement was induced by fiber dispersion.

4. Conclusion
We have proposed a novel bidirectional protection scheme for WDM-PONs. By incorporating simple optical switches and optical filters into the ONUs; and by connecting two ONUs in the same group by a single piece of fiber, bi-directional signal re-routing can be achieved. Thus the isolated ONU can still communicate with the OLT in case of fiber cut. The automatic protection switching mechanism and the transmission aspect of the 2.5Gb/s signals were experimentally characterized.

5. References
[1] D. W. Faulkner, et al, IEEE J. Lightwave. Technol., vol. 7, pp. 1741-51, 1989.
[2] N. J. Frigo, et al, IEEE Photon. Technol. Lett., vol. 6, no. 11, pp. 1365-67, 1994.
[3] P. P. Iannone, et. al, IEEE Photon. Technol. Lett., vol. 10, no. 9, pp. 1328-30, 1998.

FQ7   **12:15 PM**

Shared Sub-Path Protection with Overlapped Protection Areas in WDM Networks

J. Li, H. Park, *Information and Communications University, Daejeon, Republic of Korea;* H. Lee, *Electronics and Telecommunications Research Institute, Daejeon, Republic of Korea, Email: jqli@icu.ac.kr.*

A partitioning configuration that divides a given network into overlapped protection areas for shared sub-path protection is investigated. The performances of capacity requirement and resto-

ration time are improved without any significant degradation of other performances.

I. Introduction
A sub-path is defined as a subset of the links along a path. To find protection paths for the sub-paths of a working path is called sub-path protection. How to divide a working path into several sub-paths is an important problem in the sub-path protection scheme. One idea is to divide each working path into several protection domains [1]. The other idea is to partition a larger network into several smaller areas [2]. However, partitioning configuration in [2] is not practicable for most actual networks. Moreover, sub-path protection requires more resources [2]. This is critical for network dimensioning.

We propose a new partitioning configuration that divides a given network into overlapped protection areas where a wavelength on the link that belongs to the overlap can be shared for protection sub-paths whose corresponding working sub-paths belong to adjacent separated working areas. It not only guarantees practicability but also provides higher resource utilization and decreased restoration time without any significant degradation of other performances.

II. Partitioning Configuration
We examine two ways of partitioning a working path in detail and then describe our new partitioning configuration. We only consider link failures in this paper. For convenience, we name the method that divides a working path into several protection domains as Path Dividing (PD); we name the method that partitions a larger network into several smaller areas as Network Partitioning (NP). The main difference between PD and NP stems from the sharing method of the protection sub-paths. In PD, two protection sub-paths can share some wavelength-links as long as their corresponding working sub-paths are link-disjoint. In NP, two protection sub-paths that only belong to the same area can share some wavelength-links if their corresponding working sub-paths are link-disjoint. The NP in [2] divides a larger network into several separated areas. We called this partitioning configuration Separated Network Partitioning (SNP). However, two protection sub-paths whose corresponding two working sub-paths belong to adjacent areas can share some wavelength-links without checking the disjoint requirement because their working sub-paths belong to different areas. This motivates us to consider new partitioning configuration in order to improve the resource utilization.

The other disadvantage of SNP is that it has a requirement that the node degree of the Area Border Router (ABR) must be larger than 3. The node degree refer to the number of other nodes in the network to which a node is connected, which is also equal to the number of links connected to the node. As an ABR, it must guarantee that a working path that traverses it can be divided into two

working sub-paths and each working sub-path and its corresponding protection sub-path belong to the same area. This means that it must have at least 4 links connected to it and that at least two links belong to one area, and other two links belong to the other area. If the degree of a node is 2, it is not possible as an ABR. For a mesh network, it must have some nodes whose degree is larger than 2. Otherwise, it is a ring. If a larger network does not have suitable nodes whose degree is more than 3 as ABRs, we cannot divide the larger network into smaller separated areas according to SNP [2]. Most actual networks belong to this category. In order to partition this type of larger networks, we need to choose some nodes whose degree is 3 as ABRs. If we divide a given network into overlapped areas, the partitioning problem can be solved. However, the wavelength assignment of sub-paths for overlapped areas is more complex than for the separated areas. To deal with the wavelength assignment issue for a wavelength on the link that belong to the overlap, we must consider the wavelength assignment for adjacent areas that overlap each other. This is not benefit for ILP calculation. In order to maintain the calculation complex of ILP not to be increased significantly, we propose a new partitioning configuration.

Our partitioning configuration is described as follows. We divide a given network into several areas, but areas for working and protection sub-paths are different. Areas for the working sub-paths are called working areas. Working areas are separated. Areas for protection sub-paths are called protection areas. One protection area corresponds one working area. It can be bigger than the corresponding working area. Protection areas can be overlapped. The objective of overlapping of protection areas is to increase the sharing for the protection sub-paths that belong to the adjacent protection areas. Our partitioning configuration is called Network Partitioning with Overlapped Protection Areas (NPOPA). The difference between NPOPA and SNP is that a working area and its corresponding protection area are different. The difference between NPOPA and PD is that in NPOPA a working area and its corresponding protection area can have many pairs of working and protection sub-paths, but in PD one protection domain only has one pair of working and protection sub-paths.
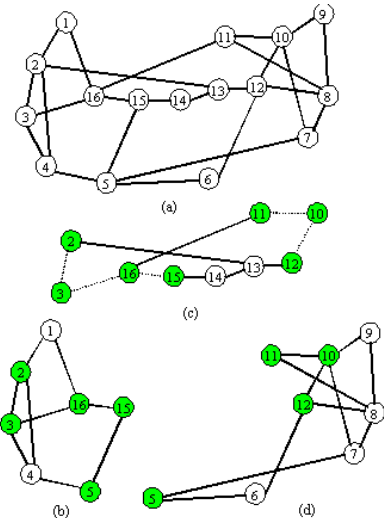

Fig. 1 (a) 16-node and 25-link NSFNET backbone. (b), (c), and (d) are three areas of (a). Working areas include only solid links. Protection areas include solid and dashed links. Node 5, 2, 3, 15, 16, 10, 11, and 12 are ABRs. The wavelengths on dashed links are permitted to be assigned only for protection sub-paths whose corresponding working sub-paths are in this working area.

We give an example to illustrate the practicability of our NPOPA. The 16-node and 25-link NSF-NET backbone is shown in Fig. 1. It can be

divided by NPOPA, but it cannot be divided by SNP.

Besides the practicability, NPOPA has another important advantage is that it provides higher resource utilization compared to SNP. We give an intuitive example in Fig. 2. Consider a connection between node pair (6,7) as shown in Fig. 2 (b). The working path is <6,5,7>, the protection path is <6,3,4,7> according to SNP, and the protection path is <6,8,7> according to NPOPA. It is obvious that the resource utilization of the connection is 5 wavelength-links for SNP while it is 4 wavelength-links for NPOPA. If one wavelength on <6,8,7> has been assigned for other protection sub-paths whose corresponding working sub-paths are in area c, the resource utilization is only 2 wavelength-links since a wavelength on the link that belong to the overlap can be assigned for two protection sub-paths whose corresponding working sub-paths are in adjacent working areas in NPOPA.
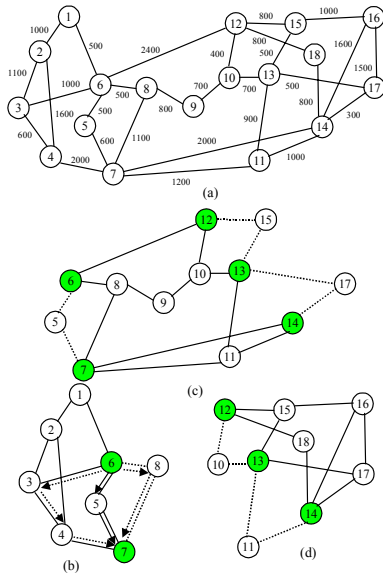

Fig. 2 (a) 18-node and 29-link nationwide network. The number besides each link is the length of the link. (b), (c), and (d) are three areas of (a). Working areas include only solid links. Protection areas include solid and dashed links. Node 6, 7, 12, 13, and 14 are ABRs. The wavelengths on dashed links are permitted to be assigned only for protection paths whose corresponding working sub-paths are in this area. The solid (dotted) arrows form the working (protection) path between node-pair (6,7).

The restoration time of our scheme is also less than or at most equal to that of SNP. The restoration time depends on the total physical distance of a pair of working and protection paths [1]. It is obvious that the total distance of a pair of working and protection paths for NPOPA is less than or at most equal to that of SNP. So the restoration time is also less than or at most equal to that of SNP. For an example, consider the connection between node pair <6,7>. The distance is 2800 for NPOPA, while it is 4700 for SNP. The restoration time must be less than that of SNP.

Let A be the number of areas. If the independence of sub-paths is guaranteed, sub-path protection can survive up to A failures as long as there is at most one failure per area. If two areas overlap, the number of simultaneous failures that the protection scheme can survive becomes less than or at most equal to A. For an example, protection areas a and b in Fig. 2 are not independent, and the sub-path protection scheme cannot guarantee to survive simultaneous failures in working areas a and b. However, it is known that the probability that more than two failures occur simultaneously is very low [3].

III. Assumptions and Calculation Procedures
The routing and wavelength assignment (RWA) problem in a WDM mesh network with shared sub-path protection can be formulated as an ILP. Our objective is to minimize the total number of wavelength-links. We assume that the network topology that is represented as a directed graph and the partitioning configuration NPOPA are given. Areas are numbered from 1 through A. We also assume that only the adjacent indexed protection areas can be overlapped. Protection area n can be overlapped with protection area n-1 and protection area n+1 when 1<n<A. Protection area 1 can only be overlapped with protection area 2 and protection area A can only be overlapped with protection area A-1. It is not difficult to extend to the general case that a protection area can be overlapped with all adjacent protection areas. We also assume that ABRs have wavelength conversion capability and other nodes do not have wavelength conversion capability.

The procedures of calculating the total number of wavelength-links are given as follows. (1) transform of connection requests. For a given inter-area connection request that traverses some areas, it is divided into some sub-paths according to working areas that it traverses, thus the inter-area connection is divided into several intra-area connections. (2) routing problem. We calculate 2 shortest link-disjoint routes between each node-pair using the Bhandari's algorithm [4] for all protection areas one by one. (3) wavelength assignment problem. We develop ILP formulation of the shared sub-path protection scheme. Due to space limitations, ILPs are not shown here.

IV. Illustrative Examples and Discussion
We apply our studies to the example network. The

algorithm was evaluated on the same network as used in [2] (Fig. 2). We assume that the number of wavelengths on each link is 10. We run the ILP formulation on random demands, where each random demand has between 25 and 40 connection requests.

We give the results of capacity utilization for the network in Fig. 3. It is shown, as expected, that our portioning configuration NPOPA has higher capacity utilization compared to SNP.

We give the average, maximum, and minimum lengths of a pair of sub-paths in Fig. 4. It is shown that the average, maximum, and minimum lengths for NPOPA are less than those of SNP. It means that the average, maximum, minimum restoration times for NPOPA are less than those of SNP.

The calculating complexity for NPOPA is almost same as that of SNP because we use the almost same time in calculation of the total number of wavelength-links for two cases.

References
[1] P. Ho and H. T. Mouftah, "A Framework for Service-Guaranteed Shared Protection in WDM Mesh Networks," IEEE Communications Magazine, vol. 40, pp. 97-103, Feb. 2002.
[2] C. Ou, H. Zang, and B. Mukherjee, "Sub-Path Protection for Scalability and Fast Recovery in WDM Mesh Networks," Proc. OFC'02, ThO6, 2002.
[3] S. Yuan and J. P. Jue, "A Shared Protection Routing Algorithm for Optical Networks," Optical Networks Magazine, Vol. 3, pp.32-39, 2002.
[4] R. Bhandari, "Optimal Physical Diversity Algorithms and Survivable Networks," Proc. Second IEEE Symposium on Computers and Communications, pp. 433 – 441, 1997.
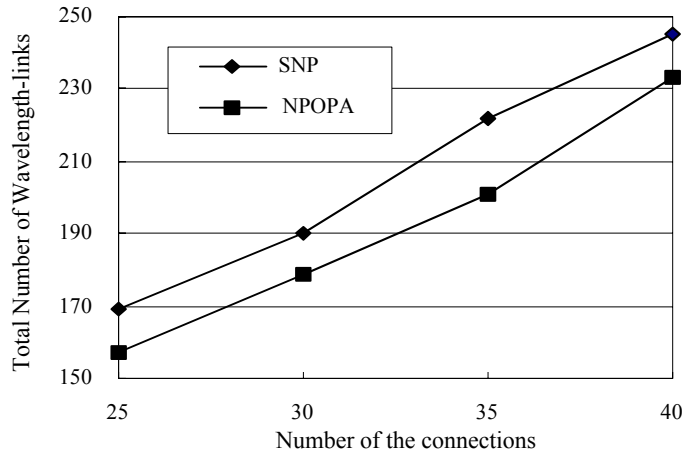
Fig. 3 The total number of wavelength-links versus the number of connections.
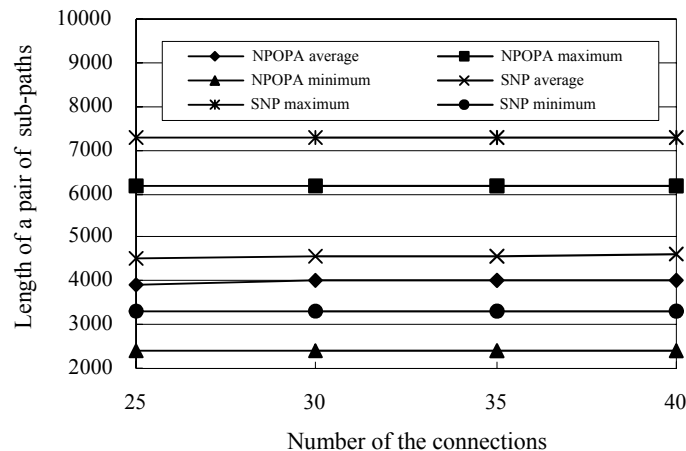

Fig. 4 The length a pair of sub-paths versus the number of connections.

FR1   **10:30 AM**

Experimental Field Trial of Waveband Switching and Transmission in a Transparent Reconfigurable Optical Network

P. Toliver, R. Runser, J. Young, J. Jackel, *Telcordia Technologies, Red Bank, NJ, Email: ptoliver@research.telcordia.com.*

We demonstrate 4-channel, 25GHz-spaced waveband transmission in a 200GHz passband through a transparent reconfigurable optical network. We investigate the impact of polarization effects on the waveband and its interaction with MEMS and LiNbO$_3$ switch fabrics.

Introduction
Waveband switching is a technique in which a subset of wavelengths are grouped together and switched optically as a single entity through a transparent network infrastructure. The individual wavelengths of a waveband are commonly assumed to be contiguous in spectrum, although they could also be interleaved or arbitrarily spaced. One of the key advantages of switching groups of wavelengths that share a common multi-hop path rather than individual wavelengths is that fewer ports are required on the switch fabrics of photonic cross-connects at transit nodes. Wavebands can also be used to upgrade the capacity of existing transparent networks without requiring any changes to the core network elements provided the waveband signals generated at the edge fit within the allowable optical passbands. This technique can also be used to support higher channel bandwidths on fiber paths that would otherwise require costly impairment compensation or regeneration.
The benefits of waveband switching have been studied by a number of groups from an architectural perspective [1, 2]. To date, however, there have been few reports discussing the practical implementation issues over real networks. Here, we present the results of waveband switching experiments that were demonstrated on the Advanced Technology Demonstration Network (ATDnet)-an optical network testbed that links a number of government agency laboratories in the Washington, D.C. metropolitan area (see Fig. 1). Under the MONET program, the original ATDnet testbed was designed to support only 8 x 2.5 Gb/s wavelengths per fiber [3]. The infrastructure of the East Ring supports network elements (NEs) that are optically transparent enabling the possibility for considerably higher bandwidths but with the need for external dispersion compensating elements. For the particular results summarized in this paper, the waveband switching experiments primarily utilized paths through the MEMS and LiNbO$_3$-based transparent wavelength selective cross-connects (WSXC) located at both the Laboratory for Telecommunication Sciences (LTS) and the Naval Research Laboratory (NRL).
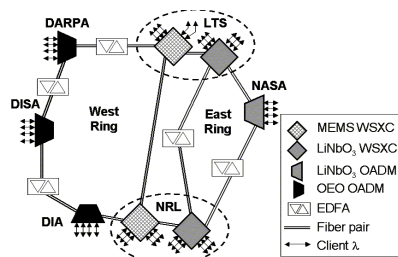

Fig. 1. ATDnet testbed comprised of both transparent and non-transparent network elements.

Experiment
The transparent network elements within ATDnet are capable of supporting at least 8 wavelength passbands on a 200 GHz ITU frequency grid. We performed our waveband switching experiments using the second 200 GHz window, which is centered at 1550.92 nm, while other single wavelength signals, such as OC-48 ATM, populated the remaining seven spectral windows.
As illustrated in Fig. 2, a 4-channel waveband transmitter (WB Tx) and a 4-channel waveband receiver (WB Rx) were constructed and connected to the add/drop ports of a WSXC located at the LTS. The WSXC allowed us to switch the waveband signal through various transparent paths of ATDnet. The four sub-channels of the WB Tx, which consists of an array of tunable lasers followed by an array of electro-optic modulators, are passively multiplexed together on a 25 GHz grid and their amplitudes are equalized before the WSXC add port. The WB Rx consists of a cascaded array of fiber Bragg grating filters (each 15 GHz wide) and circulators along with an array of four photoreceivers. Since the ATDnet NEs are optically transparent, no changes or hardware upgrades were required to support the waveband client signal. Such an upgrade would have been impossible given an OEO switched network.
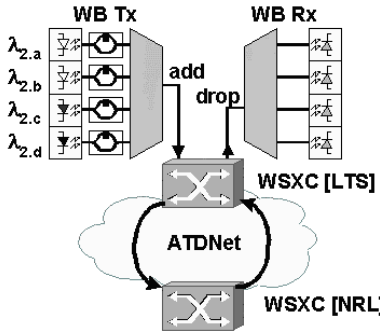

Fig. 2. Experimental setup for waveband switching demonstration.

Results
In Figure 3, we show the 4-channel waveband signal contained within a spectral window that is approximately 120 GHz wide and centered at 1550.92 nm. This particular window is defined by the optical mux and demux components inside the MEMS-based WSXC. As shown by the "add" signal plot, the four waveband sub-channels are set to the following wavelengths: λ_{2a}=1550.52, λ_{2b}=1550.72, λ_{2c}=1550.92, and λ_{2d}=1551.12 nm. The waveband was transmitted over approximately 100 km of SMF-28 fiber on a loopback path between the LTS and NRL through MEMS-based WSXCs located at each node. The entire waveband is received at the drop port, although the λ_{2a} sub-channel is attenuated slightly due to its proximity to the passband edge of the NE muxes and demuxes.
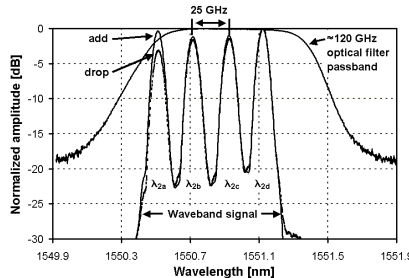

Fig. 3. Plot of add/drop waveband spectrums and passband spectral window.

The recovered bit error rates (BERs) of all four sub-channels after transmission through the two WSXCs, 100 km of fiber, and optical amplifiers (integrated into the NEs) is shown in Fig. 4. For these BER results, the waveband sub-channels are modulated with decorrelated OC-48 (2.488 Gb/s) pseudo-random data streams (2^{23}-1). The average receiver sensitivity given a BER of 10^9 is -34.4

dBm. Compared to back-to-back operation, the power penalty for the four sub-channels is only 0.1 dB. This experiment demonstrates that an existing transparent network infrastructure originally designed for 2.5 Gb/s capacity per passband can support 10 Gb/s per passband using wavebanding techniques at the edge of the network without requiring changes to core network elements or transmission fibers.
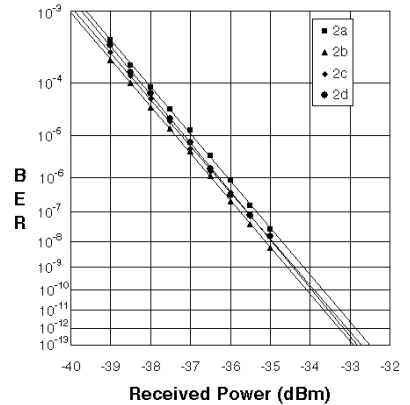

Fig. 4. Bit error rate performance with four 2.5 Gb/s channels in waveband.

We also investigated the ability to modulate the individual sub-channels at 10 Gb/s, which provides a total passband capacity of 40 Gb/s within the transmission window. In this experiment, all four wavelengths were modulated by through a common 10 Gb/s electro-optic modulator. Pre- and post-dispersion compensating fibers were used to support the 10 Gb/s sub-channels over the 100 km SMF-28 network span. The resulting BER performance for the four 10 Gb/s sub-channels is summarized in Fig. 5. The average receiver sensitivity at a BER of 10E-9 is -17.8 dBm. The average power penalty across the four sub-channels was 1.1 dB, with λ_{2a} having the largest penalty of 1.5 dB. The increased power penalty is likely to be a result of the channel proximity to the passband edge causing greater signal distortion due to filter dispersion. It would not have been possible to achieve the transmission of a single 40 Gb/s wavelength within an ATDnet passband without subsequent compensation for PMD.
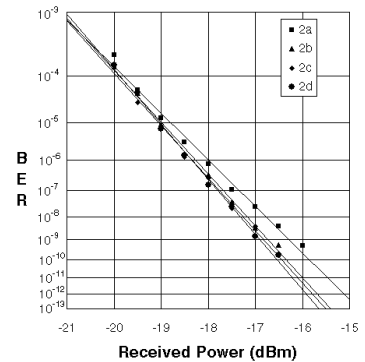

Fig. 5. Bit error rate performance of four 10 Gb/s sub-channels of the waveband.

Impact of polarization effects
An important physical layer issue to consider in a waveband switched network is the impact of how impairments may impact individual sub-channels of the waveband differently. In particular, polarization effects such as polarization dependent loss (PDL) can be particularly important for transparent NEs that use optical switch fabrics such as LiNbO$_3$. The ATDnet contains NEs with both MEMS and LiNbO$_3$ fabric technologies. The PDL for the loopback path for the MEMS-based WSXCs was less than 0.5 dB for waveband sub-channels λ_{2b}, λ_{2c}, and λ_{2d} and did not vary significantly based on the launched polarization orientation of the subchannels. The first sub-channel (λ_{2a}) had a higher PDL value of 1.0 dB due to its

proximity to the passband edge. In contrast, when the signal was sent through the LiNbO₃-based WSXC, the PDL varied within the range of 4.0-5.5 dB across the waveband. The amount of PDL experienced by each sub-channel was a function of the launch polarization orientation.

Ensuring that the sub-channels of a waveband maintain the same amplitude is important for minimizing the waveband transmission penalty. Over longer spans and multiple hops through optical networks, the amount of PDL through a network element should be kept to a minimum especially since it can coupled with second order PMD (which introduces wavelength dependent depolarization [4]) to cause additional variation in the sub-channel amplitudes.

Conclusion

Wavebanding is a technique that can be applied to existing transparent optical elements to increase the spectral efficiency within a passband without requiring costly impairment compensation or upgrades to photonic cross-connects. It can also be applied to new network designs in order to minimize the number of switch fabric ports. We have demonstrated 4-channel waveband transmission over 100 km of legacy fiber in ATDnet within a 200 GHz optical passband with aggregate capacities of 10 and 40 Gb/s. Understanding the impact of impairments and optical nonlinearities that may affect the individual sub-channels of a waveband is important for determining the ultimate reach, capacity, and channel spacing that can be achieved within a passband of existing networks and fiber infrastructure.

References
[1] L. Noirie, M. Vigoureux, and E. Dotaro, *OFC 2001*, paper TuG3, March 2001.
[2] R. Lingampalli and P. Vengalam, *OFC 2002*, paper ThP4, March 2002.
[3] W. T. Andersen, J. Jackel, G.K. Chang, et al., *J. Lightwav. Technol.,* vol. 18, no. 12, pp. 1988-2009, Dec. 2000.
[4] C. D. Poole, N. S. Bergano, R. E. Wagner, and H. J. Schulte, *J. Lightwav. Technol.,* vol. 6, no. 7, pp. 1185-1190, July 1988.

FR2   **10:45 AM**

Cost-Effective WDM Backbone Network Design with OXCs of Different Bandwidth Granularities

H. Zhu, K. Zhu, B. Mukherjee, *University of California, Davis, Davis, CA;* H. Zang, *Sprint Advanced Technology Laboratories, Burlingame, CA, Email: zhuh@cs.ucdavis.edu.*

We propose a framework for designing a WDM backbone network with OXCs of different grooming granularities. Numerical examples are presented showing that granularity-heterogeneous networks are more cost-effective than granularity-homogeneous networks.

1. Introduction

As WDM technology advances, the capacity of a wavelength channel continues to increase (OC-48, OC-192, or OC-768). However, the bandwidth requirements of typical connection requests are versatile (e.g., STS-1, OC-3, OC-12, OC-48, and OC-192), and usually of small fractions of the bandwidth of a WDM channel. To efficiently use the bandwidth, grooming switches are introduced which can pack/unpack low-speed connections onto/from high-speed WDM channels and switch at sub-wavelength granularity. Different grooming switches may have different grooming granularities. For instance, some grooming switches can groom at STS-1 level, i.e., they are capable of
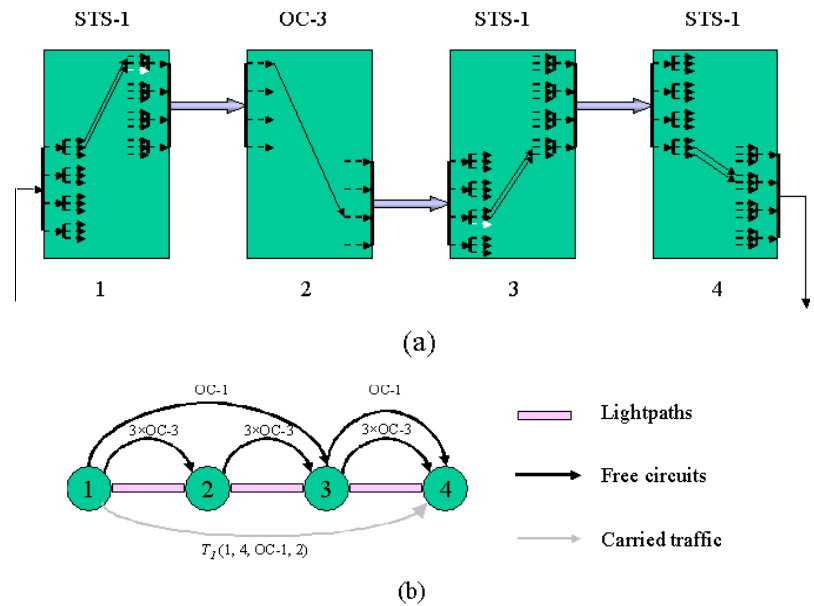

(a)

(b)

Figure 1. (a) State of the switches when routing T. (b) Network state after routing T.

OXC	Switching technology	Have grooming capability?	Capacity of the OXC port	Grooming granularity	Need transponders for bypass traffic?
Type I	OOO	No	OC-192	N/A	No
Type II	OEO	Yes	OC-192	OC-48	Yes
Type III	OEO	Yes	OC-192	STS-1	Yes

Table 1. Comparison of the three types of OXCs.

unpacking a wavelength channel down to STS-1 timeslots, switching those STS-1 timeslots, and packing them back onto wavelength channels. Some other grooming switches may do grooming only at OC-48 level (assuming the capacity of a wavelength channel is greater than OC-48). Although this kind of grooming switches provides less flexibility in grooming, the port cost may be less than that of STS-1 grooming switches. These two kinds of grooming switches are both opto-electro-opto (OEO) switches, and need to be surrounded by transponders. Meanwhile, all-optical OXCs do not need transponders for OXC ports, which is a significant saving in optical transport networks, but at the price of no grooming capability and wasting channel capacities. Since the WDM backbone network topologies are usually irregular and traffic requests are of different bandwidth granularities, it is not necessary to deploy the same kind of OXC at all the nodes. If the granularities of all the OXCs in a network are the same, we call this network *granularity-homogeneous network*; otherwise, we call it *granularity-heterogeneous network*. When designing a WDM backbone network, it is desirable to take advantage of the benefit of all types of OXCs to accommodate the traffic while reducing the network capital expenditures.

In [1], the authors compared the network cost when using different node architectures, but they assumed all the grooming nodes have the same STS-1 grooming capability. In this paper, we focus on designing a WDM backbone network with OXCs of different bandwidth granularities to minimize the network-wide OXC port cost. Specifically, we determine the type of OXC at each node, compute the route of each traffic request, and calculate the total OXC port cost.

2. Problem Statement

Given the physical topology of a network, a traffic matrix which contains various bandwidth requirement between different nodes, the types of OXCs which can be deployed in the network, and

the port cost of each type of OXCs, we need to determine the type of OXC at each node, as well as the route of each traffic request, and the objective is to minimize the total OXC port cost of the network while accommodating all the traffic demands. A traffic demand is represented by $T(s, d, g, m)$, where s and d are the source and destination nodes, respectively; g is the granularity of the traffic demand, for instance, OC-48; and m is the amount of the traffic in units of g.

3. Side-Effect of Routing Traffic in Granularity-Heterogeneous Networks

In a granularity-heterogeneous network, routing a connection request and representing the network state will become significantly more complex than in a network where only OXCs with STS-1 grooming granularity exist.

In an STS-1 grooming granularity network, if there is a lightpath between two nodes, the free capacities on the lightpath can always be accessible by the end nodes of the lightpath.

In a multi-granularity network, OXCs switch traffic at different granularities. For a given traffic demand requiring certain bandwidth, certain amount of timeslots on the lightpaths along the route of the traffic are allocated to the connection. At a STS-1 grooming switch, only the timeslots occupied by the traffic are switched from the incoming OXC port to the outgoing OXC port. However, at an OXC with a switching granularity coarser than the bandwidth granularity of the traffic request, some free timeslots may also be switched together with those timeslots taken by the traffic, causing these free timeslots to bypass this node and become unavailable to this node. The fundamental observation is that the timeslots within the switching granularity of an OXC are transparent to the OXC and these timeslots can only be operated as a whole.

Here we give a small example. To carry a traffic demand $T_1(1, 4, OC\text{-}1, 2)$, we setup lightpaths L_1 (from node 1 to node 2), L_2 (from node 2 to node 3), and L_3 (from node 3 to node 4), and then route

T_1 onto these lightpaths. The switching granularities of the nodes 1, 2, 3, and 4 are STS-1, OC-3, STS-1, and STS-1, respectively. The capacity of a wavelength channel is OC-12 for this illustration. Figure 1(a) shows the switching state of the OXCs. Since the switching granularity of node 2 (OC-3) is coarser than the bandwidth granularity of the traffic demand (OC-1), there is a free STS-1 timeslot (timeslot 3 in L_1) switched onto L_2 (timeslot 9 in L_2) by the OXC at node 2. Although this timeslot goes through node 2, it cannot be accessed by node 2. Any traffic carried by this timeslot will bypass node 2 and directly reach node 3, where it can be switched to any free outgoing grooming port. This is equivalent to having an STS-1 circuit directly connecting node 1 and node 3. Figure 1(b) shows the network state (virtual connectivity) after routing T_1. These circuits form another topology above the virtual topology, and traffic demands should be routed on this topology instead of on the virtual topology.

4. Network Design Framework

To accommodate characteristics of multi-granularity networks, we extend the graph model proposed in [2]. The graph model can route a traffic demand according to the current network state, and update the network state after carrying the traffic. The extended graph model can also intelligently choose the appropriate type of OXC to carry the current traffic demand, given there are several types of OXCs at a node. Due to space limitation, the extended graph model is not shown here.

Based on the extended graph model, we propose a design procedure as follows.

| Step 1	Place one OXC of each type at each node.
Step 2	Compute a route for each traffic demand, and choose the most suitable OXC at each node along the route using the extended graph model, until all the traffic has been carried.
Step 3	For each type of OXC at each node, move the traffic going through the other types of OXC to this type of OXC, estimate the port cost of this type of OXCs, and choose the type of OXC with the least cost at each node.
Step 4	After determining the type of OXC at each node, reroute all the traffic demands and calculate the network cost.

5. Numerical Results
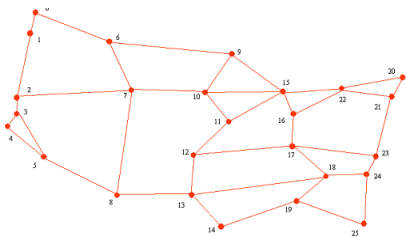
Figure 2. A 26-node nation-wide backbone network.

We conducted experiments on a typical nation-wide backbone network. The topology is shown in Fig. 2. It has 26 nodes and 40 bi-directional links. The capacity of a wavelength channel is OC-192. The bandwidth granularity of a traffic demand can be STS-1, OC-3, OC-12, OC-48, and OC-192. The total traffic bandwidth requirement distribution of these 5 granularities is α_1: α_2: α_3: α_4: α_5, respectively. The traffic is uniformly distributed between all the nodes. There are 3 types of OXCs, shown in Table 1.

The per-port cost ratio of Type I, Type II, and Type III OXCs is β_1: β_2: β_3.

We compare the port cost in four scenarios. In Scenario 1, 2, and 3, there is only a Type I, II, and III OXC at each node, respectively; in Scenario 4, we use the above network design framework to determine the type of OXC at each node, and all three types of OXCs can coexist in the network. In the experiment reported here, the ratio of α_1: α_2: α_3: α_4: α_5, is 5:1:1:3:3, which is based on the projected traffic distribution of a typical nation-wide WDM backbone network, and the per-port cost ratio β_1: β_2: β_3 is 1:3:4. Note that these ratios are just inputs to our network design procedure, and more-accurate data, when available, can be plugged into our model.
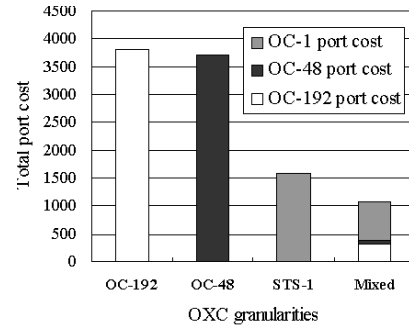
(a)
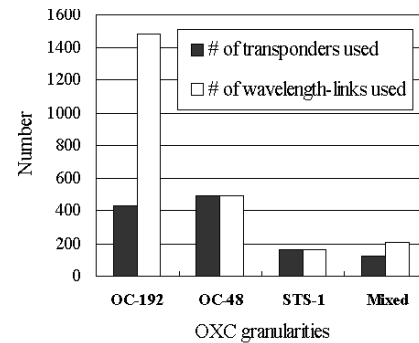
(b)
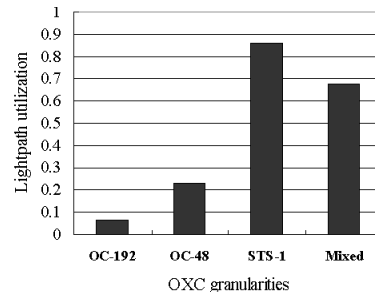
(c)

Figure 3 (a) Comparison of total port cost in the four scenarios. (b) Comparison of number of transponders and wavelength-links used in the four scenarios. (c) Comparison of the lightpath utilization in the four scenarios.

Figure 3(a) shows the total port cost, which is normalized by the per-port cost of all-optical OXCs, in the four scenarios, Fig. 3(b) shows the number of transponders used and wavelength-links used in the network, and Fig. 3(c) shows the lightpath utilization in the four scenarios. For the given traffic distribution and port cost ratio, the total port cost of the network in Scenario 1 is the highest, followed by the cost in Scenarios 2 and 3, and Scenario 4 achieves the lowest port cost. In Scenario 1, since the OXCs do not have grooming capability, the lightpath utilization is very low (6.5%) and 3822 OXC ports are used, resulting in highest total port cost despite the lowest per-port

cost. In addition, this scenario uses the largest amount of wavelength-links to carry all the traffic. In Scenario 3, although the per-port cost of the type of OXCs used is the highest, the total port cost is less than that in Scenarios 1 and 2. This is because Type III OXCs can efficiently pack low-speed connections onto high-speed wavelength channels, making the lightpath utilization relatively high (86%). Hence, the total number of OXC ports (394), WDM transponders used (160), and wavelength-links used (160) are lower than those in Scenarios 1 and 2.

However, there is still room for improvement. For instance, not all of the nodes need such high flexibility in grooming fabric; some nodes may achieve similar performance with coarser grooming granularity or even no grooming capability, with the coordination of other nodes, thus further reducing the cost. This can be observed in Scenario 4. In this scenario, we choose an appropriate type of OXC for each node. Compared with Scenario 3, although more OXC ports may be used, the total port cost and the number of transponders used in the network are reduced about 33% and 23%, respectively, at the price of using more wavelength-links and lower lightpath utilization. This is because some Type III OXCs at some nodes are replaced with Type I and Type II OXCs, which have lower per-port cost than Type III, and Type I OXCs do not need transponders for bypassing traffic.

6. Conclusion

We proposed a framework for WDM backbone network design to better utilize the benefit of different type of OXCs, which have different bandwidth granularities. Our results demonstrate that using different type of OXCs will yield better network performance, and a design using our framework can reduce the network-wide OXC port cost.

References

[1] R. Ranganathan, L. Blair, and J. Berthold, "Architectural Implication of Core Grooming in a 46-node USA optical Network," *OFC 2002*, ThP2, pp. 498-499.
[2] H. Zhu, H. Zang, K. Zhu, and B. Mukherjee, "A Novel, Generic Graph Model for Traffic Grooming in Heterogeneous WDM Mesh Networks," *IEEE/ACM Trans. Networking*, to appear, 2003.

FR3   **11:00 AM**

Pre-Emptive Reprovisioning in Mesh Optical Networks

R. Ramamurthy, A. Akyamac, J-F. Labourdette, S. Chaudhuri, *Tellium Inc., Oceanport, NJ, Email: jlabourdette@tellium.com.*

Pre-emptive reprovisioning is a method to perform reprovisioning of a backup path in advance of a second failure, to reduce the time to recover service from seconds (reprovisioning) to milliseconds (restoration). We evaluate the tradeoff between benefits and operational complexity.

1. Introduction

In shared-mesh restoration [1,2,5], each working path has a diverse backup path. In one restoration architecture [1,2], backup routes are pre-computed, and shared protection channels on the backup path are pre-assigned at the time of path provisioning. Channels on the backup path may be shared between primary paths whose working paths are diverse. Upon a single failure event, the lightpaths whose primary paths are affected by the failure are restored on their backup paths. If restoration fails (because the shared-protection channels are either in a failed state or are already being used by another lightpath - which can happen in the case of a double failure), then re-provisioning of the backup path is attempted. If reprovisioning of the backup path is successful, then the newly reprovisioned backup path is used to carry traffic. If reprovisioning fails (due to lack of capacity),

then the lightpath is not restorable. Reprovisioning is a time-consuming process since it is performed at a centralized management system, and lightpaths are sequentially reprovisioned to avoid contentions for capacity. Pre-emptive reprovisioning is a method to perform reprovisioning of a backup path in advance of a failure. The motivation for pre-emptive reprovisioning is to reduce the time it takes to restore service from several seconds or tens of seconds with reprovisioning to order of 10s to 100s of milliseconds with restoration. However, there is operational complexity in pre-emptive re-provisioning. In this paper, we evaluate the trade-off between the benefits of pre-emptive reprovisioning and the additional operational complexity.

2. Pre-emptive Reprovisioning
Pre-emptive Reprovisioning automatically "re-provisions" a new backup path for a demand whose backup path has become unavailable. As a result, upon a failure, pre-emptively reprovisioned lightpaths can be restored in the order of milliseconds as opposed to being reprovisioned in the order of seconds to minutes. Backup paths can become unavailable due to several events that include:

Backup Channel Failure: A backup shared-channel fails (for example due to failure of electronics at one of the end-switches). In Fig. 1(b), a shared channel on the backup paths of P1 and P2 fails rendering the backups B1 and B2 unavailable.

Primary Channel Failure resulting in Lightpath Switch: A shared-mesh lightpath switches to its backup (rendering the backup channels unavailable for other lightpaths that are sharing them). In fig. 1(a), P1 switches to its backup B1, rendering the backup B2 of P2 unavailable.

Fiber failure: A fiber fails resulting in several lightpaths whose primaries use the failed fiber to switch to their backups.
The value of pre-emptive reprovisioning is to allow to restore rather than reprovision upon a double failure. We evaluate the performance of pre-emptive reprovisioning on 3 representative real networks
-Network 1 (45 nodes, 75 links, 72 shared-mesh demands, 97 shared channels)
-Network 2 (17 nodes, 26 links, 102 shared-mesh demands, 203 shared channels)
-Network 3 (50 nodes, 88 links, 300 shared-mesh demands, 476 shared channels)

The goal of the study is to evaluate the benefits of performing pre-emptive reprovisioning. The three failure events listed earlier are considered. Table 1 illustrates the "average" number of lightpaths whose backup paths become unavailable for each of the three events. The averages represent the average over all possible events.
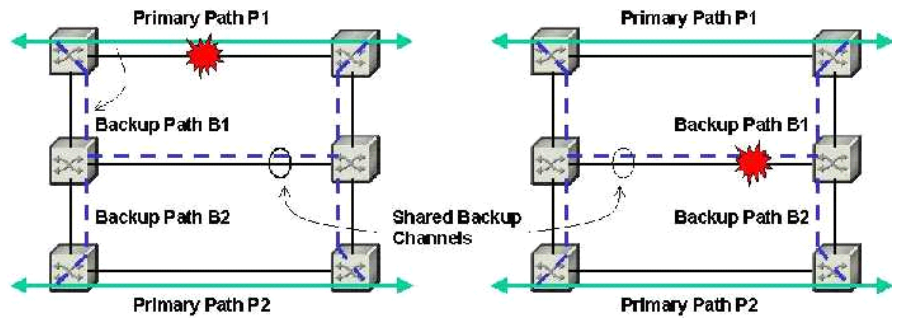

Figure 1. (a) illustrates shared-channels becoming unavailable due to a lightpath switching to protection resulting from a channel failure on the primary path, (b) illustrates a backup path becoming unavailable due to channel failure.

	Network 1	Network 2	Network 3
Backup channel failure	4	2.2	4.2
Primary channel failure	13.6	7.6	25.1
Fiber failure	17	55	192

Table 1. Number of lightpaths that would benefit from pre-emptive reprovisioning for different types of failures (average over all possible failures)

For backup channel failure, the number of lightpaths that need to be pre-emptively reprovisioned is equal to the number of lightpaths that share a protection channel [3,4,6], which is about 4 lightpaths for the above networks. For a lightpath switch to back-up, the number of lightpaths that need to be pre-emptively reprovisioned is equal to the number of backup hops multiplied by the number of lightpaths that share a protection channel, which is about 20 depending on the size of the network, but is independent of the network loading. For fiber failure, the number of lightpaths that need to be pre-emptively reprovisioned is equal to the average number of lightpaths on a fiber multiplied by the average backup hops multiplied by the average lightpaths that share a shared back-up channel, which is dependent on the network loading. Table 2 illustrates the "average" percentage of lightpaths that are successfully "pre-emptively reprovisioned" assuming that no extra capacity has been added for pre-emptive reprovisioning. Also included in the table is the percentage of lightpaths for which there is a "diversity violation" after pre-emptive reprovisioning. Diversity violation occurs when fully

diverse primary and backup routes are not available and primary and backup routes have to share links. For backup channel failure, ~90% of lightpaths can be successfully pre-emptively reprovisioned (since there are only a few lightpaths that need pre-emptive reprovisioning), for lightpath switch, ~75% can be successfully pre-emptively reprovisioned, and for a fiber failure about ~50% can be successfully pre-emptively reprovisioned. As shown in Tables 1 and 2, pre-emptive reprovisioning is not effective against fiber failures because a) a large number of lightpaths require pre-emptive reprovisioning (large operational impact) and b) only a limited percentage of lightpaths can indeed be successfully reprovisioned. In the remainder of this paper, we only consider pre-emptive reprovisioning in the case of an initial single channel failure. We now estimate the frequency of pre-emptive reprovisioning requests due to channel failures resulting from switch port failures. Given the FIT rates of switch ports, we can estimate the rate at which a given port fails within a certain duration (e.g., 1 week). We then estimate the number of channel failures in a given duration by multiplying the number of channels by the probability of a channel. We assume typical FIT rates for 2.5G, 10G ports and other equipment. We assume that 4 lightpaths need to be reprovisioned for a protection channel failure and 20 lightpaths need to be reprovisioned for primary channel failures. We find that the frequency of pre-emptive reprovisioning is dominated by primary channel failures, and the number of lightpaths pre-emptively reprovisioned depends on the size of the network. For example, we find that for Network 3, an average of 3 lightpaths are pre-emptively reprovisioned per week due to shared channel failures, whereas an average of 50 lightpaths are pre-emptively reprovisioned per week due to working channel failures.
The likelihood that pre-emptive reprovisioning is beneficial is the likelihood of a second failure impacting a lightpath during the Mean Time to Repair (MTTR) of the first failure (that caused the lightpath to become unprotected). We consider the first failure to be a primary channel failure causing a lightpath to switch to its backup, thereby resulting in 20 lightpaths to become unprotected, and pre-emptively reprovisioned. We then consider the likelihood of a second failure (being either another channel failure or a fiber failure) impacting one of 20 pre-emptively reprovisioned lightpaths. The following figure plots the likelihood that pre-emptive reprovisioning is beneficial against the MTTR of the first failure.
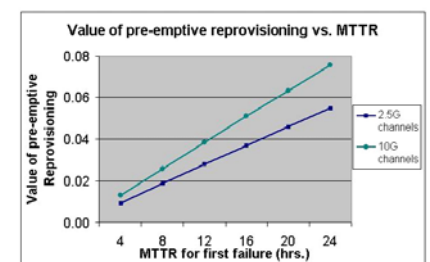

Figure 2. Probability that pre-emptive reprovisioning is successful

	Network 1		Network 2		Network 3	
	% successful	**% with diversity violation**	**% successful**	**% with diversity violation**	**% successful**	**% with diversity violation**
Backup channel failure	96	28	90	23	93	11
Primary channel failure	76	19	85	38	90	11
Fiber ailure	71	20	58	28	58	15

Table 2. Percentage of lightpaths that are successfully pre-emptively reprovisioned within existing capacity

We find that when the MTTR is about 4 hours, the probability that pre-emptive reprovisioning will be beneficial is about 1 in 100 times. As the MTTR increases, the probability that pre-emptive reprovisioning is beneficial increases proportionally.

3. Conclusion

Pre-emptive reprovisioning of backup paths improves the restoration time upon multiple failures. We evaluated pre-emptive reprovisioning on several representative real networks. We find that the success rate of pre-emptive reprovisioning is about 90% for protection channel failures, 75% for working channel failures, and about 60% for fiber failures. We find that the likelihood that pre-emptive reprovisioning is beneficial, i.e., the chance of a second-failure impacting the network within the MTTR of the first-failure, is proportional to the MTTR and is about 1 in 100 when the MTTR is 4 hours. The decision to support pre-emptive re-provisioning is thus a trade-off between the operational complexity of re-provisioning after single failures and the chances that re-provisioning would be beneficial in those (rare) cases of double failures before the first failure is repaired. The benefit is that the lightpath would then be restored (10s to 100s of msec) rather than re-provisioned (sec.) after a double failure. This work provides some preliminary results on the benefits of preemptive re-provisioning.

References

[1] J-F. Labourdette, et. al., *"Routing Strategies for Capacity-Efficient and Fast-Restorable Mesh Optical Networks,"* Photonic Network Communications, 4:3/4, pp. 219-235, July-December 2002.
[2] G. Ellinas, et. al., *"Routing and Restoration Architectures in Mesh Optical Networks,"* Optical Networks Magazine, Issue 4:1, January/February 2003.
[3] E. Bouillet, J-F. Labourdette, R. Ramamurthy, S. Chaudhuri, "Enhanced Algorithm Cost Model to Control tradeoffs in Provisioning Shared Mesh Restored Lightpaths," in Proc. OFC 2002, Anaheim, CA, March 2002.
[4] J. Doucette, W. Grover, T. Bach, "Bi-Criteria Studies of Mesh Network Restoration: Path Length vs. Capacity Tradeoffs," in Proc. of OFC 2001, Anaheim, CA, March 2001.
[5] B. Doshi, et al, "Optical Network Design and Restoration," Bell-Labs Technical Journal, Vol. 4, No. 1, pp. 58-84, January-March 1999.
[6] C. Qiao, Y. Xiong and D. Xu, "Novel Models for Shared Path Protection," in Proc. OFC 2002, Anaheim, CA, March 2002.

FR4   **11:15 AM**

Implementation of Statistical Lambda Multiplexing Network (SLAMNet)

H. Nakamura, H. Yokoyama, S. Nomoto, *KDDI R&D Laboratories Inc., Saitama, Japan, Email: nakamura@kddilabs.jp.*

This paper discusses implementation of a novel signaling-free DWDM network architecture that provides multi-wavelength service. In the service, the number of assigned wavelengths is dynamically modified according to the volume of traffic on a best-effort basis.

I. Introduction

In a future large-scale Dense Wavelength Division Multiplexing (DWDM) network, multiple wavelengths will be used by a pair of routers to transmit high-volume traffic. A basic concept of a novel architecture called Statistical Lambda Multiplexing Network (SLAMNet) was proposed for providing multi-wavelength service in the DWDM network [1]. In comparison with the other architectures proposed for the DWDM network [2-5], the most striking feature of the architecture is signaling-free wavelength path switching to dynamically adjust the number of wavelengths to the varying volume of traffic. Taking the advantage of the signaling-free wave-

length path switching, the SLAMNet can afford to be implemented to a part of a network with keeping its scalability, to be operated and maintained in a simple and economical way, and also to shorten the switching cycle regardless of a round trip time necessary for signaling. Furthermore, the signaling-free wavelength path switching can harmonize with signaling-based wavelength path management mechanisms such as GMPLS. The architecture was realized on a testbed. This paper discusses implementation of the SLAMNet and clarifies the target and effectiveness of the architecture.

II. Basic Concept of SLAMNet

A basic concept of the SLAMNet is illustrated in Figure 1. A pair of routers uses two types of optical channel (OCh) paths, referred to as initial paths and additional paths. The initial paths are fixedly established between the router pair and are used for transmission of traffic at all time. On the other hand, the additional paths are temporally utilized for transmission of burst traffic that overflows the capacity of the initial paths. The additional paths are dynamically setup and released by a pair of OCh path switches (OPSWs) and time-share wavelength resources assigned via optical

A basic configuration of an OPSW is illustrated in Figure 2. A monitor measures the volume of traffic transmitted by established initial and additional paths and observes its variation on a realtime basis. Additional paths are set up and released by making use of the variation of traffic volume as a trigger in source and destination OPSWs independently. Although the OPSWs
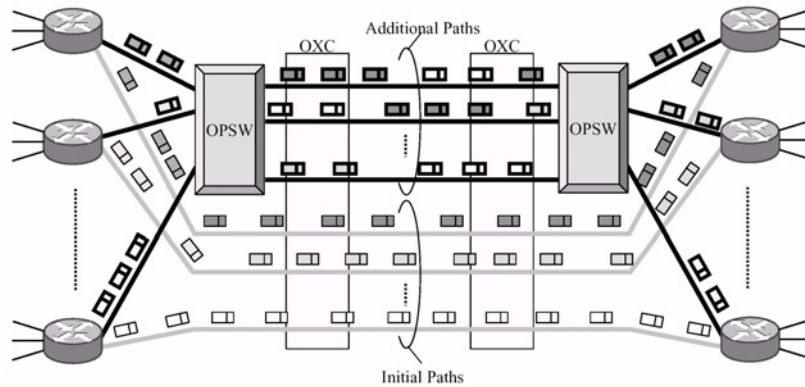

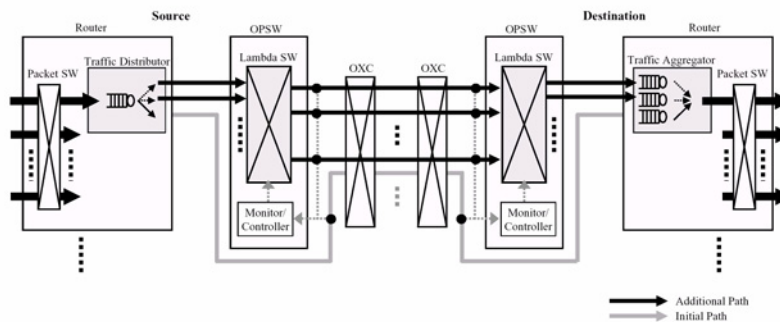Figure 1 : Basic Concept of SLAMNet
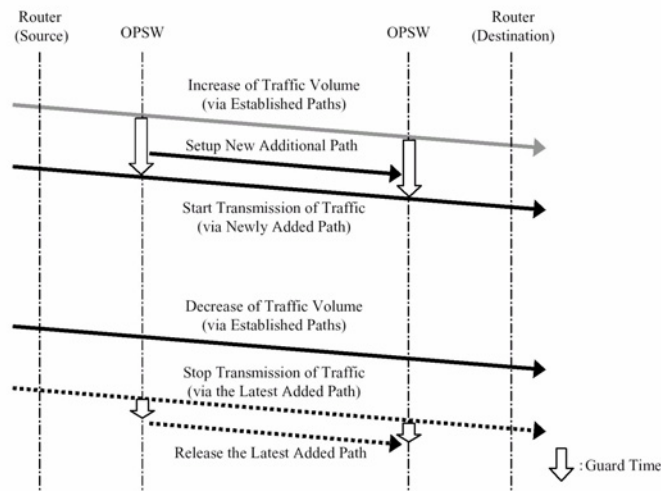

Figure 2 : Configuration of OPSW

Figure 3 : Basic Flow of Signaling-Free Path Management

exchange no signal with each other for management of the additional paths, they control to connect XC paths according to a common algorithm that selects the same path to be connected with the target path at the same status in cross-connect of the paths. Furthermore, for the purpose of keeping logical consistency in operation of the source and destination OPSWs, the algorithm employs several techniques to avoid incorrect actions and to guard against unexpected events, such as path selection based on a hash table [6]

A key point of the path switching mechanism is the difference in transmission delay among the OCh paths used by the same router pair. The difference has to be guaranteed in order to operate the switching mechanism properly and also to limit the ratio of reverse in a sequence of packets transmitted by multiple OCh paths. In this architecture, the initial and additional paths for the same router pair is routed in the physical network so that the difference in transmission delay among the paths is guaranteed to a certain extent. In the case where the paths are set up on the same physical route, the guaranteed difference is limited to that among wavelengths when they go through it. Based on the guaranteed difference in transmission delay, additional paths are managed in a sequence as shown in Figure 3. The guard time after detecting the trigger can be calculated from the guaranteed difference.

III. Logical Overlay Model

Based on a logical overlay model on a physical network, application of the SLAMNet to a DWDM network is discussed. This section focuses on management of additional paths and considers that initial paths are dealt with simply in a conventional way. Therefore, it is assumed that the overlay model is applied only to additional paths. The overlay model consists of two logical layers as shown in Figure 4. One layer is a logical management plane of OCh paths between OPSWs and OCh paths directly connecting between a router and an OPSW. The OCh path dealt with in the logical layer is referred to as a XC path and the layer is called a XC path network. The other layer is a logical management plane of end-to-end OCh paths between routers. The OCh path is a tandem connection of the XC paths and is referred to as a SW path. The logical layer for management of the SW paths is called a SW path network.
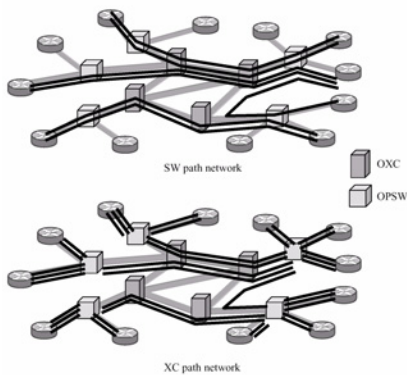

Figure 4: Overlay Model

In a XC path network, conventional optical cross-connect and add-drop facilities manages XC paths. The XC paths are logically grouped into a bundle referred to as a XC path bundle. The XC path bundle guarantees the difference in transmission delay among the paths included in itself to a certain extent. A SW path network is overlaid on the XC path network and makes use of the guaranteed difference in transmission delay of the XC path bundle in management of SW paths. The SW paths are dynamically set up and released by switching the XC paths in the OPSWs with taking a configuration of the XC path bundle into account. The SW path network is designed to
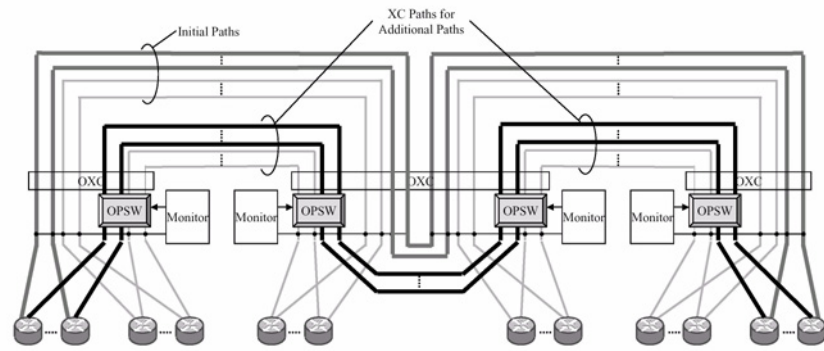

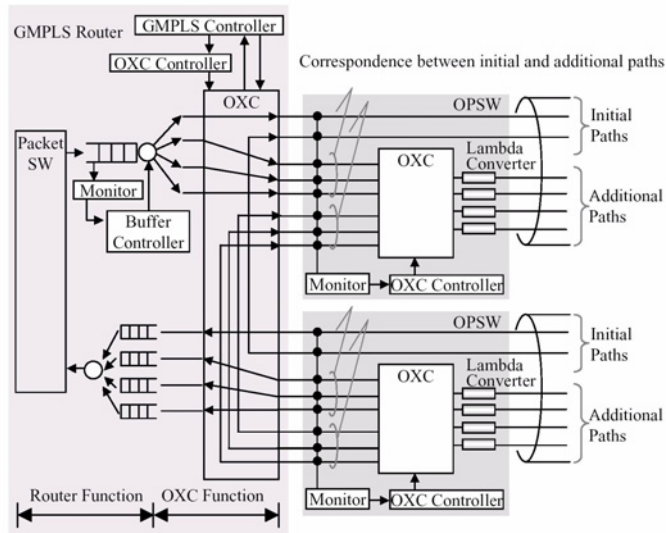
Figure 5: SW Path (XC paths in Tandem)

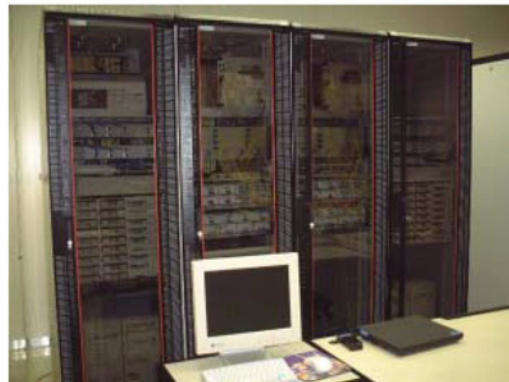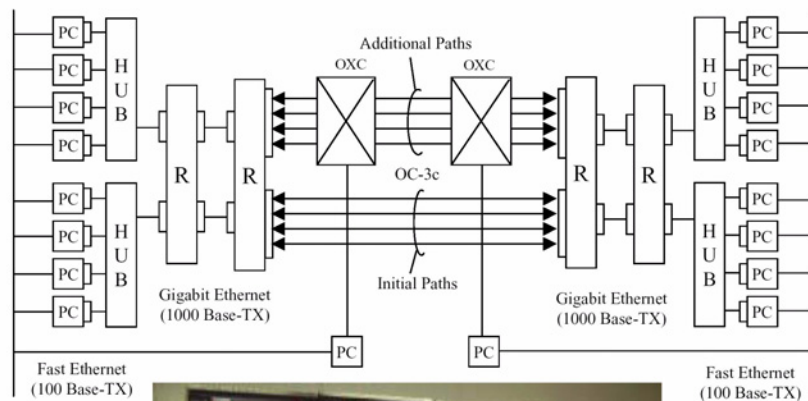Figure 6: Configuration of OPSW and GMPLS Router

Figure 7: Test system of SLAMNet

change its configuration more frequently than the XC path network that is operated in a conventional way. Statistical multiplex gain is expected in use of wavelength resources between a pair of OPSWs. Therefore, it is important for efficient network operation to implement the OPSWs with taking a tradeoff between the statistical multiplex gain and cost for implementation and operation of the OPSWs into account.

A SW path that consists of multiple XC paths is managed by multiple pairs of OPSWs as shown in Figure 5. Since each pair of OPSWs operates a XC path independently, it is not ensured that all the XC paths necessary for a SW path can be established when they are requested. The major target of this path management is transmission of burst traffic that requests wide bandwidth during a very short time period, such as high-speed download of huge files and aggregated traffic of individual streams that are apt to be highly concentrated. Furthermore, when the initial paths are established as a point-to-multipoint connection set and traffic is broadcasted via the paths, the additional path management mechanism of the SLAMNet can be simply applied for broadcasting the traffic.

IV. Harmonization with Wavelength Label Switching

The SLAMNet is applicable to a network that employs GMPLS function and can afford to work with the function in a harmonization scenario. In the scenario, initial paths and XC paths of the SLAMNet are managed as LSPs (Label Switched Paths) with signaling process by the GMPLS function. Based on the LSPs, additional paths are dynamically set up and released as SW paths by the signaling-free path management of the SLAMNet. Figure 6 illustrates a configuration of a node to support both the GMPLS function and the path management mechanism of the SLAMNet. In this configuration, a GMPLS router needs additional functions to set a cross-connect for the XC paths to be used in the additional paths according to setting of the initial paths and to control forwarding packets in output buffers of a packet switch with observing the volume of traffic. Furthermore, it is necessary for the GMPLS router to set a guard time before transmission of traffic through a newly established additional path and also to interwork with the OPSW in order to keep consistency of correspondence between the initial and additional paths.

V. Test System

For the purpose of demonstrating performance of the SLAMNet, a test system is developed as shown in Figure 7. This test system emulates the case where four router pairs share four or fewer OCh paths as additional paths on a best-effort basis. The additional paths are dynamically set up and released by a pair of OXCs representing OPSWs. Two routers in each side of the OXCs emulate four routers that share the additional paths. The router directly connected with hubs gives a tag to such the IP packet that overflows the capacity of an initial path and the other router distributes the traffic between the initial and additional paths according to the tags. A PC connected with the OXC works for monitor of traffic volume and control of the cross-connect. In a trial of this hardware, it is confirmed that the additional paths are dynamically managed in the cycle less than 28 milliseconds [6]. The cycle is expected to shorten in the further trials.

VI. Conclusions

The concept of SLAMNet is applicable to specific parts of the network, such as dense areas and bottleneck sections, and allows reduction of the necessary wavelength resources only in such portions. Thus, the architecture and path management mechanism can be introduced to conventional WDM networks in a step-by-step manner according to their usage status and operation plans. Furthermore, the SLAMNet has the possibility to shorten the cycle of additional path switching to the order of transmission time of a burst in an optical burst switching network. Based

on the SLAMNet, the short cycle operation is also pursued for optical burst switching.

References

[1] H. Nakamura, T. Kato, H. Yokoyama and S. Yamamoto, "Proposal of Statistical Lambda Multiplexing Networks (SLAMNet)," Proc. GLOBECOM2000, p. 3-6, Nov. 2000 .
[2] F. J. Janniello, "A prototype circuit-switched multi-wavelength optical metropolitan-area network," IEEE J. of Lightwave Tech., vol. 11, no. 5/6, 1993.
[3] T. Shiozawa, S. Takahashi, M. Eda, A. P. Yazaki, M. Fujiwara, "Demand Assign Wavelength Division Multiple Access (DA-WDMA) hybrid optical local area network using optical add-drop multiplexers," IEICE Trans. Commun., vol. E77-B, no. 2, 1994.
[4] T. Yasui, Y. Nakano, "Switching node consideration from the aspect of transmission characteristics in wavelength assignment photonic network (WAPN)," IEICE Trans. Commun., vol. E82-B, no. 2, 1999.
[5] T. S. El-Bawab and A. P. Jayasumana, "Modeling and performance analysis of a symmetric fast-circuit switched robust-WDM LAN with AR/LTP protocol," IEEE J. of Lightwave Tech. vol. 17, no. 6, 1999.
[6] H. Yokoyama, H. Nakamura and S. Nomoto, "Functional Architecture and Performance Analysis of Asynchronous Control between Nodes for Best Effort Multi-Wavelength Path Assignment (in Japanese)," Technical Report of IEICE, IN2002-38, pp. 29-34, July 2002.

FR5   (Invited)   **11:30 AM**

Core Mesh Optical Networks: A European Carrier's Perspective

A. Gladisch, *Deutsche Telekom T-Systems Nova Technologiezentrum, Berlin, Germany, Email: Andreas.Gladisch@telekom.de.*

Experiences with mesh restoration in a former SDH network are presented. Results of mesh core networks design studies are given with respect to opaque and transparent scenarios and problems of inter-working of mesh restoration domains are discussed.

FR6   (Invited)   **12:00 AM**

A National Mesh Network Using Optical Cross-Connect Switches

P. Charalambous, C. Dennis, *Dynegy Global Communications, Englewood, CO;* G. Ellinas, E. Bouillet, J-F. Labourdette, A. Akyamac, S. Chaudhuri, M. Morokhovich, D. Shales, *Tellium Inc., Oceanport, NJ, Email: pambos.charalambous@dynegy.com.*

This paper presents Dynegy's long-haul national network utilizing intelligent optical switches. This network offers end-to-end point-and-click provisioning, shared mesh restoration, re-provisioning of connections and network re-optimization.

Networks that transport optical connections using Wavelength Division Multiplexed (WDM) systems and route these connections using intelligent optical cross-connects (OXCs) are firmly established as the core constituent of next generation long-haul networks. In such networks, preventing and restoring link and node failures is increasingly becoming one of the most important network features [1-4]. Dynegy's network implements shared mesh restoration using intelligent optical switches to protect against single link and node failures. In shared mesh restoration (Figure 1), backup paths can share capacity if the corresponding primary paths are mutually diverse. Diversity of routes in Dynegy's optical network is defined using the notion of Shared Risk Groups [5]. A set of optical channels that have the same risk of failure is called a Shared Risk Group (SRG). SRGs are configured by Dynegy's network operators with the knowledge of the physical fiber plant of the optical network.

Compared to dedicated protection, this scheme allows considerable savings in terms of capacity required [5,6]. In addition, the backup resources can be utilized for lower priority preemptible traffic in normal network operating mode. However recovery is slower than dedicated protection in some cases, yet still within the realm of SONET restoration times, essentially because it involves signaling and path-setup procedures to establish the backup path. In particular, we note that the restoration time will be proportional to the length of the backup path and the number of hops, and if recovery latency is an issue this length must be kept under acceptable limits. However this constraint may increase the cost of the solutions, as it is sometimes more cost-effective to use longer paths with available shareable capacity than shorter paths where shareable capacity must be reserved. This tradeoff can be handled by an appropriate cost model in the route computation algorithm [7-8].

For routing purposes, the algorithms utilized by the intelligent optical switches use a cost model that assigns costs to links in the network. The policy used for assigning costs to the links is different for primary and backup paths. The weight of a link for a primary path is the real cost of using that link in the path. This is a user-defined cost that reflects the real cost of using a channel on that fiber. The weight of a link for a backup path is a function of the primary path [7-9]. Backup link e is assigned: (1) Infinite weight if it intersects with an SRG of the primary path. (2) Weight w_e if new capacity is required to provision the path, and (3) Weight $s_e = \varepsilon w_e$ 0 ? ε ? 1, if the path can share existing capacity reserved for pre-established backup paths. The routing of each lightpath attempts to minimize the total cost of all channels in the lightpath route, i.e., the goal is to share the existing capacity amongst multiple backup paths.

Mesh Restoration

Provisioning of shared mesh restored lightpaths in Dynegy's live network that utilizes Tellium's intelligent Aurora Optical Switches, was achieved by calculating the working and backup paths using the weight assignment as described above. Dynegy's network is on the order of 45 nodes and 75 trunks, and is carrying shared mesh restored
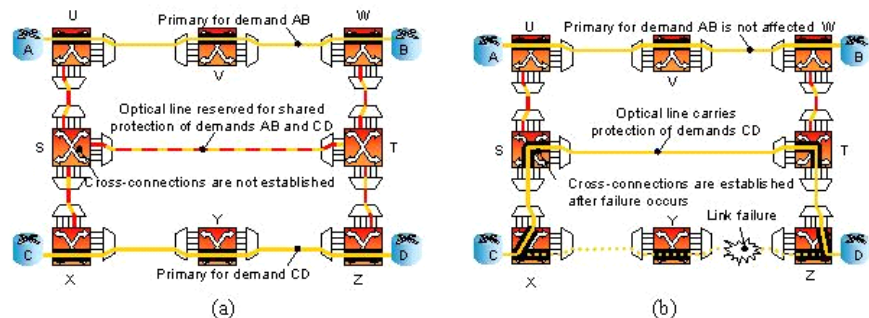

Figure 1: Shared Mesh Restoration: (a) Network connections before a failure occurs (b) Network connections after a failure occurs.

demands amounting to several hundred gigabits of service. Upon a single link or single node failure, restoration times ranging from a few tens to a couple of hundred msecs were observed. The maximum restoration times observed were less than 200 msec in the worst case (when a large number of lightpaths have to be restored simultaneously as a result of a single failure). As expected, restoration latency generally increases as more lightpaths are failed, even though there could be variations for a relatively similar number of failed lightpaths. A study presented in [10] is representative of a what-if type study to determine the range of restoration latencies that can be expected from a network upon single link or node failures.

Mesh Re-provisioning

In the case of multiple failures, Dynegy's network, utilizing intelligent OXCs, also supports lightpath re-provisioning. Lightpath re-provisioning establishes a new backup path when restoration on the original backup path does not succeed. Re-provisioning uses existing spare capacity and unused shared capacity to find a new backup path on which to immediately restore the failed lightpath. There are three conditions that result in lightpath re-provisioning: (a) A failure of the primary path followed by a failure of the backup path prior to repair of the primary path, (b) A failure of the backup path followed by a failure of the primary path prior to repair of the primary or backup path, and (c) A failure of the primary path of a lightpath (B) sharing backup capacity with a lightpath (A), followed by a failure of the primary path of lightpath (A). In this case, lightpath (B) is restored onto its backup path after the failure, thus occupying the shared backup resources. When lightpath (A) fails, it cannot restore onto its backup (because resources are being used), resulting in a re-provisioning attempt. Note that re-provisioning may fail if there is not enough capacity available. Re-provisioning a lightpath that becomes unavailable after a double failure will improve the service availability of the network, by reducing the time that the service is unavailable from hours to tens of seconds. Simulation studies showed that compared to default protection, mesh restoration provides higher reliability due to the implementation of re-provisioning after

a second failure, resulting in up to a 48% decrease in unavailability [11].

Mesh Re-optimization

During the network operation, requests for services are received and provisioned using an online routing algorithm with the cost model defined above. Both the primary and backup paths of each new demand request are computed according to the current state of the network. As the network changes with the addition or deletion of fiber links and capacity and traffic evolve, the routing of the existing demands becomes suboptimal. Re-optimization by re-routing the backup and/or primary paths gives the network operators the opportunity to regain some of the network bandwidth that is currently in use. In particular, re-routing only the backup paths is an attractive way to regain some of the protection bandwidth and reduce backup path length while avoiding any service interruption. Figure 2 illustrates how re-optimization temporarily eliminates the drift between the current solution and the best-known off-line solution that is achievable under the same conditions.

Table 1 shows the gains achieved when the backup paths in Dynegy's live network are re-routed during a maintenance window. In this case, the network consisted of 45 nodes, 75 links, and 70 shared mesh restored demands with their routes provided by the network operator, and all backup paths were re-optimized and tested. The complete re-optimization procedure, including testing took approximately 5 hours. Note that Table 1 only refers to ports used for the protection channels and it shows the port counts and number of backup hops measured before and after re-optimization. Clearly, re-optimization is beneficial both in terms of the number of protection ports used, as well as the length of the backup paths. Specifically, as shown in the table, backup path re-optimization saved 31% of the protection ports which in turn translated to 20% savings of the total number of ports. Also, the average length of the backup paths decreased from 5.87 to 4.88 hops [12]. The importance of re-optimization to the network is threefold. Firstly, the reduced number of protection ports used translates in freed protection capacity, which could then be used to carry new services. Secondly, the reduction in

backup path length translates to the reduction in protection latency. In particular, in the re-optimization of Dynegy's network, the reduction of the average length of the backup path reduced the backup latency (restoration time) by 25.61% (calculated using the average length of the backup path in miles before and after the re-optimization) [12]. Finally, re-optimization allows network operators to make use of new nodes and links that are deployed in the network.

Dynegy's long-haul national network utilizing Tellium's optical switches has clearly become an *intelligent network*. It offers end-to-end point-and-click provisioning, shared mesh restoration with a few tens to a couple of hundred msec restoration times, re-provisioning of connections in the event of double failures and network re-optimization to regain some of the network capacity that is not optimally used.

References

[1] T.E. Stern, K. Bala, Multiwavelength Optical Networks: A Layered Approach, Prentice Hall, May 1999.
[2] S. Lumetta, M. Medard, "Towards a Deeper Understanding of Link Restoration Algorithms for Mesh Networks," in Proc. of IEEE Infocom 2001, Anchorage, Alaska, April 2001.
[3] E. Modiano, A. Narula-Tam, "Survivable Routing of Logical Topologies in WDM Networks," in Proc. of IEEE Infocom 2001, Anchorage, Alaska, April 2001.
[4] B. Doshi, et al, "Optical Network Design and Restoration," Bell-Labs Technical Journal, Vol. 4, No. 1, pp. 58-84, January-March 1999.
[5] G. Ellinas, et al, "Routing and Restoration Architectures in Mesh Optical Networks," Optical Networks Magazine, Issue 4:1, January/February 2003.
[6] J-F. Labourdette, et al, "Routing Strategies for Capacity-Efficient and Fast-Restorable Mesh Optical Networks," Photonic Network Communications, vol. 4, no. 3-4, pp. 219-235, 2002.
[7] E. Bouillet, et al, "Enhanced Algorithm Cost Model to Control tradeoffs in Provisioning Shared Mesh Restored Lightpaths," in Proc. OFC 2002, Anaheim, CA, March 2002.
[8] C. Qiao, et al, "Novel Models for Shared Path Protection," in Proc. OFC 2002, Anaheim, CA, March 2002.
[9] R. Ramamurthy, et al, "Routing Lightpaths in Optical Mesh Networks with Express Links," in Proc. OFC 2002, Anaheim, CA, March 2002.
[10] A. Akyamac, et al, "Optical Mesh Network Modeling: Simulation and Analysis of Restoration Performance," in Proc. NFOEC 2002, Dallas TX, September 2002.
[11] A. Akyamac, et al, "Reliability in Single Domain vs. Multi Domain Optical Mesh Networks," in Proc. NFOEC 2002, Dallas TX, September 2002.
[12] E. Bouillet, et al, "Lightpath Re-optimization in Mesh Optical Networks," in Proc. 7th European Conference on Networks & Optical Communications (NOC), Darmstadt, Germany, June 2002.
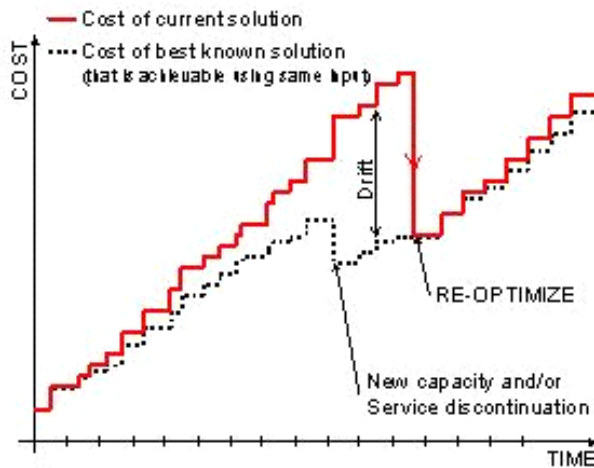
Figure 2: Current cost versus best possible cost with cost-benefit of re-optimization.

Scenario	Backup port count			Avg. backup hops		Max backup hops	
Name	Before	After	% save	Before	After	Before	After
Dynegy Network	310	214	30.97%	5.87	4.88	15	10

Table 1. Backup Path Re-optimization